Synthesis and Characterization of Poly(propyleneimine)-based Rhodium(I) Metallodendrimers and their Evaluation as Hydroformylation Catalysts

A thesis submitted to the

University of Cape Town

in fulfillment of the requirements for the degree of

Master of Science

by

Nathan Antonels

Supervisor: Dr Gregory S. Smith

Co-supervisor: Prof John R. Moss

Department of Chemistry
University of Cape Town
Rondebosch
7701
Cape Town

June 2010

Synthesis and Characterization of Poly(propyleneimine)-based Rhodium(I) Metallodendrimers and their Evaluation as Hydroformylation Catalysts

Nathan Antonels

University of Cape Town

June 2010

Declaration

I know the meaning of plagiarism and declare that all the work in the document, **"Synthesis and Characterization of Poly(propyleneimine)-based Rhodium(I) Metallodendrimers and their Evaluation as Hydroformylation Catalysts"**, save for that which is properly acknowledged by means of reference, is my own.

Signed by candidate

Mr Nathan Antonels

Date

Acknowledgements

I would like to thank:

God for always being able to confide in Him in prayer especially when situations became challenging. His spirit has given me the strength and endurance needed to undertake this degree.

My supervisors, Dr Greg Smith and Prof John Moss. Their help and patience has carried me through this learning experience. They are understanding and extremely insightful and the passing of their knowledge to me during this degree will surely serve me in the years to come especially with regards to advancing as a chemist. They truly serve by example, their passion for teaching and research is excellent, they are perfect role models for me and others to have the privilege of working with them.

The inorganic chemistry research team and especially my close friends, Prinessa, Emma, Tameryn, Preshen and Tawfeeq. They have been a great support in all matters academic and social, helping me with new angles of approach for my research and times to unwind in their company.

Mr P. Roberts and Mr N. Hendricks for the recording of my NMR spectra. Mr G. Benincasa for elemental analysis services, Dr M. Stander (University of Stellenbosch) and Dr M. Tanabe (Tokyo Institute of Technology) for mass spectral analyses and Dr B. Therrien for X-ray diffraction analyses.

For funding, I would like to thank the UCT Chemistry Equity Development Programme, UCT Equity Development, the National Research Foundation and c*change.

My mother for her constant help and support in everything during this period of time even when I was not the best person to be around, she helped keep me grounded.

Abstract

A series of new iminopyridyl- and iminophosphine-functionalized dendritic ligands were synthesized by reacting the commercially available first and second-generation DAB poly(propyleneimine) (PPI) dendrimers with 4-pyridinecarboxaldehyde and 2-(diphenylphosphino)benzaldehyde respectively via a Schiff-base condensation reaction. The ligands were characterized using NMR and IR spectroscopies, elemental analyses and mass spectrometry. Model monomeric analogues of these multimeric ligands were synthesized to aid with interpreting the more complex spectra of the dendritic ligands.

The iminopyridyl-functionalized ligands were reacted with $[RhCl(COD)]_2$ to yield a set of new mononuclear and multinuclear rhodium(I) complexes that coordinated selectively to the pyridyl nitrogen in a monodentate coordination mode. The iminophosphine functionalized ligands were reacted with $[RhCl(CO)_2]_2$. These reactions yielded a set of new mononuclear and multinuclear iminophosphine rhodium(I) complexes, where the P,N-donor iminophosphine ligands coordinated to the rhodium metal center in a heterobidentate coordination mode to form chelate complexes. The complexes were characterized using NMR and IR spectroscopies, elemental analyses and mass spectrometry. Crystals of the mononuclear iminophosphine rhodium(I) complex were obtained and the molecular structure solved using single crystal X-ray diffraction analysis. Chemical reactivity studies were conducted on the mononuclear and multinuclear iminopyridyl and iminophosphine complexes. The iminopyridyl rhodium(I) complexes were reacted with triphenylphosphine. These reactions yielded similar results to that of the reaction between the iminopyridyl-functionalized ligands and $[RhCl(PPh_3)_3]$. Methyl iodide was reacted with the mononuclear and multinuclear iminophosphine rhodium(I) complexes. Reactions of methyl iodide with the mononuclear iminophosphine rhodium(I) complex yielded a mixture of the oxidative addition and the acyl product, where the acyl product results from a subsequent alkyl migration into the metal carbonyl bond after oxidative addition has occurred. Reaction of methyl iodide with the multinuclear metallodendritic iminophosphine rhodium(I) complexes yielded the oxidative addition product exclusively. Reaction products were monitored using IR spectroscopy.

Selected mononuclear and multinuclear iminopyridyl and iminophosphine rhodium(I) complexes were evaluated as catalysts in the hydroformylation of 1-octene. The complexes showed moderate hydroformylation rates under mild conditions. The multinuclear metallodendritic rhodium(I) complexes compare favorably to that of the mononuclear

rhodium(I) complexes showing slightly enhanced catalytic activity and regioselectivity in certain cases. Hydroformylation results obtained when using these complexes compare well to results obtained when using [Rh(acac)$(CO)_2$] under similar conditions, a rhodium(I) complex commonly used in literature.

Publications

Journal Articles:

N.C. Antonels, B. Therrien, J.R. Moss and G.S. Smith, *Rhodium(I) iminophosphine poly(propyleneimine) dendrimers: Synthesis, characterization and molecular structure of a mononuclear analogue*, Inorg. Chem. Commun., **2009**, 12, 716.

P. Govender P, N.C. Antonels, J. Mattsson, A.K. Renfrew, P.J. Dyson, J.R. Moss, B. Therrien, and G.S. Smith, *Anticancer activity of multinuclear arene ruthenium complexes coordinated to dendritic polypyridyl scaffolds*, J. Organomet. Chem., **2009**, 694, 3470.

Conference Contributions:

- Oral Presentation: Nathan Antonels, Gregory Smith and John Moss, *Rhodium(I) Metallodendrimers utilized in the hydroformylation of 1-octene*, presented at the Catalysis South Africa (CATSA) conference, Cape Town, 2009.

- Poster Presentations: Nathan Antonels, Gregory Smith and John Moss, *Synthesis and Characterisation of Rhodium Metallodendrimers as Potential Hydroformylation Catalysts*, presented at the Cape Organometallic Symposium, Cape Town, 2008.

  Nathan Antonels, Gregory Smith and John Moss, *Synthesis and Characterisation of Rhodium Metallodendrimers as Potential Hydroformylation Catalysts*, presented at the Catalysis South Africa (CATSA) conference, Parys, South Africa, 2008.

  Nathan Antonels, Gregory Smith and John Moss, *Rhodium(I) Metallodendrimers utilized in the hydroformylation of 1-octene*, presented at INORGANIC 2009, Bloemfontein, South Africa, 2009.

Abbreviations

acac	-	acetylacetone
Ar	-	Aromatic
br	-	broad
Bu^n	-	n-butyl
COD	-	1,5-cyclooctadiene
d	-	doublet
DAB	-	1,4-diaminobutane
DAB-Am-4	-	N,N,N',N',-Tetrakis(3-aminopropyl)-1,4-butanediamine
DAB-Am-8	-	4,17-Bis-(3-aminopropyl)-8,13-bis-[3-[bis-(3-aminopropyl)-amino]-propyl]-4,8,13,17-tetraazaeicosan-1,20-diamin, 4,17-Bis(3-aminopropyl)-8,13-bis[3-[bis(3-aminopropyl)amino]propyl]-4,8,13,17-tetraazaeicosane-1,20-diamine
dd	-	doublet of doublets
DCM	-	dichloromethane
DMAP	-	4-dimethylaminopyridine
dppe	-	1,2-bis(diphenylphosphino)ethane
EI	-	Electron Impact
ESI	-	Electrospray Ionization
ESPHOS	-	(2R, 5S)-(1,2-phenylene)bis(-3-phenyl-1,3-diaza-2-phosphabicyclo[3.3.0^{1,5}]octane)
Et	-	Ethyl
FAB	-	Fast Atom Bombardment
FTIR	-	Fourier Transform Infrared
GC	-	Gas Chromatography
Hz	-	Hertz
IR	-	Infrared
J	-	Coupling constant
m/z	-	mass to charge ratio
m (for IR)	-	medium
m (for NMR)	-	multiplet
MALDI-TOF	-	Matrix Assisted Laser Desorption Ionization – Time Of Flight
MHz	-	Megahertz

Abbreviations

MS	-	Mass Spectrometry
NMR	-	Nuclear Magnetic Resonance
PAMAM	-	Poly(amidoamine)
Ph	-	Phenyl
POSS	-	Polyhedral Oligomeric Silsesquioxane
ppm	-	parts per million
pyr	-	pyridine
qn	-	quintet
s (for IR)	-	strong
s (for NMR)	-	singlet
SemiEsphos	-	(2R, 5S)-2-(2-methoxyphenyl)-3-phenyl-1,3-diaza-2-phosphabicyclo[3.3.0^{1,5}]octane
sx	-	sextet
t	-	triplet
THF	-	Tetrahydrofuran
TOF	-	Turnover Frequency
w	-	weak

Contents

Chapter 1

Literature Review

1.1 What are metallodendrimers?

Dendrimers are highly branched macromolecules characterized by their tree-like structure where dendritic branches propagate from the core of the dendrimers and where each new branching gives rise to a new generation. [1, 2]

The first molecules resembling a dendritic structure were synthesized in 1978 by Vögtle and co-workers who initially referred to them as "cascade molecules". [3] Tomalia and co-workers further pursued these cascade molecules and called them dendrimers. [4,5] Dendrimers can be synthesized with various functional groups in the branches or at the termini. This provides potential coordination sites for transition metals and hence the potential application in transition metal catalysis. [6,7] As a result different metallodendrimer topologies can be formed such that the metal can be coordinated at the periphery (Fig. 1.1a,b), within the branches (Fig. 1.1c), the core (Fig. 1.1d) and within interstitial sites (Fig. 1.1e) of the dendrimer.[8]

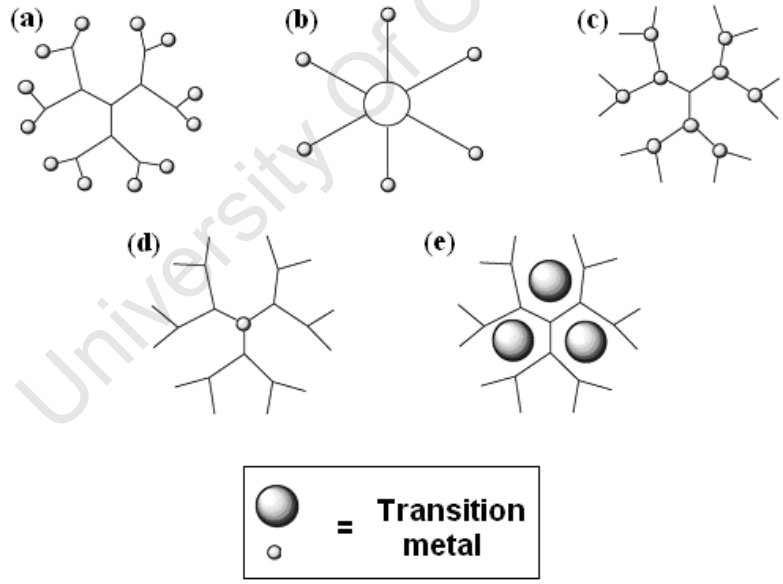

Figure 1.1: Illustration of the various metallodendrimer topologies. [8]

1.2 Synthetic routes to metallodendrimers

Dendrimers can be synthesized via two approaches, the convergent or the divergent method. The divergent method entails synthesis from the core outwards by continual coupling of monomeric units. The coupling involves alternating steps of deprotection and then subsequent coupling of multifunctional monomeric units (Fig. 1.2).[9]

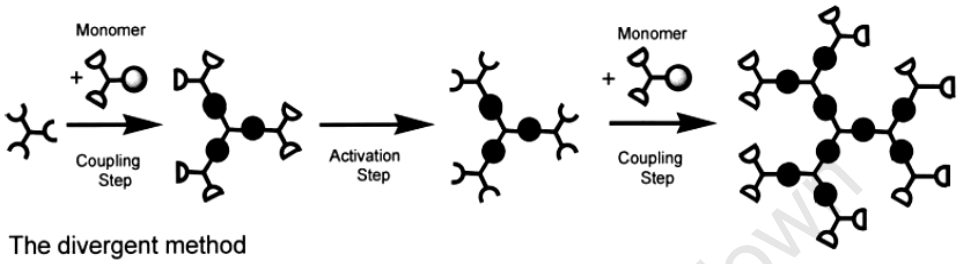

Figure 1.2: Illustration of the divergent method for dendrimer synthesis. [9]

The convergent method entails synthesis of dendritic units/wedges which are coupled to the core molecule (Fig. 1.3).[9]

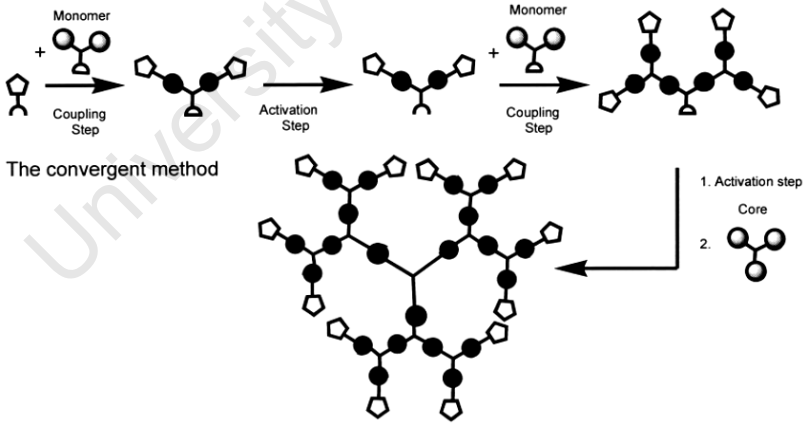

Figure 1.3: Illustration of the convergent method for dendrimer synthesis. [9]

These synthetic methodologies allow the synthesis of dendrimers of various generations but incur difficulties for synthesis of higher generation dendrimers as steric crowding between branches can hinder the coupling reactions. [9,10] These methodologies can also be utilized to synthesize metallodendendrimers.

1.3 Synthesis and examples of transition metal metallodendrimers with different topologies

The synthesis of the multinuclear metallodendrimer compounds can be synthesised in a similar manner to that of the mononuclear compounds. As previously discussed, metallodendrimers can have different topologies with metals coordinating at various sites on the dendrimer. Suitable synthetic routes are therefore required to realize these various topologies.

Work by van Leeuwen and co-workers involved the synthesis of a novel poly(propyleneimine) (PPI)-based metallodendrimer functionalized with alkoxycarbonylcyclopentadienyl complexes of rhodium.[11] Prior to the attachment of the metal precursor to the dendrimer, the metal complex **1.1**, was reacted with 1,1-carbonyldiimidazole (**1.2**) to afford the complex **1.3** (Scheme 1.1).

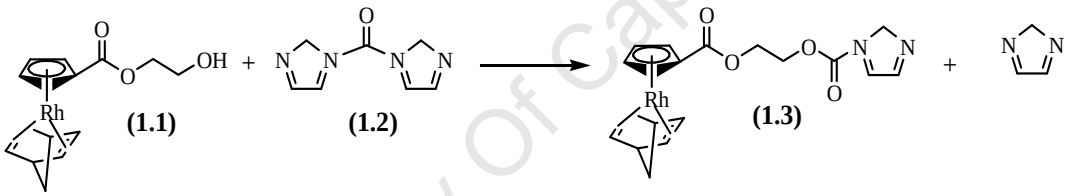

Scheme 1.1

An excess of **1.3** was then reacted with the first generation 1,4-diaminobutane (DAB) PPI dendrimer (Scheme 1.2) via a carbamate formation reaction to afford the metallodendrimer, **1.4**. Any unreacted **1.3** and side products can be removed by washing with diethyl ether. This exemplifies a typical route utilized to synthesize metallodendrimers with transition metal centers located on the periphery of the dendrimer.

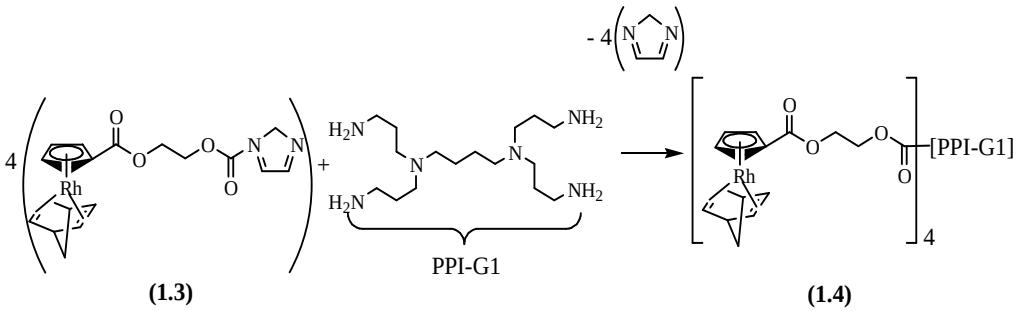

Scheme 1.2

A second example of a peripherally metallated dendrimer was reported by Govender *et al.* [12] The first- and second-generation metallodendrimer complexes were reported. Scheme 1.3 illustrates the reaction between the first generation iminopyridyl functionalized dendrimer, and di-μ-chlorobis[(*p*-cymene)chlororuthenium] to afford the first generation ruthenium(II) *p*-cymene dichloride metallodendrimer, **1.5**.

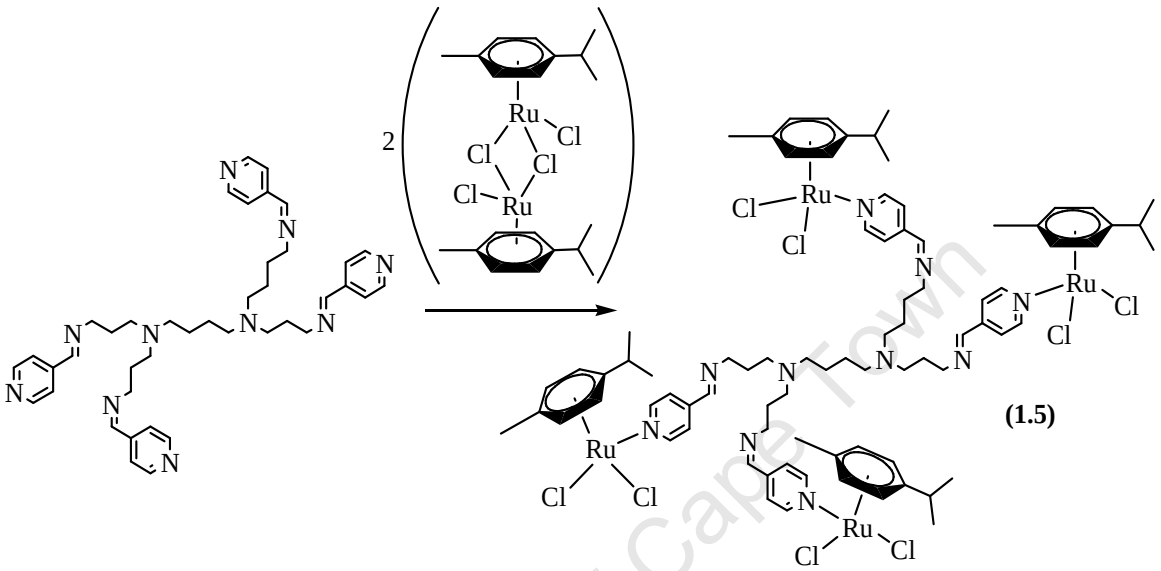

Scheme 1.3

Peripherally coordinated metals allow for the dispersal of metal centres on the outside of the dendritic scaffold. In the case where a metal is located at the core of the dendrimer, a sterically hindered macro-environment is created. Majoral and co-workers reported the synthesis and characterization of an octa-substituted pthalocyanine core dendrimer. [13] The dendrimer, **1.6**, was reacted with cobalt dichloride in the presence of triethylamine in tetrahydrofuran (THF) (Scheme 1.4). The reaction resulted in the coordination of cobalt to the phthalocyanine nitrogens to afford complex **1.7**.

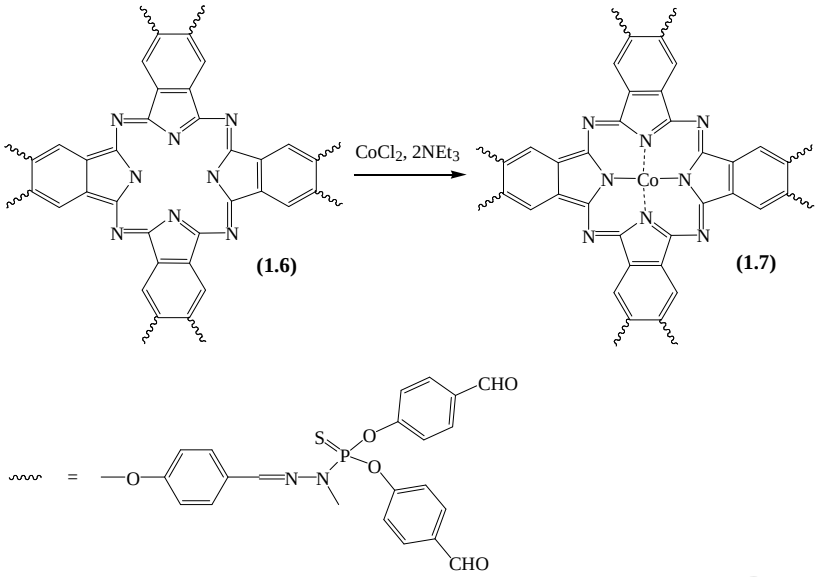

Scheme 1.4

Smith and co-workers investigated the effect of the dendritic macro-environment on the oxidation potential of ferrocene. [14] They synthesized metallodendrimers with ferrocene as the core (Scheme 1.5). The synthesis of the first generation dendrimer, **1.9**, was achieved by a convergent synthesis by reacting 1,1'-bis(chlorocarbonyl)ferrocene with two equivalents of the pre-formed dendron, **1.8**, in the presence of 4-dimethylaminopyridine (DMAP) and dichloromethane (DCM).

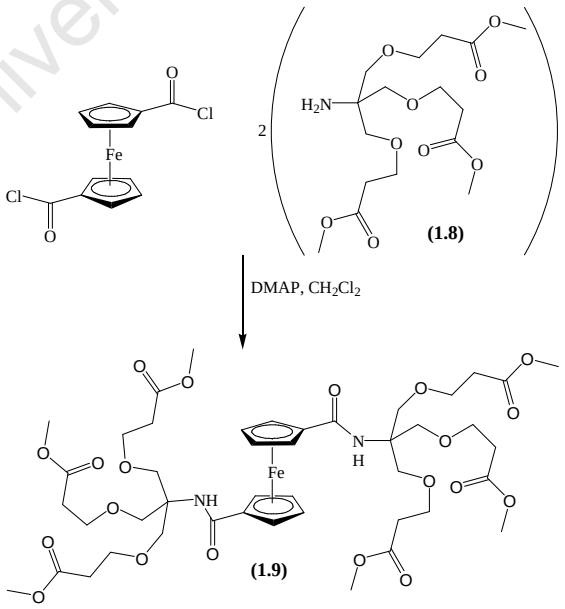

Scheme 1.5

A third type of topology exists where the metals are coordinated within the branches of the dendrimer. Takahashi and co-workers synthesized a platinum-acetylide containing dendrimer.[15] These dendrimers have platinum-acetylide groups within the branches of the dendrimer that are linked by phenyl groups. Synthesis of the first generation dendron was easily achieved by Cu(I) catalyzed coupling of the platinum complex with acetylide species as shown in Scheme 1.6.

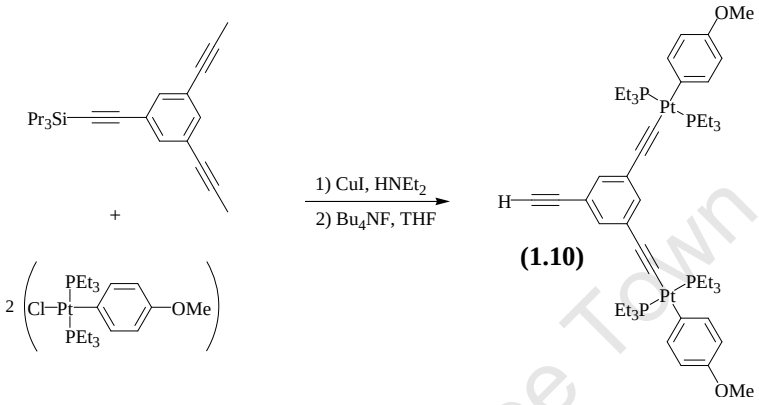

Scheme 1.6

A first-generation metallodendrimer, **1.11**, based on this topology can be synthesized by replacing the H group of **1.10** with a pyridyl group (Fig 1.4, **G_1 Dendron**) and reacting this dendron with a tri-substituted palladium acetylide core.

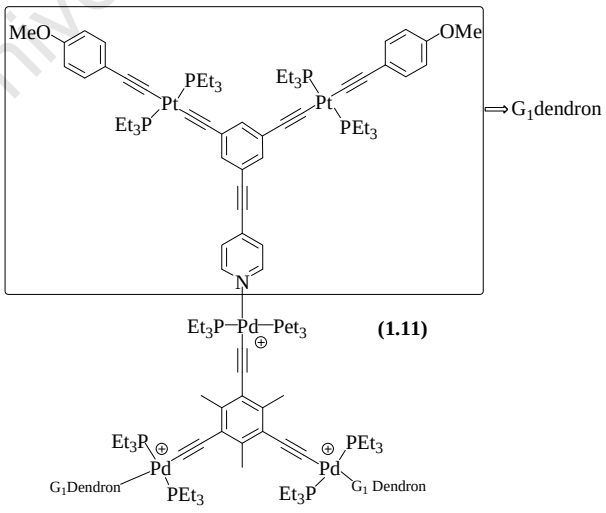

Figure 1.4: Takashi's pyridine-substituted Pt acetylide dendrimer.

A similar dendritic framework was employed by Humphrey and co-workers who synthesized a metallodendrimer where the ruthenium metal atoms are bound within the branches of the dendrimer. [16, 17] These dendrimers were investigated for their non-linear optical properties. Synthesis of the ruthenium functionalized dendritic core was achieved by reacting the phenyl acetylide core, **1.12**, with three equivalents of *cis*-$[RuCl_2(dppe)_2]$ to give **1.13** (Scheme 1.7).

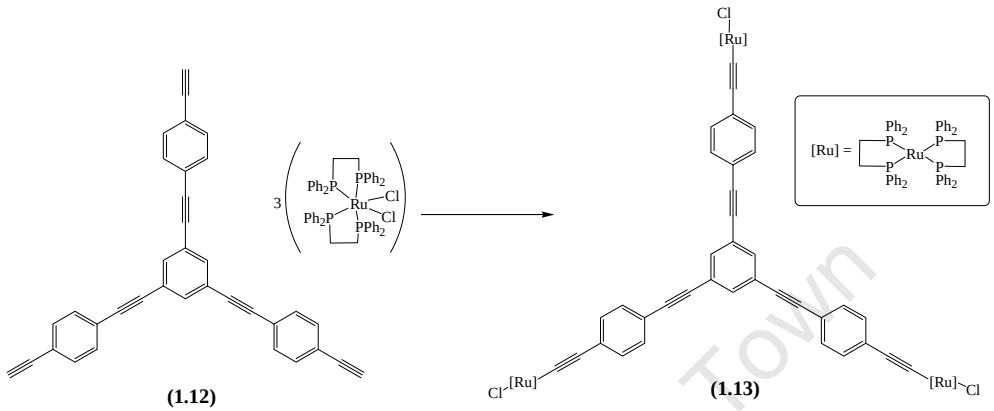

Scheme 1.7

This ruthenium functionalized phenyl acetylide core (**1.13**) was then reacted with three equivalents of the dendron **1.14**, in the presence of $NaPF_6$ and NEt_3 to give the first generation dendrimer, **1.15** (Scheme 1.8).

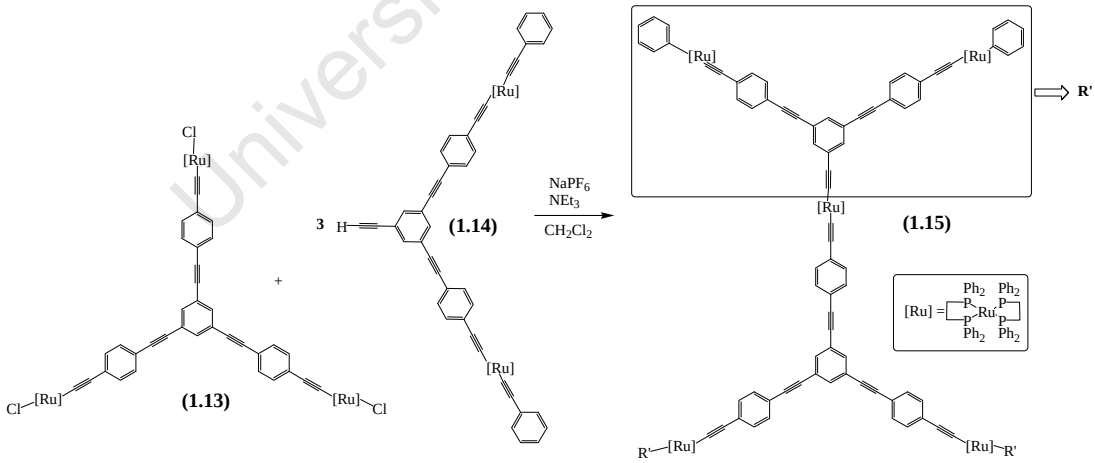

Scheme 1.8

These examples demonstrate the various types of metallodendrimers that exist and some of their applications. This project deals with the use of metallodendrimers in hydroformylation a topic to be discussed in the following sections.

1.4 Discovery of hydroformylation

Hydroformylation is the catalyzed addition of carbon monoxide and hydrogen to an olefin, to form aldehydes (Scheme 1.9).

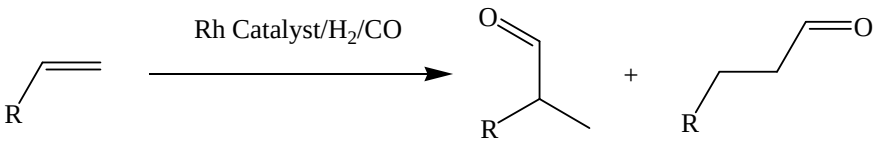

R = alkyl or aromatic group

Scheme 1.9

These aldehydes can subsequently be hydrogenated to alcohols that can have a variety of uses including their use as detergents or solvents.[17-21] This process is catalyzed by homogeneous transition metal catalysts normally based on cobalt or rhodium. On an industrial scale, this reaction produces in excess of 7 million tons of aldehyde annually. Hydroformylation was discovered in 1938 by Otto Roelen during an investigation of the oxygenated products formed during the Fischer-Tropsch reaction.[18] Roelen noted that CO, H_2 and ethylene were converted to propanal and that at higher pressures diethyl ketone was formed. This sparked interest in the process of hydroformylation and since its initial discovery up until the 1960's, cobalt catalysts were used in industry as hydrogenation catalysts under catalytic reaction conditions. The cobalt catalyzed hydroformylation mechanism proposed by Heck and Breslow is now the generally accepted mechanism for hydroformylation.

The hydroformylation mechanism consists of the following steps (Scheme 1.10):

- Dissociation of CO and addition of alkene to cobalt complex.
- Anti-Markovnikov (for linear aldehydes) addition of hydrogen to alkene to form the linear alkyl.
- Alkyl migration to form the acyl intermediate of the complex.
- Reductive elimination of acyl to form the aldehyde and regenerate the active complex.

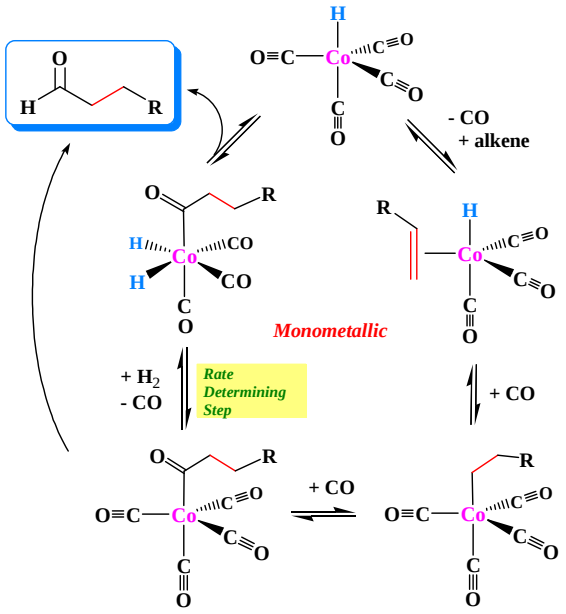

Scheme 1.10

When developing homogeneous and heterogeneous hydroformylation catalysts, areas of concern include the chemoselective conversion of olefin to aldehyde, regioselectivity to linear or branched aldehyde (n:iso ratio), separability of catalyst from the reaction medium and hydroformylation products, stability and lifetime of the catalyst and recyclability of the catalyst. Organometallic hydroformylation catalysts and catalyst precursors are mainly based on rhodium and cobalt. Each metal allows different levels of selectivity towards catalytic products. Great importance is placed on developing a catalyst with a high level of chemo- and regioselectivity. This is demonstrated by the need for branched aldehydes in pharmaceutical industry for the preparation of drugs such as ibuprofen obtained from the hydroformylation of 4-isobutylstyrene and subsequent oxidation of the branched aldehyde.[19,20]

A variety of rhodium and cobalt transition metal catalysts are available for the catalysis of this reaction but they are expensive and difficult to recover. Immobilizing these catalysts on a support such as a dendrimer can ensure a degree of catalyst recoverability and promising catalytic activity as demonstrated by Bourque and co-workers.[21]

1.4.1 Cobalt hydroformylation catalysts

Cobalt catalysts are prepared *in situ* by treating cobalt salts with synthesis gas (CO/H_2; 1:1). The instability of this complex under high temperature dictates the conditions required for

catalysis. High temperature leads to the formation of metallic cobalt. To counteract the high instability of the catalyst at these temperatures, an increase in CO partial pressure is required. Increasing CO partial pressure can negatively affect the catalytic rate despite the positive effect on the stability of the complex. The rate of hydroformylation therefore shows a negative order with respect to the CO partial pressure. [22]

Problems with unmodified cobalt catalyst precursors and catalysts like $Co_2(CO)_8$ and $HCo(CO)_4$ respectively, are their volatility and that they are difficult to separate from the catalytic products. Complexes with tertiary alkyl phosphine ligands show an increase in the stability of the complex and are referred to as modified complexes. This results in lower CO pressure needed to stabilize the cobalt complex when subjected to catalytic conditions. Shell developed the cobalt complex, $[Co(CO)_3(PBu_3^n)]_2$, with the active catalyst being $[HCo(CO)_3(PBu_3^n)]$. The catalyst shows lower activity than $HCo(CO)_4$ but higher selectivity giving an n:iso ratio of 7:1 compared to 4:1 for the unmodified cobalt catalyst . [22] The modified catalyst shows good activity at 100 atm compared to 200-300 atm. In turn, the stability of the complex allows for the distillation of alcohols from the catalytic mixture.[22]

1.4.2 Rhodium hydroformylation catalysts

Compared to cobalt catalysts, most rhodium catalysts can catalyze the hydroformylation reaction under milder conditions. Table 1.1 compares the general conditions utilized by the various catalytic systems.[23]

Table 1.1: Operating conditions for the most common hydroformylation catalysts.

	Co (Unmodified)	**Co (PR_3)**	**Rh (PPh_3)**
Temp. (ºC)	140-180	160-200	80-120
Pressure (bar)	250-350	50-100	15-25
Co/Rh: alkene (%)	0.1-1.0	0.5-1.0	10^{-2}-10^{-3}
n:iso ratio	3-4:1	8-9:1	12-15:1
Aldehydes (%)	~80	---	~96
Alcohols (%)	~10	~80	---

From the data depicted in Table 1.1 it can be seen that there is a decrease in the temperature requirement going from the unmodified cobalt complexes to the modified rhodium complexes. In the case of the modified cobalt and rhodium catalysts, the former is

chemoselective for alcohol formation and the latter for aldehydes. Modified cobalt catalysts can therefore be advantageous if alcohols are needed as it removes the need for a separate hydrogenation step after hydroformylation. In the case of the modified rhodium catalyst, a higher catalytic rate is realized, in comparison to unmodified cobalt catalysts, for a lower metal loading.[22]

To substantiate the above information with respect to rhodium catalysts they afford the hydroformylation of propylene to *n*-butyraldehyde at 10-20 atm and 100 °C. This is important especially in industry where energy conservation can lead to increased revenue. The linear aldehyde is favored with yields of approximately 90% when an excess of phosphine ligand is employed.

The phosphine ligand plays a vital role in stabilizing the catalyst during the product recovery as well as directing the reaction to form the desired linear aldehyde. Little to no alcohol is formed but the propylene can be hydrogenated to propane. Rate and regioselectivity of hydroformylation reactions can be greatly affected by changes in reaction conditions such as temperature and syngas pressure. [19]

To better understand and classify the observations noted in hydroformylation studies, two governing effects need to be considered, viz, the electronic and steric effects. Similar to cobalt catalysts, alkylphosphine ligands lead to a decrease in catalytic rate and to counteract this, higher temperatures are needed to increase reaction kinetics.[18, 24, 25]

On the other hand, the use of phosphine ligands with more electron withdrawing groups results in faster catalytic reaction rates. The rhodium-carbonyl bond is therefore weakened by the decrease in electron density on the metal centre. Comparitive studies show that arylphosphine ligands with more electron withdrawing groups allow faster catalytic reaction rates than conventional alkylphosphine ligands.[26-28]

Steric effects govern what is bound to the rhodium centre at any moment, where bulky ligands will lead to the dissociation of other bulky ligands and coordination of less bulky carbonyls to the metal complex. [29] Phosphine ligands can operate by introducing steric hindrance and

drive the formation of the linear aldehyde instead of the branched aldehyde. However, if one of the bulky phosphines should be replaced by a smaller carbonyl, there would be a greater propensity for the formation of the bulkier branched aldehyde.[29]

1.5 Metallodendrimers used as hydroformylation catalysts

Dendrimers have been investigated for their potential applications in catalysis. [30, 31] They have the ability to incorporate the advantages of both homogeneous and heterogeneous catalysts. This is due to the possibility of separation of the catalytic product from the metallodendrimer by nanofiltration employed in a continuous feed system.[32] Table 1.2 details the general properties of heterogeneous and homogeneous catalysts.

Table 1.2: Properties of heterogeneous and homogeneous catalysts.[33]

Heterogeneous Catalysts	Homogeneous Catalysts
Facile separation from catalytic product	Difficult separation of catalytic product from catalyst
Increased catalyst lifetime	Short catalyst lifetime
Lower catalytic rates	High catalytic rate
Harsher reaction conditions required	Mild catalytic conditions required
	Catalyst is easily fine tuned

The ideal catalyst would combine the advantages of these two types of catalysts hence:

- Have separate well-defined catalytic sites.
- Be stable with a long lifetime.
- Have a high catalytic rate.
- Be easily separated from the catalytic product and be recyclable.

Dendrimer synthesis affords a degree of freedom allowing customization of the functional groups on the dendrimer, the size and the crowding of the dendrimer. This can lead to various effects on catalytic performance such as enhanced activity [34] and selectivity [35] or sometimes total inhibition [36] of the catalyses. The objective is therefore to obtain a metallodendrimer that has enhanced activity and selectivity, allows for dispersal of distinct catalytic metal centers on the dendritic scaffold and facile separation from the products.

Phosphine terminated dendrimers show versatile complexation abilities towards rhodium complexes.[37] One of the first metallodendritic complexes to be employed in hydroformylation was synthesized by Reetz and co-workers. They utilized the DAB poly(propyleneimine) dendritic scaffold and functionalized it with phosphorous at the termini to give a multiphosphine functionalized dendrimer (Figure1.5). [38,39]

Iridium, palladium and nickel metal complexes were coordinated to these dendrimers to give various metallodendrimers. These were evaluated as potential catalysts in the Heck cross coupling reaction.

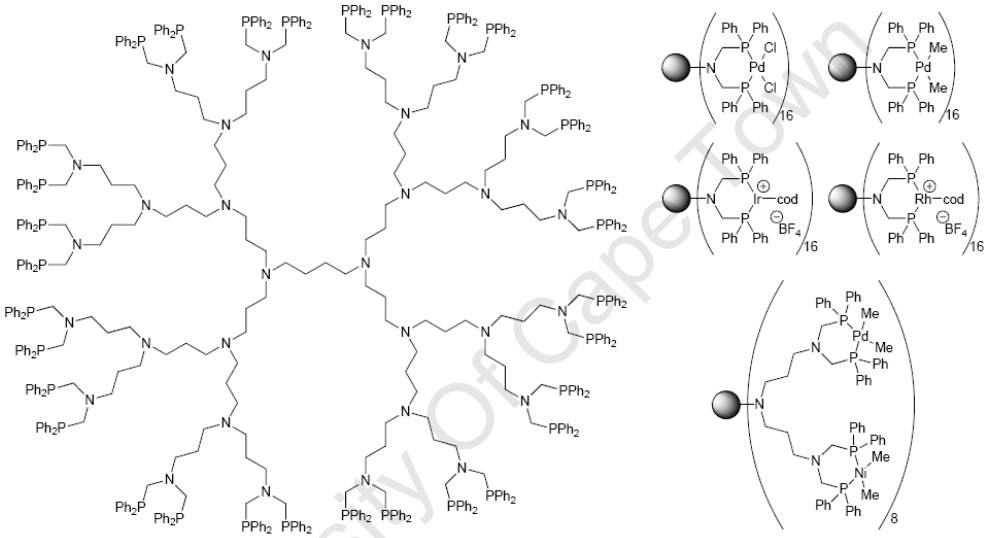

Figure 1.5: DAB rhodium, palladium and iridium metallodendrimers employed in catalytic reactions. [38,39]

Of more relevance to this project, is the synthesis of rhodium metallodendrimers. $[Rh(COD)_2]BF_4$ was reacted with the diphosphine dendrimers and the resulting metallodendrimers tested as catalysts in the hydroformylation of 1-octene. Model mononuclear complexes were also synthesized and compared to the dendritic complexes. Quantitative conversion of the olefin to aldehyde was observed, when using the multinuclear metallodendrimer complex, with an n:iso ratio of 60:40 and turnover frequency of 360 h^{-1}.

The mononuclear compound yielded similar results to that of the multinuclear metallodendrimer. In this case there is an indication that the metallodendrimer catalyst can contend with mononuclear complexes where catalyst performance is concerned.

Due to their unique macromolecular environments, dendritic molecules can influence the regioselectivity and chemoselectivity of a catalytic reaction. Enhanced regioselectivity can be observed as was the case with research conducted by Cole-Hamilton and co-workers, who synthesized a dendrimer based on a polyhedral oligomeric silsesquioxane (POSS) core. [40, 41]

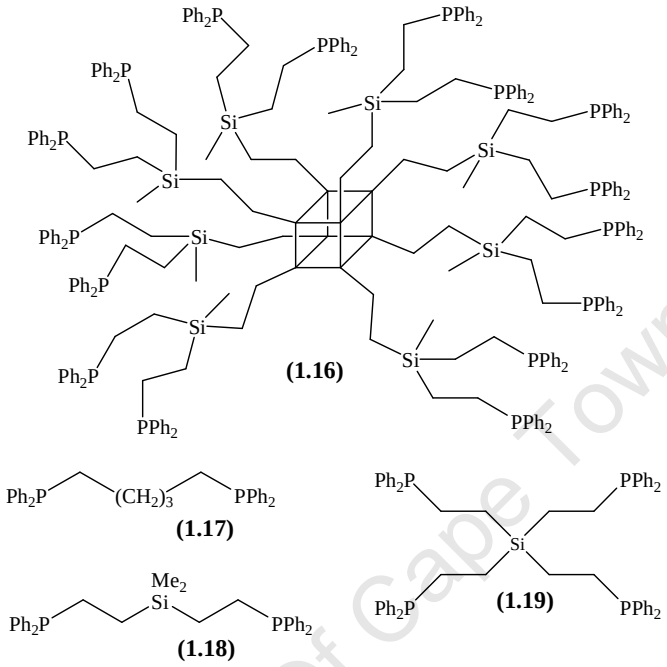

Figure 1.6: POSS dendrimer and ligand analogues utilized in hydroformylation to investigate effect of ligands size

The dendrimer has 16 diphenylphosphine functionalized arms. The catalyst was prepared *in situ* from the POSS dendrimer (**1.16**) (Fig. 1.6) and [Rh(acac)$(CO)_2$] (acacH = pentane-2,4-dione). The hydroformylation reactions were conducted using 1-octene. This combination gives n:iso ratios of approximately 14:1.

This ligand, **1.16**, was compared to other less constrained ligands, **1.17-1.19** (Fig. 1.6). The bar graph summarizes the results obtained (Fig. 1.7) and it is evident that there is a definite increase in the n:iso ratio as the ligand increases in size and steric bulk.

The use of the more constrained higher generation dendritic ligands favored an increase in the formation of the linear aldehyde. The dendrimer therefore has a positive effect on the regioselectivity of this reaction.

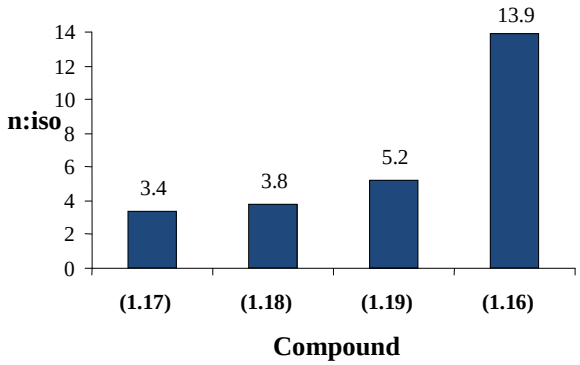

Figure 1.7: Bar graph of n:iso selectivity for different ligands

Dendrimers with increased water solubility have great appeal especially if utilized in greener processes such as biphasic catalysis. Gong and co-workers designed one such dendrimer based on the poly(amidoamine) (PAMAM) scaffold with terminal sulfonyl and amine groups to increase water solubility (Fig. 1.8). [42] These dendrimers were utilized as ligands in the hydroformylation of 1-octene and styrene at mild conditions of 40 ºC and 20 atm syngas pressure (1:1, $CO:H_2$). High catalytic rates were seen for the hydroformylation of both substrates in this biphasic system and a pronounced regioselectivity for the branched product was observed using styrene as the substrate. In the case of 1-octene, the linear product was favored and this is due to the steric bulk introduced by the dendritic ligand.

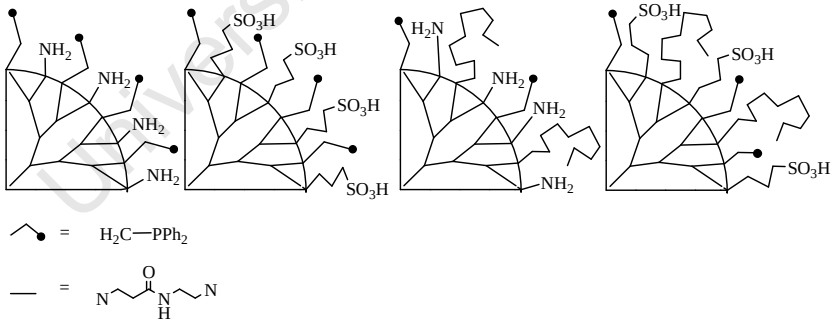

Figure 1.8: Sulfonyl and amine terminated dendritic ligands for increased water solubility.[42]

A similar trend for regioselectivity was observed by Huang and co workers for increased generation of dendritic ligand.[43] They employed poly (aryl ether) (PAE) dendrimers peripherally functionalized with triphenylphosphine as dendritic ligands (Fig. 1.9). The catalyst was prepared *in situ* from $[Rh(acac)(CO)_2]$ and the dendritic ligand under a syngas (1:1, $CO:H_2$) pressure of 20 bar. Styrene and 1-octene were employed as substrate in the

hydroformylation reaction and they found that there was not much difference in the selectivity for these different dendrimers. The n:iso ratios ranged from 3:1 to 3.6:1. However these values do increase with an increase in dendrimer generation and are in accordance with the common trend of proportional increase in linear product with increasing steric bulk.

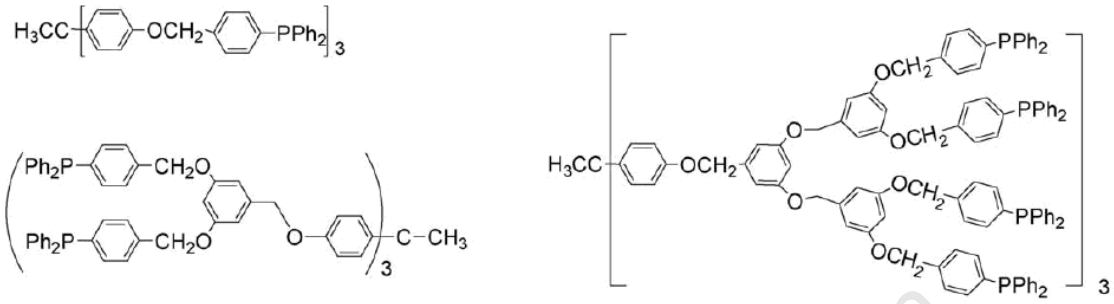

Figure 1.9: Triphenylphosphine functionalized poly(aryl ether) dendrimers.

Reek and co-workers synthesized a series of core-functionalized dendrimers, an example of which is seen in Figure 1.10 and investigated them as potential ligands in the design of rhodium hydroformylation and hydrogenation catalysts. [44] Table 1.3 details the hydroformylation data for the triphenylphosphine functionalized dendritic ligands utilized. The catalyst was prepared *in situ* by reacting the $[Rh(acac)(CO)_2]$ metal precursor with the dendritic ligand. The system was active in the hydroformylation of 1-octene and showed high regioselectivities for nonanal of 69% and above (Table 1.3).

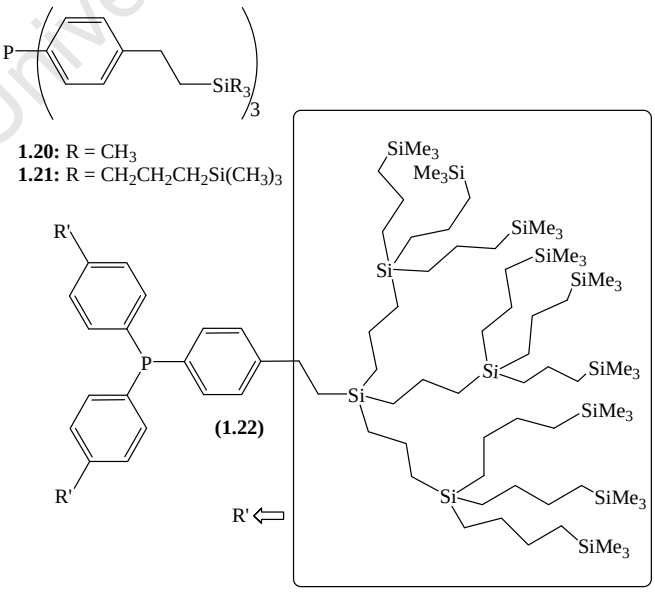

Figure 1.10: Core functionalized dendrimer with phosphorous at core.

Table 1.3: Hydroformylation data of 1-octene using dendrimeric ligands based on PPh_3.

Entry	Ligand	TOF[b] (x 10^2)	nonanal (%)	n/iso ratio[c]
1	PPh_3	29	73	2.9
2	**1.20**	28	69	2.2
3	**1.21**	27	71	2.6
4	**1.22**	16	71	2.6

[a] 1.0 μmol $[Rh(acac)(CO)_2]$, 10.0 μmol monophosphine or 5.0 μmol diphosphine ligand, 0.637 mmol 1-octene, 0.257 mmol decane, 1.1 cm^3 toluene, 20 bar (CO/H_2 = 1), 80 ºC, incubation time 90 min, reaction time 15 min (~60% conversion).
[b]Average turnover frequency, in (mol aldehyde)(mol Rh)$^{-1}h^{-1}$.
[c]n/iso product ratio.

Significantly, the reaction rate for the hydroformylation using the bulkier substrate was significantly decreased as can be seen by the almost two-fold decrease in the turnover frequency going from entries 2 and 3 to 4. They ascribed this to the bulkiness of the dendrimer rendering the metal centre somewhat inaccessible to the substrate. Despite the positive effects of increased steric bulk on the regioselectivity, tentative fine-tuning of the ligand is needed to avoid a decrease in catalytic activity.

Bulky diphosphine ligands are known to cause increased selectivities in the hydroformylation of various olefins to aldehydes; however the opposite is sometimes true for the bulky monodentate phosphines. ESPHOS (Fig 1.11, **1.23**) ligands and rhodium utilized in the *in situ* hydroformylation of vinyl acetate showed high regio- and stereoselectivities. [45] The unidentate analogue SemiEsphos however shows a diminished performance in this regard. [45]

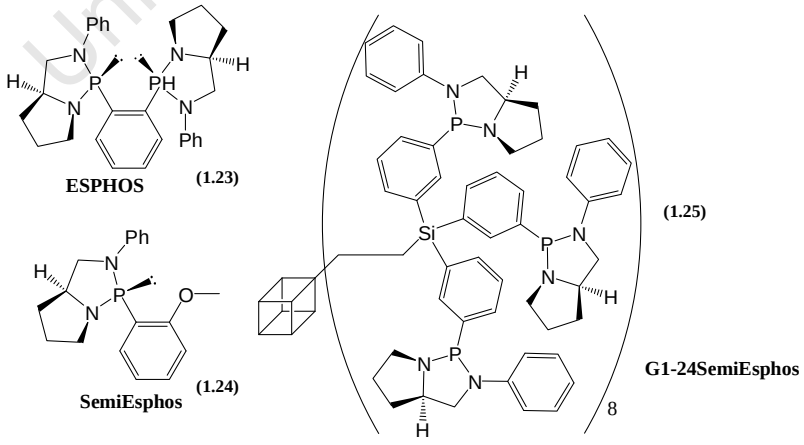

Figure 1.11: ESPHOS, SemiEsphos and dendritic SemiEsphos ligand G1-24SemiEsphos

Cole-Hamilton *et al.* conducted research in trying to increase the efficacy of certain unidentate ligands by using a dendritic scaffold. They utilized the SemiEsphos (**1.24**) ligands by functionalizing a first generation POSS dendrimer with SemiEsphos moieties.

Three types of POSS dendrimers were synthesized by functionalization with SemiEsphos ligands, with 8, 16 or 24 SemiEsphos moieties equally distributed on the 8 arms of the dendrimer. [46] Compound **1.25** in Figure 1.11 shows the first generation POSS dendritic ligand with 24 SemiEsphos moieties. The increase in SemiEsphos moieties on the periphery and their close proximity to each other could force the SemiEsphos moieties to coordinate to the rhodium in a multidentate fashion hence acting in a similar manner to an ESPHOS ligand. The SemiEsphos-based ligands were then utilized in the hydroformylation of vinyl acetate employing a syngas pressure of 40 bar ($CO:H_2$, 1:1), temperature of 80 ºC and reaction time of 20 hours. Table 1.4 shows some of the catalytic data obtained using the various systems.

The data clearly shows a low catalytic rate when using SemiEsphos even after 20 hours while a marked increase in activity is seen when using ESPHOS since quantitative conversion of 1-octene is realized after only 3 hours. In the case of the dendrimer bound SemiEsphos ligand, G1-16SemiEsphos, only an 11% conversion was realized after 20 hours with a Rh:P ratio of 1:6 and using rhodium concentration of 0.005 $mol.L^{-1}$.

Table 1.4: Hydroformylation of vinyl acetate with catalysis by rhodium complexes.[a]

Entry	Ligand	P:Rh	Conversion (%)	Aldehyde Yield (%)[b]	n/iso[c]
1	SemiEsphos	6.0	12.9	2.3	0.4
2	SemiEsphos	3.0	10.2	2.5	0.3
3	ESPHOS[d]	1.5	100.0	34.9	15.9
4	G1-16SemiEsphos	6.0	11.0	6.7	1.5
5	G1-24SemiEsphos	6.0	60.2	42.0	11.6
6	G1-24SemiEsphos	3.0	51.5	48.4	15.5
7	G1-24SemiEsphos	6.0	13.6	9.2	2.1

[a] Catalyst prepared *in situ* from $[Rh(acac)(CO)_2]$ and the phosphine in toluene (4 cm^3) containing vinyl acetate (1 cm^3). P ($CO:H_2$, 1 : 1) = 40 bar. Temp = 80 ºC, t = 20 h.

[b] Yield refers to 2-acetoxypropanal (1-acetoxypropanal decomposes under the reaction conditions to acetic acid and propenal).

[c] Refers to aldehyde formation before aldehyde decomposition/hydrogenation. Determined from the ratio of branched chain product (aldehyde + alcohol) to acetic acid. [d] t = 3 h

The G1-24SemiEsphos, showed more promising results. In this case they postulated that the SemiEsphos molecules are constrained by the dendritic architecture hence possibly leading to a bidentate coordination to rhodium. This would explain the enhanced activity seen for entry 5 where the catalytic behavior slowly starts approaching that of ESPHOS. This is a good demonstration of a synergistic effect between the dendritic architecture and the SemiEsphos moiety.

The aforementioned examples have all demonstrated that these multinuclear transition metallodendrimer catalysts can compete with mononuclear complexes where chemoselectivity and regioselectivity is concerned. Recyclability of the catalyst is still a concern, and even though nanofiltration can be employed in hydroformylation, there is no assurance that the membrane filters can endure the full range of reaction conditions employed. To overcome this problem and to allow for facile separation of catalyst from catalytic products, dendritic ligands can be anchored on solid supports thus heterogenizing the system while ensuring that separate catalytic sites are available.

Alper and co workers investigated the activity of first to fourth generation Rh(I) coordinated diphosphine functionalized PAMAM dendrimers supported on silica (Fig. 1.12) in the hydroformylation reaction. [21] Styrene was employed as one of the substrates.

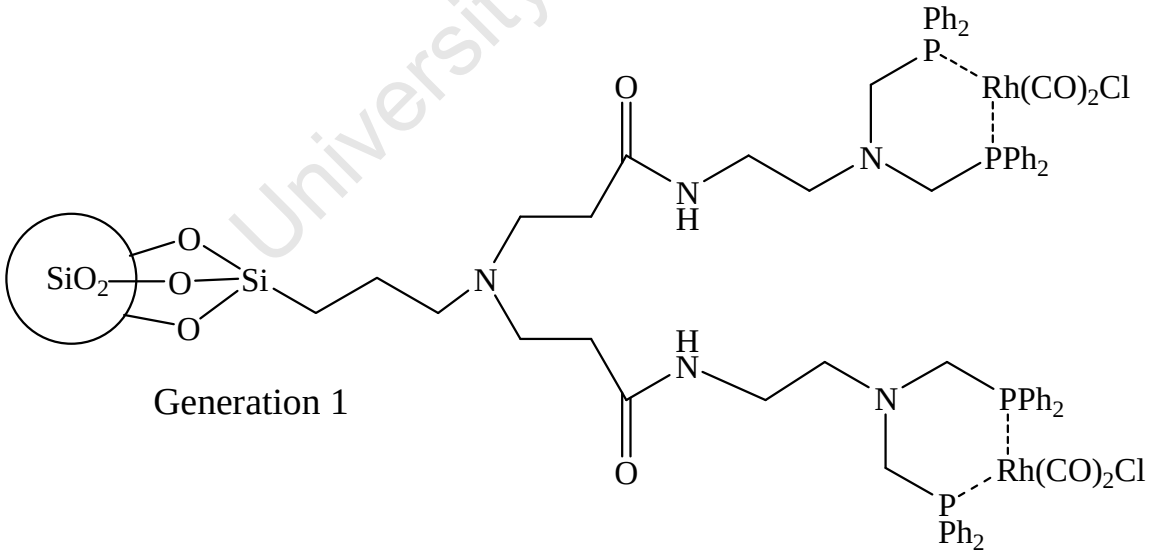

Figure 1.12: First generation Rh(I)-PAMAM metallodendrimer supported on silica.

The catalytic system was prepared by treating the metallodendritic rhodium complex with syngas in a 1:1 $CO:H_2$ ratio. Each catalytic system yielded aldehyde in close to quantitative

yields (Table 1.5, entries 1-9 and 11) but metal leaching was noted for generations 0 to 2, as evident by the yellowing of the reaction mixture. Metal leaching was not as evident in generations 3 and 4. The second generation catalyst was recovered by microporous filtration, washed with distilled hexane and was used 4 times over with no significant loss of activity or selectivity. A further study was conducted to investigate the effect of sterics and flexibility of the dendritic ligand. [47] This was achieved by varying the spacer length within the dendritic arms. They noticed that with an increase in spacer length there is a significant increase in catalytic activity. This is possibly due to better dispersal of the dendritic arms and increased metal complex accessibility.

Table 1.5: Hydroformylation of styrene with various generations of PAMAM dendrimers.[21 a]

Entry	Catalyst generation	Pressure (bar)[b]	Temp (°C)	Conversion (%)[c]	n/iso[d]
1	0	1000	25	98	25
2	1	1000	25	98	27
3	2	1200	75	>99	9
4	2	1000	75	>99[e]	8
5	2	800	75	>99	6
6	2	500	75	>99	3
7	2	1000	65	>99	13
8	2	1000	25	>99	30
9	3	1000	75	>99	8
10	3	1000	25	5	ND[f]
11	4	1000	75	>99	8
12	4	1000	25	2	ND[f]

[a] 2.0 mmol of styrene, 10 cm^3 CH_2Cl_2, 22hrs.
[b] Syngas 1:1 of CO:H_2. Determined by GC.
[d] Determined by ^{1}H NMR.
[e] Catalyst was recovered by microporous filtration, washed with distilled hexanes, and reused four times without significant loss of activity or selectivity.
[f] Not determined.

Lu and co workers [48] immobilized their dendrimer on resin beads to heterogenize it. A rhodium complex was coordinated to these dendrimers functionalized with bidentate diphenylphosphine groups and tested in the hydroformylation of styrene. The catalyst showed a great selectivity for the branched product when employed in styrene hydroformylation, a nearly quantitative conversion of 99% of the substrate to the catalytic product was observed for the majority of the catalytic conditions utilized. The catalyst was recycled more than five times while maintaining this percentage conversion. Recovery was accomplished by simple filtration.

Alper and co-workers, immobilized their dendrimers on a resin solid support as well (Fig 1.13).[49] This was to heterogenize the catalytic system and allow for ease of separation, improved recyclability and to minimize metal leaching. They synthesized two metallodendritic catalysts based on a biomimetic and supported it on resin beads (**1.26** and **1.27**).

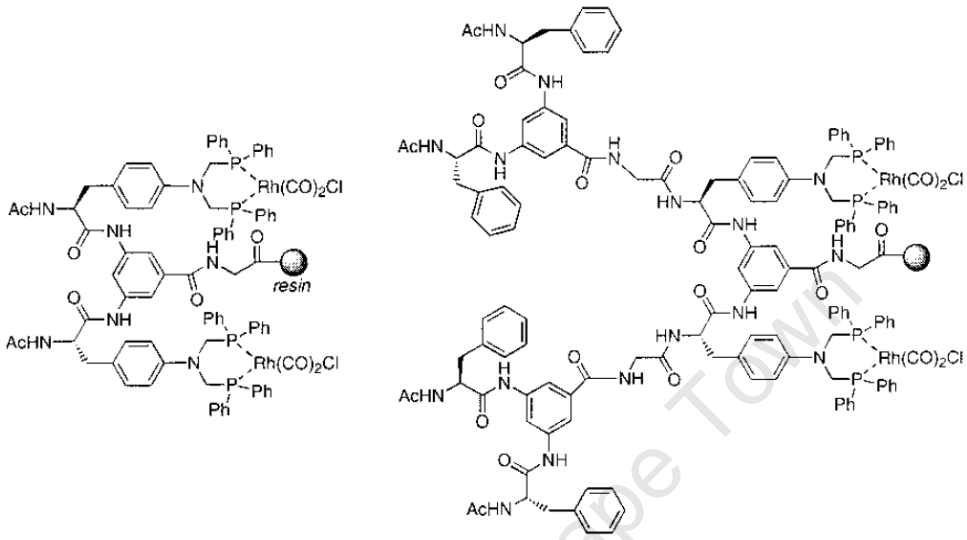

1.26 **1.27**

Figure 1.13: Heterogenized, bivalent dendritic Rh(I) catalysts.

The complexes were tested as catalysts in the hydroformylation of styrene and vinyl acetate. The focus was on decreasing the problem of metal leaching by introducing metal centers along the inner dendritic arms. They proposed that submersion of the metal centers helped preserve the catalytic centers from degradation by the outside catalytic environment.

The catalysts gave high conversions of the substrate and a pronounced selectivity for the branched aldehyde. Both catalysts were recyclable with appreciable catalytic rates even after being re-used for four catalytic cycles. Complex **1.27** showed an improved recyclability compared to that of **1.26**. They proposed that it could be due to the metal centers of **1.27** being more shielded from the reaction environment than that of complex **1.26** as the metal centers are within the branches of the dendrimer.

1.6 Concluding Remarks

Dendrimers are well defined molecules that can be designed to suit the needs of their specific application. Whenever considering the design of a catalyst there are a few factors to consider. These are the activity of the catalyst, selectivity for the desired products, lifetime of the catalyst and recyclability. The use of dendrimers in hydroformylation allows for ease of separation of the catalyst from the catalytic products and increased selectivity of catalytic products. Although not all the factors of a catalyst or the catalytic process are simultaneously positively favored, the flexibility where dendrimer design is concerned allows for the synthesis of more stable architectures and are versatile enough to allow for fine modifications where steric and electronic factors are concerned. Solid supported dendrimers show great promise as good selectivities are retained while separability from the reaction mixture is facilitated. This potential application of dendrimers in catalysis drives the focus of this project.

1.7 Aims and Objectives

1.7.1 Aims:

The project is designed around the preparation of various imino-functionalized dendritic ligands functionalized on the periphery, the coordination of metal complexes to these ligands and the evaluation of the resulting metallodendrimers in the hydroformylation of 1-octene.

1.7.2 Objectives:

The research objectives for this dissertation are:

- The synthesis of iminopyridyl- and iminophosphine-functionalized dendritic ligands with functional groups on the periphery based on the PPI dendritic scaffold (Scheme 1.11).

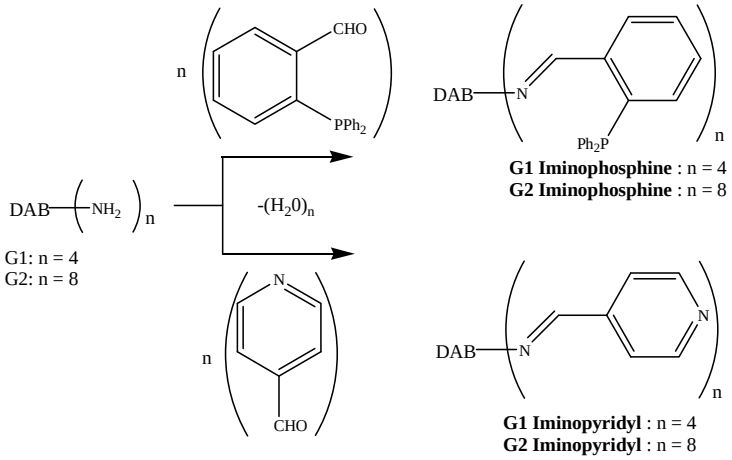

Scheme 1.11

- The synthesis of iminopyridyl (Scheme 1.12) and iminophosphine (Scheme 1.13) rhodium(I) metallodendrimer complexes.

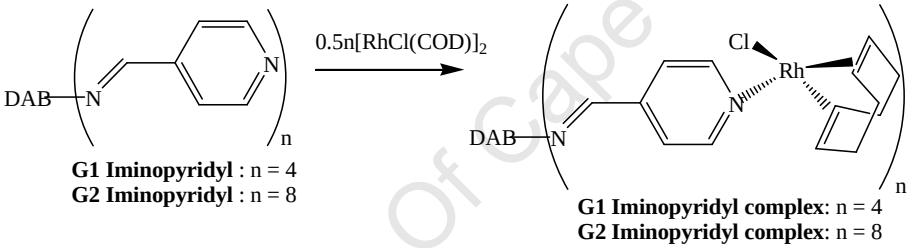

Scheme 1.12

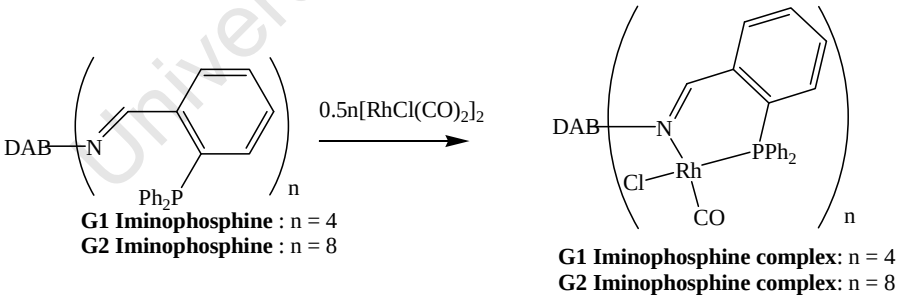

Scheme 1.13

- Evaluation of metallodendrimers as potential catalysts in the hydroformylation of 1-octene (Scheme 1.14).

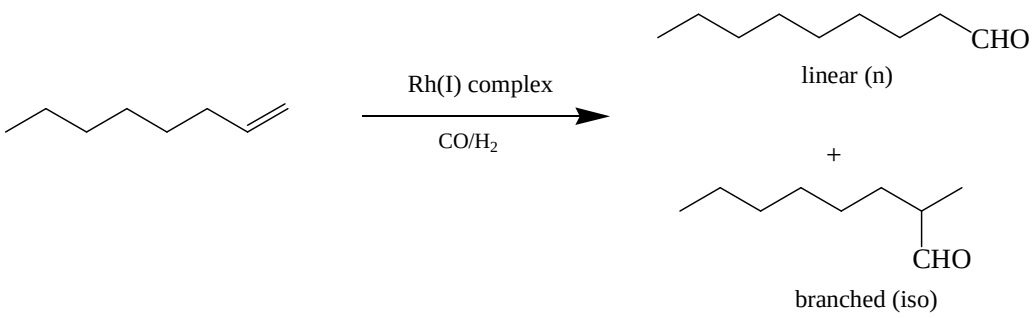

Scheme 1.14

1.8 References

1. U. Boas, J.B. Christensen and P.M.H. Heegard, *J. Mater. Chem.*, **2006**, 16, 3785.
2. D.A. Tomalia, A.M. Naylor and W.A. Goddard III, *Angew. Chem., Int. Ed. Engl.*, **1990**, 29, 138.
3. E. Buhleier, W. Wehner and F. Vögtle, *Synthesis*, **1978**, 155.
4. D.A. Tomalia, J.R. Dewald, M.R. Hall, S.J. Martin and P.B. Smith, *Preprints 1st SPSJ Polym. Conf., Soc. Polym. Sci. Jpn., KyotoI*, **1984**, pp. 65.
5. D.A. Tomalia, H. Baker, J. Dewald, M. Hall, G. Kallos, S. Martin, J. Roeck, J. Ryder and P. Smith, *Polym. J.*, **1985**, 17, 117.
6. M.A. Hearshaw and J.R. Moss, *Chem. Commun.*, **1999**, 1.
7. I. Cuadrado, M. Morán, C. M. Casado, B. Alonzo and J. Losada, *Chem. Rev.*, **1999**, 193-195, 395.
8. D. Méry and D. Astruc, *Coord. Chem. Rev.*, **2006**, 250, 1965.
9. A. Dahan and M. Portnoy, *J. Polym. Sci. Part A: Polym. Chem.*, **2005**, 43, 235.
10. L.J. Twyman and A.S.H. King, *J. Chem. Res. (S)*, **2002**, 43.
11. L. Busetto, M.C. Cassani, P.W.N.M. van Leeuwen and R. Mazzoni, *Dalton Trans.*, **2004**, 2767.
12. P. Govender, N.C. Antonels, J. Mattsson, A.K. Renfrew, P.J. Dyson, J.R. Moss, B. Therrien and G.S. Smith, *J. Organomet. Chem.*, **2009**, 694, 3470.
13. J. Leclaire, R. Dagiral, A. Pla-Quintana, A.M. Caminade and J.P. Majoral, *Eur. J. Inorg. Chem.*, **2007**, 2890.
14. D.L. Stone, D.K. Smith and P.T. McGrail, *J. Am. Chem. Soc.*, **2002**, 5, 856.
15. K. Onitsuka, A. Iuchi, M. Fujimoto and S. Takahashi, *Chem. Commun.*, **2001**, 741.
16. A.M. McDonagh, C.E. Powell, J.P. Morrall, M.P. Cifuentes and M.G. Humphrey, *Organometallics*, **2003**, 22, 1402.
17. M.G. Humphrey, C.E. Powell, M.P. Cifuentes, J.P. Morrall and M. Samoc, *Pol. Preprints*, **2004**, 45, 367.
18. J.K. MacDougall, M.C. Simpson, M.J. Green and D.J. Cole-Hamilton, *J. Chem. Soc., Dalton Trans.*, **1996**, 1161.
19. J.P. Rieu, A. Boucherle, H. Cousse and G. Mouzin, *Tetrahedron*, **1986**, 42, 4095.
20. A.J. Lewis and D.E. Furst, *Nonsteroidal Antiinflammatory Drugs: mechanisms and clinical uses*, 2nd edn., Marcel Dekker, Inc, New York, 1994.

21. S.C. Bourque, F. Maltais, W.J. Xiao, O. Tardif, H. Alper, P. Arya and L.E. Manzer, *J. Am. Chem. Soc.*, **1999**, 121, 3035.
22. G.W. Parshall and S.D. Ittel, *Homogeneous Catalysis The Applications and Chemistry of Catalysis by Soluble Transition Metal Complexes*, 2nd edn., Wiley- Interscience, Canada, 1992.
23. C. Masters, *Homogeneous Transition-metal Catalysis*, Chapman and Hall, London, 1981.
24. A. Oswald, D.E. Hendrikse, R.V. Kastrup, K. Irikura, E.M. Mozeleski and D.A. Young, *Phosphorus and Sulfur*, **1987**, 30, 237.
25. A.A. Oswald, J.S. Merola, E.J. Mozeleski, R.V. Kastrup and J.C. Reisch, *Adv. Chem. Ser.*, **1981**, 104, 503.
26. A. Buhling, P.C.J. Kamer and P.W.N.M. van Leeuwen, *J. Mol. Catal. A: Chem*, **1996**, 98, 69.
27. W.R. Moser, C.J. Papite, D.A. Brannon, R.A. Duwell and S.J. Weininger, *J. Mol. Catal.*, **1987**, 41, 271.
28. J.D. Unruh and J.R. Christenson, *J. Mol. Catal.*, **1982**, 14, 19.
29. P.W.N.M van Leeuwen and C.F. Roobeek, *J. Organomet. Chem.*, **1983**, 258, 343.
30. D. Astruc and F. Chardac, *Chem. Rev.*, **2001**, 101, 2991.
31. D. Astruc, E. Boisselier and C. Ornelas, *Chem. Rev.*, **2010**, 110, 1857.
32. D. de Groot, E.B. Eggeling, J.C. de Wilde, H. Kooijman, R.J. van Haaren, A.W. van der Made, A.L. Spek, D. Vogt, J.N.H. Reek, P.C.J. Kamer and P.W.N.M. van Leeuwen, *Chem. Commun.*, **1999**, 1623.
33. A. Corma and H. Garcia, *Top. Catal.*, **2008**, 48, 8.
34. V. Maraval, R. Laurent, A.M. Caminade and J.P. Marjoral, *Organometallics*, **2000**, 19, 4025.
35. L. Ropartz, R.E. Morris, D.F. Foster and D.J. Cole-Hamilton, *Chem. Commun.*, **2001**, 361.
36. A.W. Kleij, R.A. Gossage, J.T.B.H. Jastrzebski, J. Boersma and G. van Koten, *Angew. Chem., Int. Ed.*, **2000**, 39, 176.
37. M. Slany, M. Bardaji, A.M. Caminade, B. Chaudret and J.P. Majoral, *Inorg. Chem.*, **1997**, 36, 1939.
38. M.T. Reetz, G. Lohmer and R. Schwickardi, *Angew. Chem., Int. Ed. Engl.*, **1997**, 36, 1526.
39. M.T. Reetz, G. Lohmer and R. Schwickardi, *Angew. Chem.*, **1997**, 109, 1559.

40. L. Ropartz, R.E. Morris, D.F. Foster and D.J. Cole-Hamilton, *J. Mol. Catal. A: Chem.*, **2002**, 182–183, 99.
41. L. Ropartz, K.J. Haxton, D.F. Foster, R.E. Morris, A.M.Z. Slawin and D.J. Cole-Hamilton, *J. Chem. Soc., Dalton Trans.*, **2002**, 4323.
42. A. Gong, Q. Fan, Y. Chen, H. Liu, C. Chen and F. Xi, *J. Mol. Catal. A: Chem.*, **2000**, 159, 225.
43. Y. Huang, H. Zhanga, G. Dengb, W. Tanga, X. Wanga, Y. Heb and Q. Fan, *J. Mol. Catal. A: Chem.*, **2005**, 227, 91.
44. G.E. Oosterom, S. Steffens, J.N.H. Reek, P.C.J. Kamer and P.W.N.M. van Leeuwen, *Top. Catal.*, **2002**, 19, 61.
45. S. Breeden, D.J. Cole-Hamilton, D.F. Foster, G.J. Schwarz and M. Wills, *Angew. Chem., Int. Ed.*, **2000**, 39, 4106.
46. N.R. Vautravers and D.J. Cole-Hamilton, *Chem. Commun.*, **2009**, 92.
47. S.C. Bourque, H. Alper, L.E. Manzer and P. Arya, *J. Am. Chem. Soc.*, **2000**, 122, 956.
48. S.M. Lu and H. Alper, *J. Am. Chem. Soc.*, **2003**, 125, 13126.
49. P. Arya, G. Panda, N.V. Rao, H. Alper and L.E. Menzer, *J. Am. Chem. Soc.*, **2001**, 123, 2889.

Chapter 2

Synthesis and Characterization of Iminophosphine and Iminopyridyl Dendritic Ligands and their Rhodium(I) Complexes

2.1 Introduction

Various dendritic scaffolds have been synthesized and described extensively in the literature, with some of the more commonly used scaffolds being the polyamidoamines (PAMAM)[1], polybenzyl ethers (Fréchet-type)[2], polycarbosilanes[3], polyhedral oligomeric silsesquioxanes (POSS)[4] and more specific to this project, the poly(propyleneimine) (PPI)[5] scaffold. Numerous reviews have been written surrounding the employment of dendrimers in catalytic reactions and various other applications. [6-11] A few of the applications include catalyst supports,[12-14] Magnetic Resonance Imaging (MRI) contrast agents,[15] DNA intercalation compounds[16] and drug delivery systems. [17, 18] Dendrimers therefore show great versatility in various applications.

Dendrimers vary in the degree of sizes depending on the generation and this could also aid in catalyst recovery by nanofiltration should the dendrimers act as a suitable support for a transition metal catalyst precursor.[19] As demonstrated in the previous chapter, not only does the use of dendritic supports allow for ease of separation but they can also affect the selectivity for specific catalytic products when employed as transition metal catalyst supports. The dendritic system employed in this research is the DAB poly(propyleneimine) dendrimer, one of the first types of dendrimers initially designed by Vögtle, with a 1,4-diaminobutyl core and polypropylamine side chains.[20] The amine termini can be further functionalized by employing Schiff-base and amide chemistry as examples.

An example of a functionalized dendritic ligand is the dendritic phosphine synthesized by Reetz and co-workers.[21] Catsoulacos and co-workers[22] pursued the synthesis of iminophosphine functionalized dendrimers. Their methodology was used for the iminophosphine functionalized dendrimers discussed in this chapter. Additionally, iminopyridyl functionalized ligands were prepared [23] as well as the rhodium complexes of these imino-functionalized dendrimers. This chapter fully discusses the synthesis and characterization of these iminopyridyl- and iminophosphine-functionalized ligands and their respective Rh(I) complexes.

2.2 Synthesis and characterization of the iminophosphine ligands and their rhodium(I) complexes

Bidentate ligands with "hard" and "soft" donor groups have been the subject of great interest.[24-27] P-N heterobidentate ligands are one of the common ligands used and combine the soft donor ability of phosphorous that can bind strongly to a soft metal centre such as palladium and the hard donor ability of the nitrogen that can be weakly bound. This combination of soft donor, hard donor properties is known as hemilability. There are not many examples of heterobidentate P-N metallodendritic complexes. These hemilabile ligands can have potential advantages when employed as ligands in catalysis.

2.2.1 Synthesis of the mono- and multimeric iminophosphine ligands

The known compound, **2.1**, was synthesized using a method adapted from Ghilardi and co-workers (Scheme 2.1). [28] This monomeric analogue was synthesized to assist with characterization of the more complex dendritic system. The synthesis involves a Schiff-base condensation reaction between 2-(diphenylphosphino)benzaldehyde and a slight excess of propylamine. The authors suggest removal of excess propylamine by distillation but compound **2.1** was purified by first removing the solvent and then washing the residual orange oil with water to remove any traces of water-soluble propylamine.

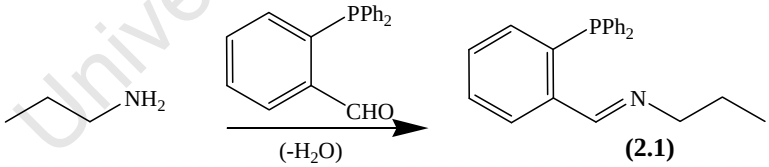

Scheme 2.1

The new first-generation iminophosphine dendrimer, compound **2.2**, was synthesized by reacting 2-(diphenylphosphino)benzaldehyde with the first-generation DAB dendrimer in a 4:1 ratio (Scheme 2.2) in an ethanol/dichloromethane (50:50, v/v%) solution for 48 hours at room temperature. [29] Anhydrous magnesium sulphate was added to remove water generated during the reaction. The extended reaction time is needed to ensure full functionalization of the amine termini on the dendrimer.

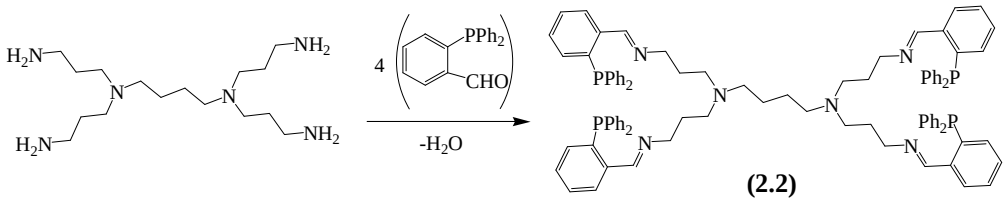

Scheme 2.2

According to Catsoulacos and co-workers, this solvent combination provides better yields than either solvent on its own. This could be due to a solvent effect as was investigated by Chai and co-workers where various solvents affect the molecular structure of DAB differently. [30] It was proposed that due to the presence of ethanol, there is better solvent inter-penetration between the dendritic arms due to hydrogen bonding between solvent and amine groups of the dendrimer. This helps minimize the dendritic arm backfolding and hence allows exposure of the terminal amines for Schiff-base reaction with 2-(diphenylphosphino)benzaldehyde. Dichloromethane is added to aid the solubility of the resulting dendritic ligand which is poorly soluble in pure ethanol. The new second-generation iminophosphine dendrimer, **2.3**, (Scheme 2.3) was synthesized in a similar manner to the first-generation iminophosphine functionalized dendrimer.

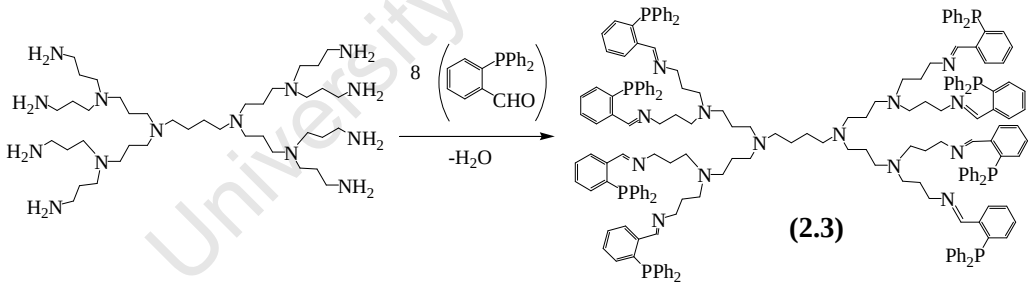

Scheme 2.3

2.2.2 Spectroscopic and analytical data of the mono- and multimeric iminophosphine ligands

Infrared Spectral Analysis

Infrared spectra for compounds **2.1-2.3** were recorded to further confirm the Schiff-base condensation and hence formation of the imine bond. All spectra were obtained as solutions

in dichloromethane. The typical stretching frequencies for the C=N double bond of an imine occurs in the range 1590-1660 cm^{-1}. The imine absorption is seen as a band of medium intensity at 1637 cm^{-1} for compounds **2.1-2.3**, confirming formation of the imine bond.

^{1}H NMR Spectral Analysis

The ^{1}H NMR spectra consist of two distinct regions in which the resonance peaks occur for these ligands, δ 0.76-3.45 ppm and δ 6.85-8.89 ppm. The region δ 0.76-3.45 ppm contains a set of resonances for the protons of the dendritic core and aliphatic side chains.

The ^{1}H NMR spectral characterization for the model monomeric ligand, **2.1**, assisted in the interpretation of the more complex spectra for the dendritic ligands **2.2** and **2.3**. The alkyl side chain of the monomeric ligand analogue, **2.1**, has a triplet resonance peak at δ 0.76 ppm for the terminal methyl protons ($CH_2C\underline{H}_3$), a sextet at δ 1.55 ppm for the protons of the secondary carbon ($C\underline{H}_2CH_3$), and a triplet at δ 3.45 ppm for the protons on the carbon adjacent to the imine nitrogen ($NC\underline{H}_2$). The resonance peaks for the aromatic protons occur as multiplets at δ 6.89 ppm, δ 7.34 ppm and δ 7.99 ppm. The doublet observed at δ 8.89 ppm corresponds to the methine proton coupling to phosphorous and has a $^{4}J_{PH}$ = 4.5 Hz that agrees well with literature. [31-33]

The peaks for the dendritic core and side arm protons of compound **2.2** occur in the range δ 1.29-3.44 ppm. The diaminobutane core proton resonances for **2.2** appear as a set of broad singlets at δ 1.29 ppm ($N(CH_2)_2C\underline{H}_2CH_2N$) and δ 2.28 ppm ($NCH_2(CH_2)_2C\underline{H}_2N$). The resonances for the aliphatic protons of the side arms of the dendritic ligand occur at δ 1.59 ppm for ($C\underline{H}_2CH_2NCH$) and δ 2.28 ppm for ($C\underline{H}_2CH_2CH_2NCH$) where the latter resonance overlaps with the resonance for the DAB core protons previously discussed. This data is similar to ^{1}H NMR spectroscopic data from another study investigating this scaffold.[5]

The peaks for the aliphatic protons of the dendritic ligands show considerable peak broadening due to the degrees of freedom they possess. [10] The aliphatic resonance peak for the carbon adjacent to the imine nitrogen, ($C\underline{H}_2NCH$), occurs at δ 3.44 ppm. This is a downfield shift in resonance frequency from δ 2.70 ppm when compared to that of the DAB

dendrimer prior to functionalization and serves to confirm formation of the imine bond during the Schiff base condensation reaction. The observed downfield shift is due to the electron withdrawing effect of the imine bond deshielding the respective protons. The aromatic protons for **2.2** show resonances peaks similar to that of the mononuclear complex.

In the case of compound **2.3**, the splitting patterns are similar to that of compound **2.2**. There is considerable broadening of the resonance peaks more than the first-generation due to the increased complexity of the scaffold and degrees of freedom of the dendritic arms. The resonance peaks for the aliphatic protons occur in the range δ 1.55 ppm – δ 3.42 ppm and that of the aromatic peaks in the range δ 6.85 ppm – δ 7.94 ppm. The resonance peak for the imine proton occurs as a doublet with a ^{4}J-coupling constant of 4.5 Hz indicative of coupling of phosphorous to the imine proton. [33]

^{13}C NMR Spectral Analysis

The proton-decoupled ^{13}C NMR spectra were recorded in $CDCl_3$ for both mononuclear and dendritic ligands. The spectral data were used to confirm the desired compounds by noting the characteristic resonance for the imine carbon and by the number of signals that correspond with the various carbon atoms.

Compounds **2.2** and **2.3** show resonance signals in the range of δ 23.7 – 59.6 ppm for the aliphatic carbons, $\underline{C}H_2$, of the diaminobutane core and propyl chains within the dendritic side arms. Due to the higher generation of **2.3**, there is a higher number of resonance peaks when compared to **2.2**. A series of resonance peaks occur in the range, δ 126.7 – 139.8 ppm for both **2.2** and **2.3** and these are assigned to the carbons of the aromatic rings. The methine carbon has a resonance peak at δ 159.4 ppm and δ 158.2 ppm for **2.2** and **2.3** respectively. Both resonance peaks are doublets with a ^{3}J-value of 20.7 Hz ascribed to coupling of phosphorous to carbon. [31-33]

^{31}P NMR Spectral Analysis

^{31}P NMR spectroscopy was used to further confirm that compounds **2.1**-**2.3** had formed. This is noted in a downfield shift of the singlet resonance peak for the phosphorous of 2-(diphenylphosphino)benzaldehyde at δ -11.45 ppm to δ -13.45 ppm for the Schiff-base product.

Elemental Analysis

Elemental analysis was conducted on compounds **2.2** and **2.3**. Due to the architecture of this dendrimer there is a possibility for solvent inclusion and this can be seen in the ^{1}H NMR as a DCM peak for each compound. This has been seen for other PPI dendrimers functionalized at the periphery. [34] Elemental analysis values re-calculated with DCM solvent inclusion gave values that correlate with those found experimentally.

Mass Spectrometry

The first-generation iminophosphine dendritic ligand **2.2**, was analyzed using ESI mass spectrometry in the positive ion mode. The compound shows a doubly charged molecular ion at m/z 703. The second-generation iminophosphine ligand, **2.3**, was analyzed using (MALDI-TOF) mass spectrometry that shows a peak for the molecular ion at m/z 2952.

2.2.3 Reactions of the iminophosphine ligands with $[RhCl(CO)_2]_2$

The chelating hetero-bidentate (P,N) iminophosphine rhodium(I) complexes **2.4**, **2.5** and **2.6** (Schemes 2.4 - 2.6) were synthesized by syringing a tetrahydrofuran (THF) solution of the iminophosphine ligand into a stirring THF solution of the rhodium complex, $[RhCl(CO)_2]_2$. [29] Compound **2.4** precipitates as an orange solid in a moderate yield of 54%.

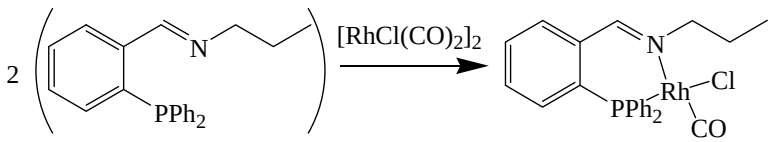

(2.4)

Scheme 2.4

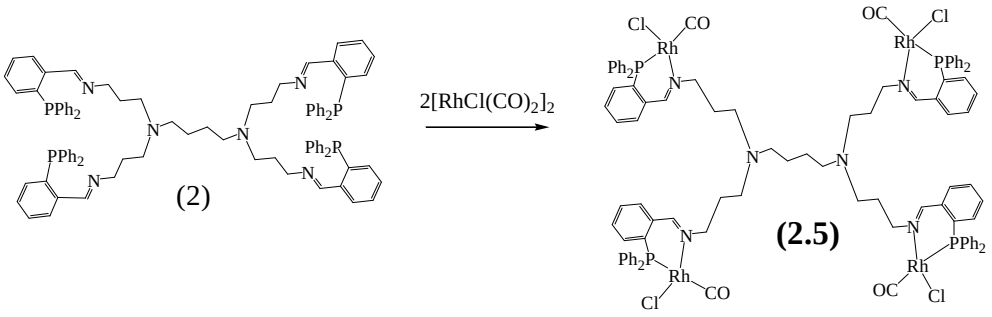

Scheme 2.5

In the case of the dendritic complexes, **2.5** and **2.6** the solvent was reduced *in vacuo* to half its original volume and the dendritic complexes precipitated as orange and yellow-brown solids by the addition of *n*-pentane in moderate to good yields of (63%-88%).

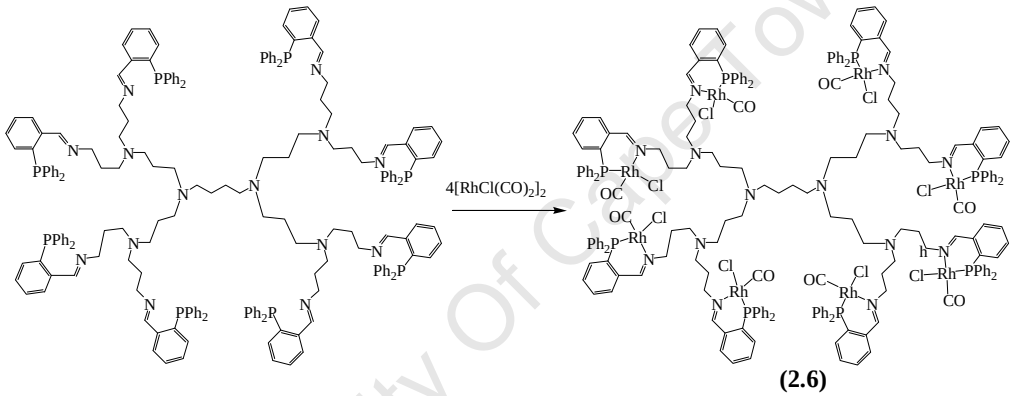

Scheme 2.6

2.2.4 Spectroscopic and analytical data of the mono- and multimeric iminophosphine Rh(I) complexes

Infrared Spectral Analysis

The iminophosphine ligand, compound **2.4** acts as a chelating ligand when complexed to a rhodium metal centre. A weak to medium intensity band can be seen at approximately 1628 cm^{-1} belonging to the imine C=N double bond stretching vibrations. Coordination of the imine nitrogen to the rhodium metal centre is confirmed by a shift from 1637 cm^{-1} for the free ligand to 1628 cm^{-1} for the complex. This decrease in stretching frequency is due to sigma donation of electrons on the imine nitrogen to the rhodium centre and hence slight loss in the double bond character of the imine bond. The infrared spectral data for this model

compound is similar to that obtained for **2.5** and **2.6** despite the latter two being multinuclear complexes. A single strong carbonyl (C=O) absorption band at 2000 cm^{-1} for **2.4** was also noted and confirms the formation of one preferred isomer. The dendritic complexes **2.5** and **2.6** show strong intensity bands at 2001 cm^{-1} and 1995 cm^{-1} for the carbonyl ligand respectively.

^{1}H NMR Spectral Analysis

The mononuclear Rh(I) complex **2.4**, and multinuclear Rh(I) complexes **2.5** and **2.6** were characterized using ^{1}H NMR spectroscopy. The data obtained helps to confirm that the organic framework of both the mononuclear and multinuclear complexes are intact, and that there is coordination of the imine nitrogen to rhodium.

Coordination of the imine nitrogen to the Rh(I) complex is confirmed by the shifting of two resonance peaks upon coordination, one for the methine proton and the other for the two protons on the propyl chain carbon adjacent to the imine nitrogen. The resonance peak of the methine proton therefore shows an upfield shift from δ 8.89 ppm for the free ligand, **2.1**, to δ 7.93 ppm for the complex, **2.4**. The protons on the carbon adjacent to the imine nitrogen show a downfield shift from δ 3.45 ppm to δ 4.11 ppm clearly indicating a movement of electron density from the imine nitrogen to the rhodium metal centre and hence deshielding of these protons.

The dendritic complexes **2.5** and **2.6** showed the same shift of the resonance peaks for protons on either carbon adjacent to the imine nitrogen. For the methine proton, there is an upfield shift from δ 8.85 ppm to δ 8.49 ppm for compound **2.5** and from δ 8.84 ppm to δ 8.54 ppm for compound **2.6** upon coordination. For the protons of the propyl arm carbon adjacent to the imine nitrogen, these show a downfield shift from δ 3.44 ppm to δ 4.07 ppm for **2.5** and from δ 3.42 ppm to δ 4.11 ppm for **2.6** upon coordination.

The aliphatic protons of the dendritic scaffold are observed as a set of broad peaks from δ 1.45 ppm – δ 2.27 ppm for **2.5** and δ 1.64 ppm – δ 2.35 ppm for **2.6**. The resonance peaks for the aromatic protons occur as sets of multiplets in the ranges δ 6.82 ppm – δ 7.91 ppm for **2.5** and δ 8.84 ppm – δ 8.54 ppm for **2.6**.

^{13}C NMR Spectral Analysis

Complex **2.4** shows three signals in the region δ 10.8 – 66.9 ppm which belong to the aliphatic protons of the propyl side chain of the ligand. Resonances for the aromatic protons are observed in the range, δ 128.8 – 135.4 ppm with J_{PC} values from 24 – 36 Hz. The singlet for the imine carbon appears at δ 163.8 ppm. The carbonyl peak appears at δ 189.5 ppm as a doublet of doublets with $^{2}J_{PC}$ = 17.0 Hz and $^{1}J_{RhC}$ = 72.0 Hz. These coupling constants are in agreement with a carbonyl carbon being *trans* to the imine nitrogen in the complex. [33]

The dendritic complexes **2.5** and **2.6** show a more complex resonance peak pattern in the aliphatic region δ 22.4 ppm – δ 62.0 ppm to account for the dendritic scaffold. The aromatic carbons can be seen as a set of resonance peaks in the region δ 125.6 - δ 136.6 ppm. Coordination of nitrogen is confirmed by a downfield shift in the resonance peaks for the carbons adjacent to the imine nitrogen upon coordination to rhodium. The resonance peak for the methine carbon shows a downfield shift from δ 159.4 ppm to δ 167.1 ppm for **2.5** and from δ 158.2 ppm to δ 166.2 ppm for **2.6**. The carbon adjacent to the imine nitrogen from the dendritic propyl scaffold shows a downfield shift from δ 59.6 ppm to δ 68.2 ppm for **2.5** and δ 58.6 ppm to δ 62.1 ppm for **2.6**. A doublet of doublets is seen for the carbonyl of both **2.5** and **2.6** at δ 189.4 ppm and δ 190.0 ppm respectively. The doublet of doublets for the carbonyl carbons of complexes **2.5** ($^{2}J_{PC}$ = 17.0 Hz and $^{1}J_{RhC}$ = 72.0 Hz) and **2.6** ($^{2}J_{PC}$ = 17.0 Hz and $^{1}J_{RhC}$ = 72.0 Hz) show the same coupling constants to that of complex **2.4** and confirm that the carbonyl is *trans* to the imine nitrogen. [33]

^{31}P NMR Spectral Analysis

^{31}P NMR spectroscopy was used to further confirm coordination of phosphorous to rhodium. This is noted in a downfield shift of the ligand's phosphorous resonance peak from δ -13.45 ppm to approximately δ 49 ppm. The resonance peak observed in the ^{31}P NMR spectrum is a

doublet with a coupling constant of approximately $^{1}J_{RhP}$ = 160 Hz, consistent with rhodium coupling to phosphorous.[33] This shift in resonance peak along with spectroscopic evidence of imine nitrogen coordination confirms the coordination of the ligand to the Rh(I) metal center in a hetero-bidentate manner and hence formation of a chelate complex.

Elemental Analysis

The elemental analysis results for compound **2.4** are in agreement with those calculated for the compound. For the dendritic complexes **2.5** and **2.6**, similar to that of their respective ligands, there are solvent molecules encapsulated in the dendritic scaffold (DCM resonsance peak observed in ^{1}H NMR spectra). The observed and calculated elemental analysis data agrees once this inclusion is taken into account.

Mass Spectrometry

The mass spectrum for complex **2.4** was recorded using EI-mass spectrometry run in the positive mode and shows a molecular ion peak at m/z 497 that corresponds to the calculated molecular mass of 497.77 g.mol^{-1}. The mass spectral data for complex **2.5** was collected using ESI-mass spectrometry in the positive mode. The compound shows a doubly charged molecular ion peak at m/z 1038.

X-ray Molecular Structure

Single crystals of compound **2.4** were grown by layering *n*-pentane on a DCM solution of **2.4**. Table 2.1 details the crystallographic data for the molecular structure obtained while Table 2.2 lists selected bond lengths and angles. Complex **2.4** was crystallized in the triclinic system and space group P1. The molecular structure of the complex (Figure 2.1) shows the iminophosphine ligand coordinating to the rhodium metal center in a heterobidentate coordination mode thus forming a six-membered chelate ring. The geometry surrounding rhodium is square-planar with the carbonyl ligand trans to the imine nitrogen and chloride ligand *trans* to phosphorus.

Table 2.1: Crystallographic data for complex **2.4**

Empirical formula	$C_{23}H_{22}NPORhCl$
Empirical weight	497.75
Crystal size	0.15 x 0.14 x 0.10 mm
Crystal system, space group	triclinic, P1 (No. 2)
a	8.7765(12) Å
b	10.2179(16) Å
c	13.180(2) Å
alpha	109.904(18)º
beta	101.832(18)º
gamma	13.180(2)º
Volume	1083.0(3) $Å^3$
Z	2
Calculated density	1.526 $g.cm^{-3}$
F(000)	504.0
R indices (all data)	R = 0.0697, wR2 = 0.2568

Bite angles and other geometrical parameters around the rhodium atom correspond to those of similar compounds. [35-37] The bond lengths for the bonds Rh-P and Rh-N are 2.188(4) Å and 2.118(11) Å respectively. The Rh-C(23) bond length measures at 1.806(14) Å. This short bond length is due to π-back-bonding from the rhodium metal centre to the carbonyl carbon antibonding orbitals causing a stronger Rh-C bond.

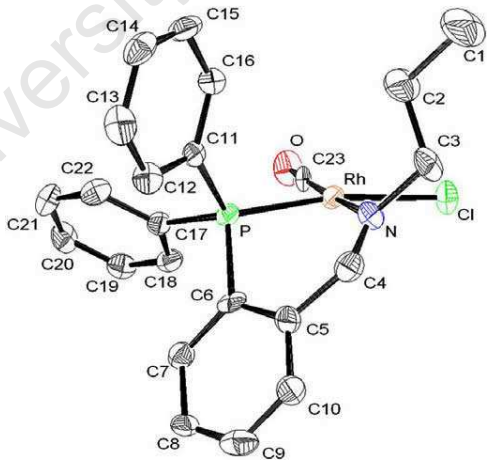

Figure 2.1: Molecular structure of **2.4** showing ellipsoids at the 50% probability level with hydrogen atoms omitted for clarity.

Table 2.2: Selected bond lengths and angles for complex **2.4**

Rh–P	2.188(4) Å
Rh–Cl	2.394(4) Å
Rh–N	2.118(11) Å
Rh–C(23)	1.806(14) Å
N–C(4)	1.284(16) Å
N–C(3)	1.468(15) Å
P–Rh–Cl	170.60(11)º
P–Rh–N	86.1(3) º
P–Rh–C(23)	93.7(4) º
Cl–Rh–N	90.0(3) º
Cl–Rh–C(23)	90.6(4) º
N–Rh–C(23)	177.1(5) º
C(3)–N–C(4)	116.9(11) º

The six-membered ring formed causes a slight distortion in the geometry surrounding the rhodium metal center. The P-Rh-Cl angle [170.60(11)°] is smaller than the expected value 180º and is most likely due to the strain from the six-membered chelate ring. There is essentially a co-planar geometry between Rh, Cl, N, C(23) and O with a slight deviation of 0.0218 Å from the mean plane with the P atom 0.39(1) Å away from the plane.

2.3 Synthesis and characterization of the iminopyridyl ligands and their Rh(I) complexes

2.3.1 Synthesis of the mono- and multimeric iminopyridyl ligands

The known compound **2.7** was synthesized by reacting 4-pyridinecarboxaldehyde with an excess of propylamine (Scheme 2.7). [23] This afforded a yellow-orange oil in a moderate yield of 52%, most likely due to some loss of the product during copious washings with water during purification.

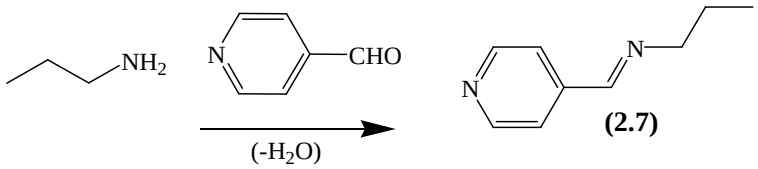

Scheme 2.7

The first-generation iminopyridyl functionalized dendrimer, compound **2.8** was synthesized by reacting the first-generation DAB dendrimer with 4-pyridinecarboxaldehyde in a 1:4 ratio, using a slight excess of the aldehyde (Scheme 2.8). [23] Reaction time was increased to 48 hours to ensure full functionalization of the dendrimers.

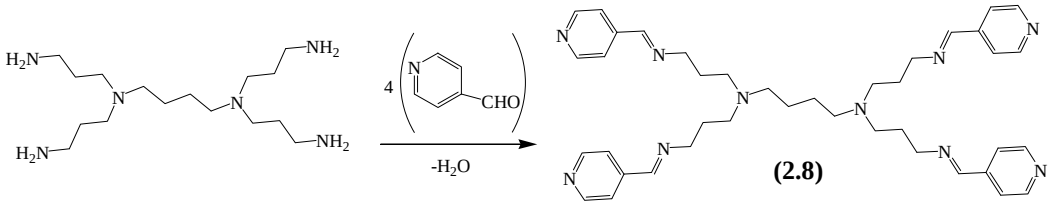

Scheme 2.8

The purification of **2.8** was achieved in a similar manner to compound **2.7**. Compound **2.8** was obtained as a yellow oil in a moderate yield of 51%. Compound **2.9** (Scheme 2.9) was synthesized in the same manner but reaction time was increased to 72 hours to account for the increase in terminal amine sites available for functionalization. Compound **2.9** was obtained as an orange oil in a good yield of 76%.

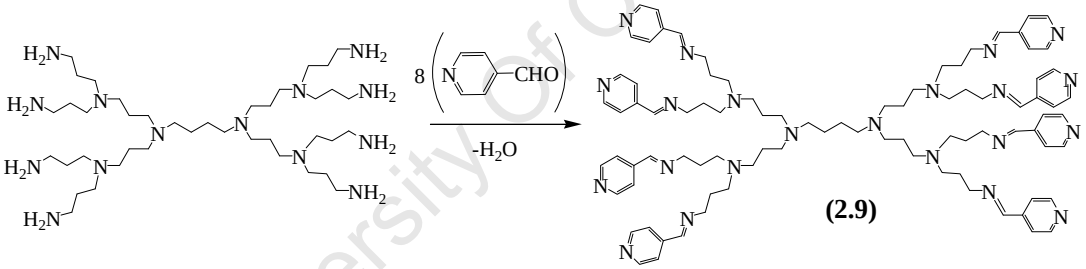

Scheme 2.9

2.3.2 Spectroscopic and analytical data of the mono- and multimeric iminopyridyl ligands.

Infrared Spectral Analysis

The imine C=N double bond occurs as a strong absorption band at 1647 cm^{-1} for compounds **2.7-2.9**. In addition, there is a medium intensity band at approximately 1598 cm^{-1} for the C=N double bond of the pyridyl ring. The presence of the peak at 1647 cm^{-1} serves to confirm the Schiff-base condensation reaction and the formation of the imine bond.

^{1}H NMR Spectral Analysis

The region δ 0.95-3.63 ppm contains a set of resonances for the aliphatic protons in the propyl chain of compound **2.7**. The alkyl side chain of the monomeric ligand analogue, **2.7**, has a resonance peak at δ 0.95 ppm for the terminal methyl protons ($CH_2C\underline{H}_3$), δ 1.73 ppm for the protons of the secondary carbon ($C\underline{H}_2CH_3$), and a triplet at δ 3.61 ppm for the protons on the carbon adjacent to the imine nitrogen ($NC\underline{H}_2$). The methine and aromatic protons appear as a set of three resonance peaks. The resonance peak at δ 7.57 ppm is a doublet for the proton on the carbon *meta* to the pyridyl nitrogen, (NCHC$\underline{H}$C), and the resonance peak at δ 8.66 ppm for the proton on the carbon *ortho* to the pyridyl nitrogen, (NC$\underline{H}$CHC). Splitting is due to the protons coupling to each other. The methine proton resonance peak occurs as a singlet at δ 8.24 ppm.

The peaks for the dendritic core and side arm protons of compounds **2.8** and **2.9** occur in the range δ 1.39-3.63 ppm. Peak broadening occurs for this system as for the iminophosphine dendrimers. The aromatic resonances occur as doublets at, δ 7.52 ppm and δ 8.63 ppm. The singlet at δ 8.25 ppm is that of the methine proton, (NC$\underline{H}$C) further confirming formation of the imine bond. Similarly, compound **2.9** has the same distribution of resonance peaks as these two compounds are similar despite their difference in generation.

^{13}C NMR Spectral Analysis

The proton-decoupled ^{13}C NMR spectra were recorded in $CDCl_3$ for both mononuclear (**2.7**) and dendritic ligands (**2.8** and **2.9**). The spectral data was used to confirm the structural integrity of the ligand as well as the formation of the imine bond. Compound **2.7** shows seven peaks with three in the range δ 11.8-63.6 ppm assigned to the carbons of the propyl side chain, $N\underline{C}H_2\underline{C}H_2\underline{C}H_3$. Four resonance peaks occur in the range δ 121.9-158.8 ppm for the aromatic and methine carbon of **2.7**. The inductive effect of the pyridyl ring conjugated with the imine nitrogen causes the methine carbon to have the most downfield resonance peak at δ 158.8 ppm.

Compounds **2.8** and **2.9** show signals in the range of δ 24.8 – 59.8 ppm for the aliphatic carbons, $\underline{C}H_2$, of the diaminobutane core and propyl chains within the dendritic side arms.

Due to the higher generation of **2.9**, there is a larger number of resonance peaks when compared to **2.8**. The aromatic region, δ 121.7 – 150.4 ppm for both **2.8** and **2.9** shows three signals at roughly the same shift. The methine carbon resonance peak appears at approximately δ 159.0 ppm.

Elemental Analysis

The elemental analyses for compounds **2.8** and **2.9** were obtained. Both compounds are oils and were dried for 24 hours. As for the iminophosphine ligands, these ligands trap DCM as well. The calculated values include solvent encapsulation (DCM solvent resonance peak observed in ^{1}H NMR spectra) within the dendritic arms and agree with the observed values for the elemental analyses.

Mass Spectrometry

The mass spectrum for complex **2.8** was recorded using MALDI-TOF mass spectrometry and shows a molecular ion peak at m/z 673 that corresponds to the calculated molecular mass of 672.95 g.mol^{-1}.

2.3.3 Reactions of the iminopyridyl ligands with $[RhCl(COD)]_2$

The iminopyridyl ligands were reacted with the Rh(I) metal complex precursor $[RhCl(COD)]_2$ in the appropriate stoichiometric ratios (Scheme 2.10-2.12) similar to a method used by Rajput and co-workers.[38] The respective ligand was therefore dissolved in dichloromethane and syringed into a stirring solution of $[RhCl(COD)]_2$ to afford the mononuclear complex **2.10** or dendritic complexes **2.11** and **2.12**. The complexes were all obtained as yellow solids where complex **2.10** was isolated in a moderate yield of 58%, whilst both dendritic complexes **2.11** and **2.12** were obtained in good yields of 70% and 74% respectively.

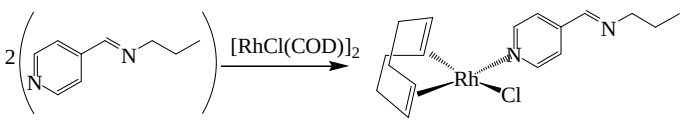

(2.10)

Scheme 2.10

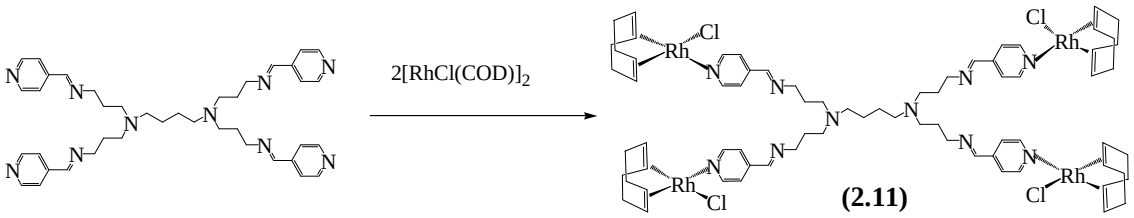

Scheme 2.11

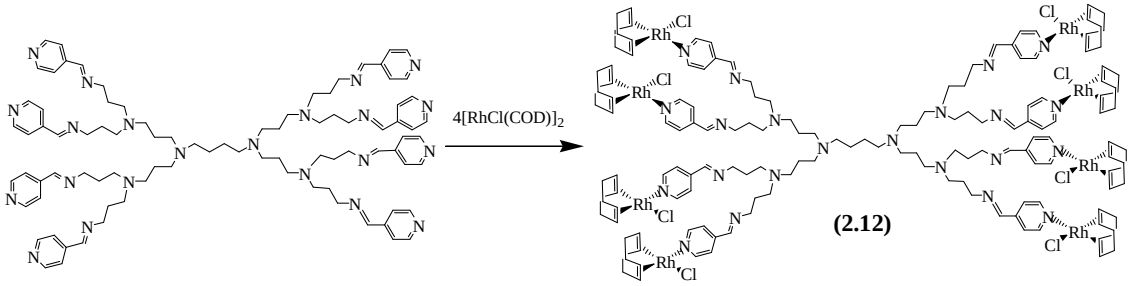

Scheme 2.12

Infrared Spectral Analysis

Infrared spectroscopy was used to confirm coordination of the ligand to rhodium. The free ligand shows a [*ν*(C=N)] absorption band at 1647 cm^{-1} and 1598 cm^{-1} for the imine and pyridyl functional groups in **2.10** respectively. The absorption band observed at 1598 cm^{-1} shows a shift to a higher frequency, found as a medium intensity band at 1612 cm^{-1}. There is no significant shift for the band at 1647 cm^{-1} associated with the imine. This confirms selective coordination of the rhodium metal centre to the pyridyl nitrogen and the bonding of this ligand in a monodentate coordination mode to the rhodium metal center. This shift to higher frequencies instead of lower frequencies is attributed to the pyridyl nitrogen being a good σ-donor. As seen for the mononuclear analogue, there was no significant shift in frequency for the imine [*ν*(C=N)] band which shows a band at 1646 cm^{-1} for both Rh(I) complexes **2.11** and **2.12**. Upon coordination, the pyridyl [*ν*(C=N)] band shows a shift to higher frequency from 1598 cm^{-1} and 1599 cm^{-1} to 1612 cm^{-1} and 1614 cm^{-1} for **2.11** and **2.12** respectively.

^{1}H NMR Spectral Analysis

The ^{1}H NMR spectrum of **2.10** was used to confirm the coordination of the pyridylimine, **2.7**, to the Rh(I) precursor, [RhCl(COD)]. There is not a dramatic change in the shifts for the protons of the propyl chain. Three new signals appear in the aliphatic region as broad

multiplets at δ 1.81 ppm, δ 2.51 ppm and δ 4.17 ppm. These signals correspond to the COD ligand coordinated to the complex. The aromatic protons show the same resonance pattern for the imine and aromatic protons. There is an upfield shift from δ 8.66 ppm to δ 8.79 ppm for the proton on the carbon adjacent to the pyridyl nitrogen.

The resonance pattern for the dendritic complex, **2.11**, shows a set of broad peaks. This is due to the multinuclear nature of the dendritic complex. The aliphatic core is discernable as a set of broad signals in the range δ 1.29-4.18 ppm. In contrast to the mononuclear complex, **2.10**, one cannot discern the COD peaks from that of the aliphatic DAB core as most of these peaks overlap. The only discernable COD peak is at δ 4.18 ppm. A downfield shift in resonance from δ 8.66 ppm to δ 8.75 ppm occurs for the methine proton of the pyridine ring upon coordination to rhodium. Similarly, the second generation complex, **2.12**, shows a set of broad signals in the region δ 1.36 - 4.13 ppm for the aliphatic DAB core and the COD protons. The pyridyl methine proton resonance shows a downfield shift from δ 8.64 ppm to δ 8.74 ppm upon coordination. This further corroborates that there is selective coordination of the pyridyl nitrogen to the Rh(I) metal center.

^{13}C NMR Spectral Analysis

The ^{13}C NMR spectrum of **2.10** shows two extra signals for the carbons of COD. These COD resonance signals occur at δ 30.89 ppm for the alkyl carbons $\underline{C}H_2$ and δ 80.55 ppm, for the alkene carbons, $\underline{C}H$.

The spectra for complexes **2.11** and **2.12** show an additional two peaks for the carbons of COD, similar to that of **2.10**, at δ 30.85 ppm and δ 30.77 ppm for the $\underline{C}H_2$ and δ 80.40 ppm and δ 80.62 ppm for the $\underline{C}H$ methylene carbons. The number of resonances expected for each of these complexes agrees with that observed in each spectrum further confirming the formation of the complexes.

Elemental Analysis

Elemental analyses were conducted on compounds **2.10-2.12**. Values obtained are in agreement once solvent inclusion of DCM is taken into account for compounds **2.11-2.12**.

2.3.4 Reactions of the iminopyridyl ligands with $[RhCl(PPh_3)_3]$

Complexes **2.13-2.15** (Schemes 2.13-2.15) were synthesized by reacting the iminopyridyl ligands **2.7-2.9** with Wilkinson's catalyst, $[RhCl(PPh_3)_3]$. The compounds are isolated as fine beige powders. Satisfactory elemental analyses could not be obtained for the respective compounds. Despite this, other spectral data including NMR and infrared spectral data was used to confirm coordination.

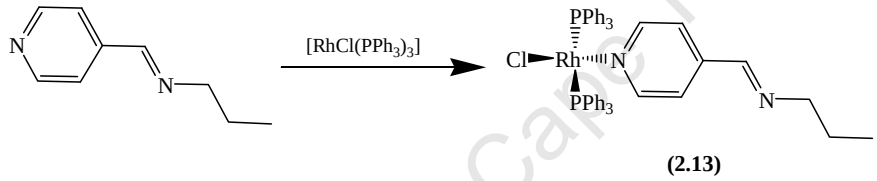

(2.13)

Scheme 2.13

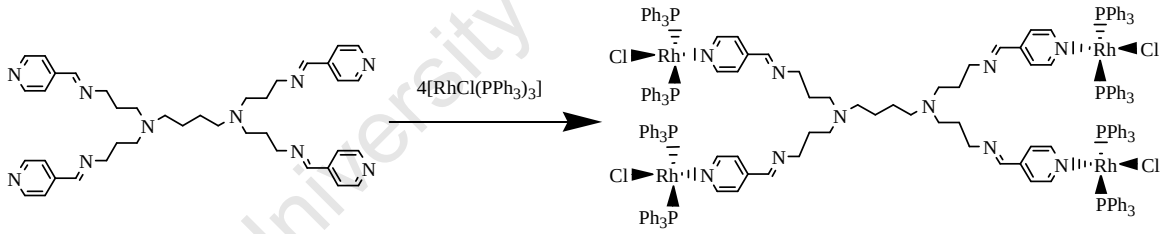

(2.14)

Scheme 2.14

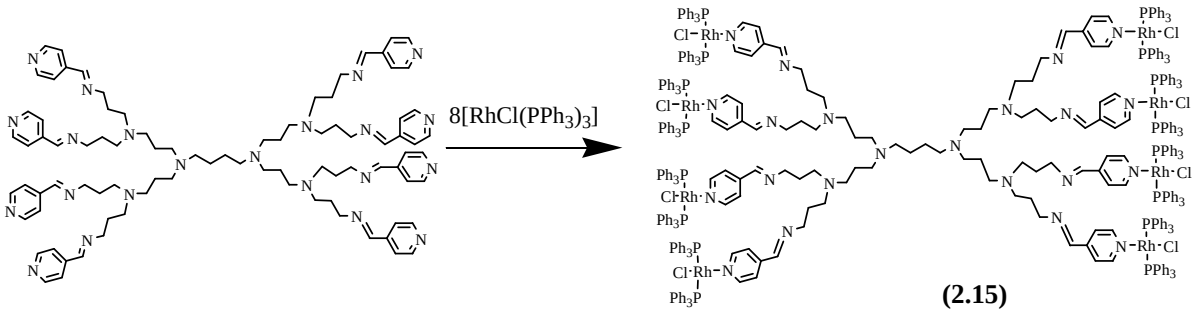

(2.15)

Scheme 2.15

Infrared Spectral Analysis

Infrared spectral data was used to confirm coordination of the ligand to the Rh(I) precursor. As for the [RhCl(COD)] pyridyl complexes, the free ligand, **2.7**, shows a shift for the [*v*(C=N)] band of the pyridine ring upon coordination from 1598 cm^{-1} to 1614 cm^{-1}. The imine [*v*(C=N)] band shifts from 1647 cm^{-1} to 1646 cm^{-1} which is not a significant enough shift to warrant any coordination to rhodium. Coordination therefore occurs exclusively at the pyridyl nitrogen.

The same mode of coordination is observed for the dendritic complexes. These show a shift in the [*v* (C=N)] band of the pyridine ring from ~1598 cm^{-1} to 1614 cm^{-1} upon coordination of the ligand for both **2.14** and **2.15** respectively. The [*v* (C=N)] band for the imine shifts from 1647 cm^{-1} to 1646 cm^{-1}.

^{1}H NMR Spectral Analysis

^{1}H NMR spectra for complex **2.13** was used to further confirm that coordination of the pyridylimine ligand occurred to the Rh(I) centre. In the case of the mononuclear complex, the aliphatic protons can be seen as three resonance signals at δ 0.92 ppm, δ 1.70 ppm and δ 3.61 ppm for the propyl chain confirming that the ligand is still present. The aromatic protons are all clustered as a multiplet around δ 7.48 ppm with the imine resonance signal included.

The dendritic complexes **2.14** and **2.15** both show a set of broad signals for the aliphatic protons of the dendritic core in the range δ 1.27-3.73 ppm. The aromatic protons of the phenyl rings show an intense multiplet between δ 7.00-8.98 ppm and the imine peak can be seen at δ 8.25 ppm for compound **2.14**. The methine proton of the pyridyl ring shows a downfield shift from δ 8.57 ppm to δ 8.98 ppm consistent with the coordination of the pyridyl nitrogen to the Rh(I) centre.

Similarly, compound **2.15** shows a set of broad resonance signals for the aliphatic protons of the dendritic core in the range δ 1.42-3.57 ppm. The aromatic protons for triphenylphosphine occur as an intense multiplet resonance signal at δ 7.34 ppm. The imine

peak is hidden underneath the resonance signals for the aromatic protons and the pyridyl methine resonance signal occurs as a broad singlet at δ 8.68 ppm showing a downfield shift when compared to the free ligand signal that occurs at δ 8.58 ppm.

^{31}P NMR Spectral Analysis

Phosphorous NMR only shows an unexpected singlet at δ ~29 ppm which is due to free triphenylphosphine oxide that forms while in solution. It is possible that the intensity of the phosphorous resonance peak for the triphenylphosphine oxide present is obscuring the product peaks. Despite this observation all previous characterization confirms that there is formation of the complex and that the dendritic architecture stays intact.

2.4 Chemical reactivity studies

2.4.1 Reaction of the iminopyridyl Rh(I) COD complexes (**2.10**-**2.12**) with triphenylphosphine

Reactivity studies were conducted on the rhodium pyridylimine COD complexes by reacting them with triphenylphosphine (Schemes 2.16-2.18). Scheme 2.16 details the reaction between the pyridyl complex **2.10** and triphenylphosphine. A colour change from yellow to orange was noted during the course of the reaction. Upon completion hexane was used to precipitate a beige solid from solution. Further purification was attempted by using hot hexane to wash away any triphenylphosphine oxide formed but this has proved unsuccessful.

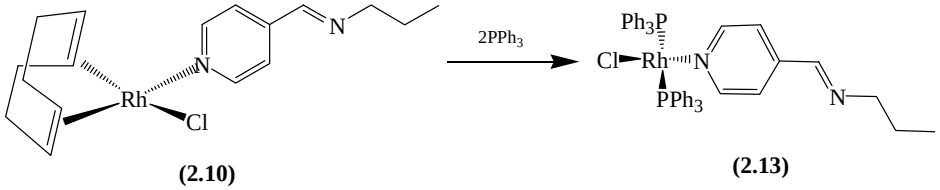

(2.10) **(2.13)**

Scheme 2.16

The dendritic complexes **2.11** and **2.12** were reacted with triphenylphosphine in a similar method to that described for the reaction of compound **2.10** with triphenylphosphine. The reaction yielded a beige solid. Elemental analysis and mass spectral analyses was not conducted on these samples as they could not be sufficiently purified.

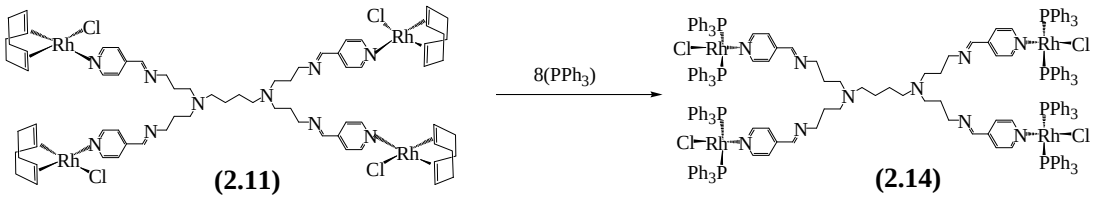

Scheme 2.17

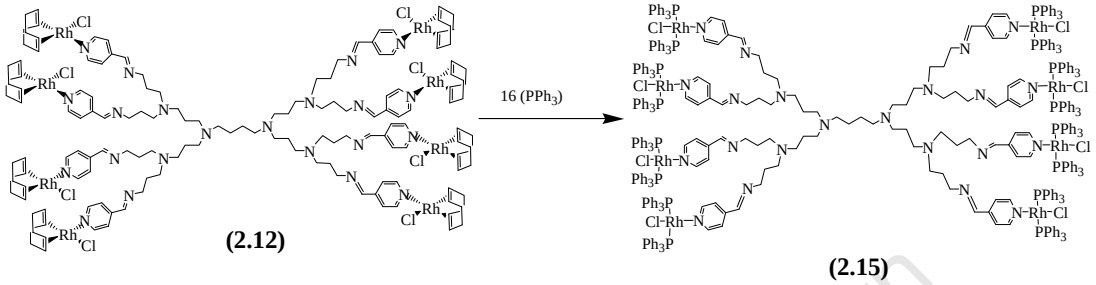

Scheme 2.18

IR Spectral Analysis

Infrared spectral data was used to help confirm whether the pyridyl nitrogen remains coordinated to the Rh(I) metal center. The infrared spectrum shows a stretch at 1613 cm^{-1} for the C=N bond of the pyridine ring. The stretch for the C=N double bond of the imine nitrogen remains unchanged at 1647 cm^{-1}. These two stretches indicate that rhodium is not coordinated to the imine nitrogen but to the pyridyl nitrogen exclusively. The stretch at 1613 cm^{-1} further confirms that the iminopyridyl ligand was not displaced by the triphenylphosphine ligands. If this had been the case an expected shift of the pyridyl C=N stretch from 1613 cm^{-1} to approximately 1598 cm^{-1}, corresponding to the free ligand, would have occurred. These values agree with those observed for compound **2.13**. The reactivity studies conducted on the analogous dendritic complexes **2.14** and **2.15** show similar values for the vibrational stretches of the imine and pyridyl C=N double bond. This suggests that the dendritic ligands are still coordinated to the rhodium metal centres and that no displacement of the dendritic ligand by triphenylphosphine took place.

^{1}H NMR Spectral Analysis

^{1}H NMR spectral analyses were conducted on the compounds obtained from reactivity studies conducted (Schemes 2.19–2.21). The reaction employing the mononuclear complex, **2.10**, shows three broad peaks in the range δ 0.95-3.62 ppm. The peaks for the COD ligand usually occurs at δ 1.81 ppm, δ 2.51 ppm and δ 4.17 ppm but are absent in this spectrum. This confirms that there is displacement of the COD ligand by triphenylphosphine.

In the case of the dendritic ligands, these show peaks in the range δ 1.25 ppm - δ 3.74 ppm for the alkyl framework of the dendritic scaffold and another from δ 7.33 ppm - δ 8.24 ppm for the aromatic and methine protons.

Similar to that of the mononuclear complex, the resonance peaks for the COD ligand are absent and confirms that the COD ligand has been displaced by triphenylphosphine. The spectra obtained resemble that of the dendritic complexes **2.14** and **2.15** previously discussed.

^{31}P NMR Spectral Analysis

^{31}P NMR spectral analyses were conducted on the complexes discussed. Similar to complexes **2.13-2.15**. The same resonance peak at δ ~29 ppm is seen and most likely denotes a strong presence of triphenylphosphine oxide in the prepared sample. Where isolation and purification is concerned, it is evident that the oxide forms quite readily and that the complex is therefore quite air sensitive. Further characterization was not conducted as pure enough samples could not be obtained.

2.4.2 Reactions of the iminophosphine Rh(I) carbonyl complexes (**2.4-2.6**) with methyl iodide

The Rh(I) chlorocarbonyl complexes **2.4-2.6** were reacted with an excess of methyl iodide (Schemes 2.19 – 2.21) as part of a preliminary reactivity study. The reactions were monitored using infrared spectroscopy. In the case of the reaction using the mononuclear complex **2.4**, a mixture of products **2.16** and **2.17** were formed.

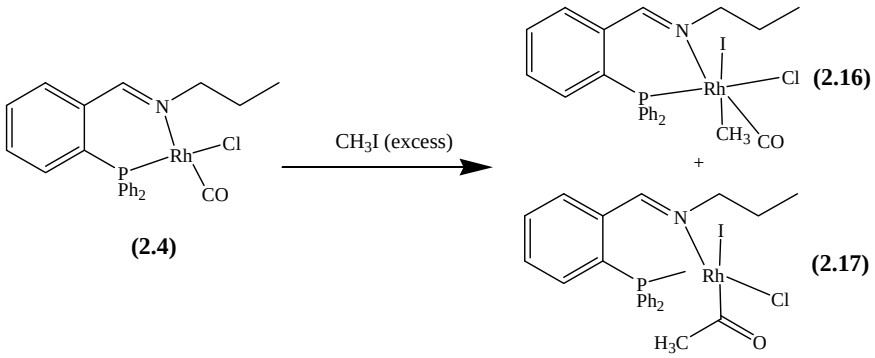

Scheme 2.19

Schemes 2.20 and 2.21 detail the reactivity studies conducted on compounds **2.5** and **2.6**. These reactions were carried out in a similar manner to that depicted in Scheme 2.19. The dendritic complexes **2.5** and **2.6** were reacted with methyl iodide for a total of 72 hours at room temperature. These reactions were monitored by infrared spectroscopy as well.

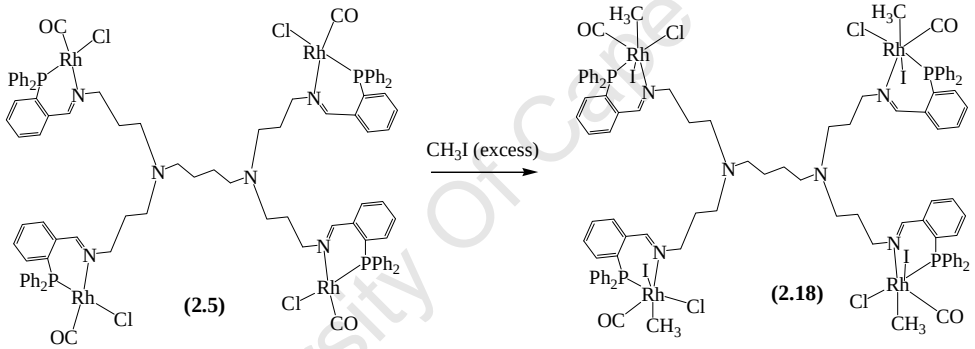

Scheme 2.20

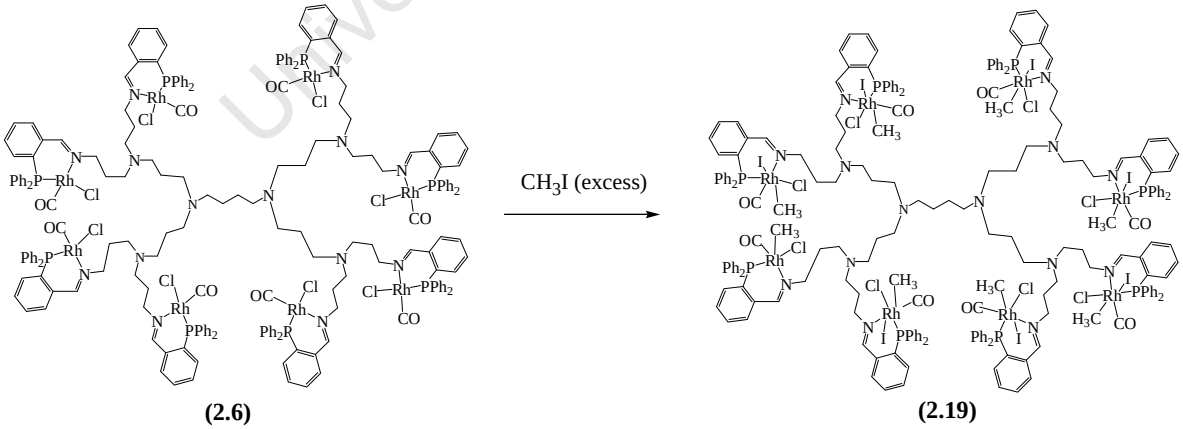

Scheme 2.21

Infrared Spectral Analysis

The reaction of compound **2.4** with methyl iodide was monitored by Fourier Transform Infrared Spectroscopy (FTIR). Infrared data shows the disappearance of the terminal carbonyl band at 2001 cm^{-1} for compound **2.4** and the subsequent growth of a higher frequency band at 2071 cm^{-1} and lower frequency band at 1725 cm^{-1}. The band at 2071 cm^{-1} is indicative of the formation of the oxidative addition product **2.16** and appears first and then there is subsequent growth in the band at 1725 cm^{-1} for the Rh(I) acyl product, **2.17**. The growth in these bands reaches a steady state after an hour of reaction. Kinetic and reactivity studies conducted on Rh(I) carbonyl complexes show a seemingly increased rate for carbonyl insertion when there is high steric demand within the complex whereas a slower rate is noticed for complexes with a higher electron density surrounding the metal. [33] The system investigated does not meet the steric demands to exclusively drive the formation of an acetyl product and therefore a mixture of both oxidative addition and Rh(I) acyl products are noted. Systems typical of this behaviour have the N-aryl iminophosphine ortho-substituted with alkyl groups to increase steric bulk and promote acetyl formation. [33]

Reactivity studies were conducted on dendritic complexes **2.5** and **2.6** as well. In contrast to the reactivity study conducted on compound **2.4**, only oxidative addition occurred and there was no formation of the acetyl species. Upon oxidative addition of methyl iodide to the Rh(I) complex, there is an increase in the oxidation state from +1 to +3. This causes a decrease in the electron density on the rhodium metal center. This decrease in electron density on the metal center results in a decrease in π-back-bonding to the anti-bonding orbitals of the coordinated carbonyl carbon. This results in a stronger C≡O bond. This was noted by a shift to higher frequency of the terminal carbonyl band at 1996 cm^{-1} for **2.5** to 2071 cm^{-1} for **2.18**. The reactivity study conducted on the second generation complex, **2.6**, showed the same increase in the [ν(CO)] at 2001 cm^{-1} to 2069 cm^{-1} for **2.19**. Steric bulk in the immediate environment of the rhodium complex facilitates acetyl formation. It would be expected that the steric constraints introduced by the dendritic scaffold would facilitate acetyl formation as well but this is not the case.

This could be ascribed to electronic factors. Should there be coordination of the Rh(I) complexes to the amine nitrogens on the dendritic scaffold facilitated by back-folding of the dendritic arms, the electronic properties of the complexes would be affected. This can possibly lead to inhibition of alkyl insertion into the Rh-CO bond and hence prevent formation of the acyl species.

^{1}H NMR Spectral Analysis

^{1}H NMR spectral data for oxidative addition of methyl iodide to compound **2.4** corroborates the formation of a mixture of products **2.16** and **2.17**. This is evident in an increase and even doubling of signals for the aliphatic protons in the region δ 0.5 ppm to δ 4.6 ppm. Due to the complexity of the dendritic scaffold, definite resonance peaks were not observed but rather extensively broadened peaks.

2.5 Conclusion

A series of model iminopyridyl- and iminophosphine-functionalized and multimeric iminopyridyl- and iminophosphine-functionalized ligands were synthesized employing Schiff-base chemistry and were fully characterized. These ligands were reacted with various Rh(I) metal precursors to prepare monodentate iminopyridyl and chelating bidentate iminophosphine complexes. The molecular structure helped confirm the coordination geometry around the metal centre as square-planar. In the case of the iminopyridyl complexes reacted with Wilkinson's complex, full characterization was not achieved as the complex was not stable enough. This was due to the facile oxidation of triphenylphosphine coordinated to the rhodium complex.

Preliminary reactivity studies were conducted to investigate the type of products formed by reaction of the iminopyridyl-COD complexes with triphenylphosphine and the reaction between the iminophosphine-carbonyl complexes and methyl iodide. The results gained from the former reaction show similarities to results obtained for the reaction between the iminopyridyl ligands and Wilkinson's complex. The methyl iodide reactions show the formation of oxidative addition and acyl products in the case of the mononuclear complex. The dendritic complexes however only show the formation of the oxidative addition product.

2.6 References

1. D.A. Tomalia, H. Baker, J. Dewald, M. Hall, G. Kallos, S. Martin, J. Roeck, J. Ryder and P. Smith, *Polym. J.*, **1985**, 17, 117.
2. C.J. Hawker and J.M.J. Fréchet, *J. Chem. Soc., Chem. Commun.*, **1990**, 1010.
3. R. van Heerbeek, P.C.J. Kamer, P.W.N.M. van Leeuwen and J.N.H. Reek, *Org. Biomol. Chem.*, **2006**, 4, 211.
4. L. Ropartz, R.E. Morris, D.F. Foster and D.J. Cole-Hamilton, *Chem. Commun.*, **2001**, 361.
5. E.M.M. de Brabander-van den Berg and E.W. Meijer, *Angew. Chem.*, **1993**, 32, 1308.
6. D. Astruc and F. Chardac, *Chem. Rev.*, **2001**, 101, 2991.
7. P.A. Chase, R.J.M.K. Gebbink and G. van Koten, *J. Organomet. Chem.*, **2004**, 689, 4016.
8. A. Dahan and M. Portnoy, *J. Polym. Sci., Part A: Polym. Chem.*, **2005**, 43, 235.
9. W.D. Jang, K.M.K. Selim, C.H. Lee and I.K. Kang, *Prog. Pol. Sci.*, **2009**, 34, 1.
10. D. Méry and D. Astruc, *Coord. Chem. Rev*, **2006**, 100, 1965.
11. R.K. Tekade, P.V. Kumar and N.K. Jain, *Chem. Rev.*, **2009**, 109, 49.
12. R. Andres, E. de Jesús and J.C. Flores, *New J. Chem.*, **2007**, 31, 1161.
13. L.H. Gade, *Dendrimer Catalysis*, Springer GmbH edn., Berlin, Germany, 2006.
14. C. Omelas, J.R. Aranzaes, L. Salmon and D. Astruc, *Chem. Eur. J.*, **2008**, 14, 50.
15. S. Langereis, A. Dirksen, T.M. Hackeng, M.H.P. van Genderen and E.W. Meijer, *New J. Chem.*, **2007**, 31, 1152.
16. B. Felber and F. Diederich, *Helv. Chim. Acta*, **2005**, 88, 120.
17. M. Goldberg, R. Langer and X. Jia, *J. Biomater. Sci. Polym. Ed.*, **2007**, 18, 241.
18. H.S. Parekh, *Curr. Pharm. Design*, **2007**, 13, 2837.
19. N.J. Hovestad, E.B. Eggeling, H.J. Heidbüchel, J.T.B.H. Jastrzebski, U. Kragl, W. Keim, D. Vogt and G. van Koten, *Angew. Chem. Int. Ed.*, **1999**, 38, 1655.
20. E. Buhleier, W. Wehner and F. Vögtle, *Synthesis*, **1978**, 155.
21. M.T. Reetz, G.S. Lohmer and R. Schwickardi, *Angew. Chem., Int. Ed. Engl.*, **1997**, 36, 1526.
22. D.P. Catsoulacos, B.R. Steele, G.A. Heropoulos, M. Micha-Screttas and C.G. Screttas, *Tetrahedron Lett.*, **2003**, 44, 4575.
23. P. Govender, N.C. Antonels, J. Mattsson, A. K. Renfrew, P. J. Dyson, J. R. Moss, B. Therrien and G. S. Smith, *J. Organomet. Chem.*, **2009**, 694, 3470.

24. J.R. Dilworth, S.D. Howe, A.J. Hutson, J.R. Miller, J. Silver, R.M. Thomson, M. Harman and M.B. Hursthouse, *J. Chem. Soc., Dalton Trans.* , **1994**, 3553.
25. J.R. Dilworth, A.J. Hutson, J.S. Lewis, J.R. Miller, Y. Zheng, Q. Chen and J. Zubieta, *J. Chem. Soc., Dalton Trans.*, **1995**, 1093.
26. G.R. Newkome, *Chem. Rev.*, **1993**, 93, 2067.
27. G. Sánchez, J.L. Serrano, M.A. Moral, J. Pérez, E. Mollins and G. López, *Polyhedron*, **1999**, 3057.
28. C. A. Ghilardi, S. Midollini, S. Moneti, A. Orlandini and G. Scapacci, *J. Chem. Soc., Dalton. Trans.*, **1992**, 3371.
29. N.C. Antonels, B. Therrien, J.R. Moss and G.S. Smith, *Inorg. Chem. Commun.*, **2009**, 12, 716.
30. M. Chai, Y. Niu, W.J. Youngs and P.L. Rinaldi, *J. Am. Chem. Soc.*, **2001**, 123, 4670.
31. S. Antonaroli and B. Crociani, *J. Organomet. Chem.*, **1998**, 560, 137.
32. G. Bandoli and A. Dolmella, *Transition Met. Chem.*, **2000**, 25, 17.
33. J. Best, J.M. Wilson, H. Adams, L. Gonsalvi, M. Peruzzini and A. Haynes, *Organometallics*, **2007**, 26, 1960.
34. J.F.G.A. Jansen, E.M.M. de Brabander-van den Berg and E.W. Meijer, *Science*, **1994**, 266, 1226.
35. S. Burling, L.D. Field, B.A. Messerle, K.Q. Vuong and P. Turner, *Dalton Trans.*, **2003**, 4181.
36. P.W. Dyer, J. Fawcett and M.J. Hanton, *J. Organomet. Chem.*, **2005**, 690, 5264.
37. K.N. Gavrilov, O.G. Bondarev, R.V. Lebedev, A.A. Shiryaev, S.E. Lyubimov, A.I. Polosukhin, G.V. Grintselev-Knyazev, K.A. Lyssenko, S.K. Moiseev, N.S.Ikonnikov, V.N. Kalinin, V.A. Davankov, A.V. Korostylev and H.J. Gais, *Eur. J. Inorg. Chem.*, **2002**, 1367.
38. J. Rajput, A.T. Hutton, J.R. Moss, H. Su and C. Imrie, *J. Organomet. Chem.*, **2006**, 691, 4573.

Chapter 3

Iminopyridyl and Iminophosphine Multinuclear Metallodendritic Rhodium(I) Complexes Utilized in the Hydroformylation of 1-octene

3.1 Introduction

Rhodium-catalyzed hydroformylation is one of the most important industrial processes involving the use of a homogeneous catalyst. [1] As discussed in the Chapter 1.4.2, catalysts containing rhodium are more stable during hydroformylation reactions and require milder reaction conditions to give high catalytic rates and chemoselectivity towards the aldehyde product. Because the catalyst is homogeneous, problems arise when separation of catalyst from the product is required. One way to overcome this is to anchor the complex on a support that helps facilitate this separation.

Dendrimers are suitable for this purpose as transition metal complexes can be coordinated to them and easily recovered by ultrafiltration. [2-8] This is however not the only advantage of using dendrimers as supports for transition metals. Dendrimers can help stabilize metal complexes which helps maintain or enhance catalytic rates observed, an important factor when considering the kinetics of the reaction. In the hydroformylation of olefins, it is imperative to find a catalytic system that gives good chemoselectivity for aldehydes and good regioselectivity for either the branched or linear aldehyde depending on which one is the desired product. Dendrimers provide a complex microenvironment for the coordinated catalysts that can either positively or negatively affect these selectivities.

A series of mono- and multinuclear Rh(I) complexes that were previously synthesized and thoroughly discussed in the previous chapter are shown in Figure 3.1. In order to evaluate the catalytic performance of these Rh(I) complexes, we chose to study the hydroformylation reaction using 1-octene as the model substrate.

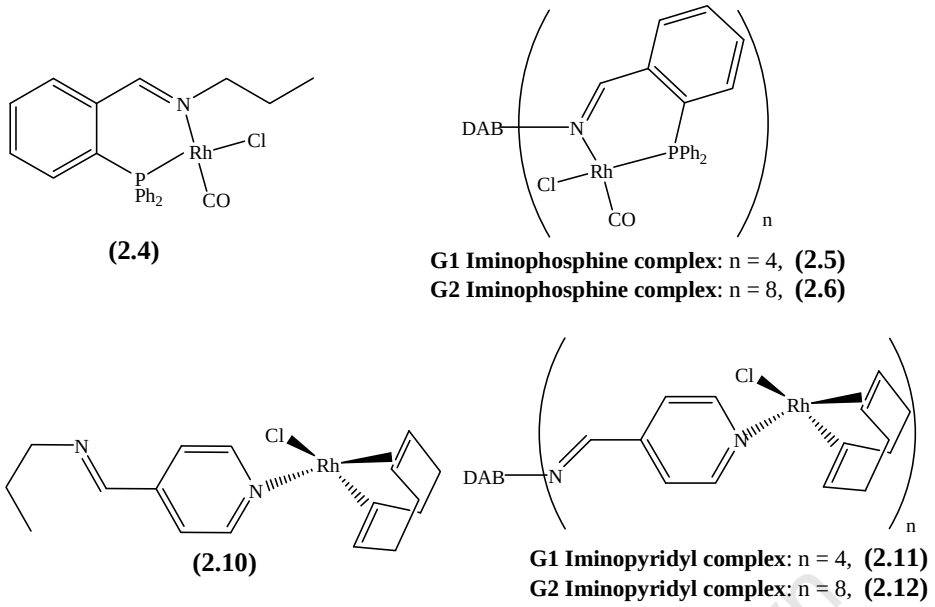

(2.4)

G1 Iminophosphine complex: n = 4, **(2.5)**
G2 Iminophosphine complex: n = 8, **(2.6)**

(2.10)

G1 Iminopyridyl complex: n = 4, **(2.11)**
G2 Iminopyridyl complex: n = 8, **(2.12)**

Figure 3.1: Rh(I) mononuclear and multinuclear iminopyridyl and iminophosphine complexes utilized in hydroformylation of 1-octene.

Hydroformylation is the catalyzed addition of syngas (H_2/CO) across an olefinic substrate to produce aldehydes as products. In our case the hydroformylation of 1-octene can lead to the formation of either nonanal (linear product) and/or 2-methyloctanal (branched product) as shown in Scheme 3.1.

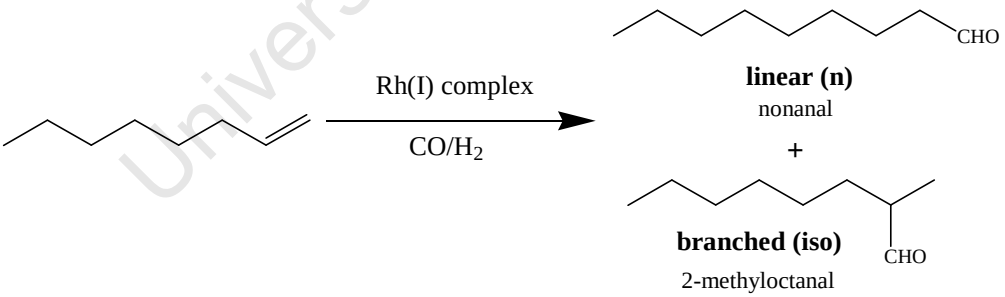

Scheme 3.1

This chapter describes the use of the previously prepared mononuclear and multinuclear Rh(I) complexes in the hydroformylation of 1-octene, investigating the effects of the dendritic scaffold on reaction rate and chemo- and regioselectivities.

3.2 Comparison of various catalytic systems

3.2.1 Conversion of 1-octene versus time

The percentage conversion of 1-octene observed per unit time provides a measure of the rate of reaction when using a particular catalyst with Rh = 0.0028 mmol for each reaction. The substrate conversion was investigated over an eight hour period with samples of the hydroformylation reaction mixture taken every two hours for the iminophosphine Rh(I) complexes, **2.4-2.6** and the iminopyridyl Rh(I) complexes, **2.10-2.12**, and the percentage 1-octene conversion calculated after each sampling.

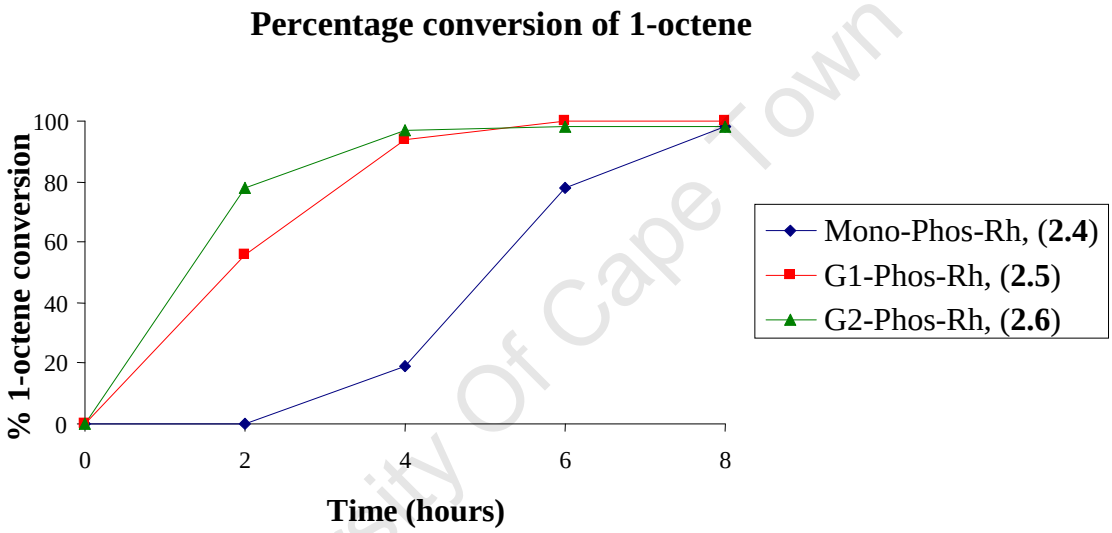

Figure 3.2: Percentage conversion of 1-octene over an 8 hour period using Rh(I) iminophosphine complexes.

Figure 3.2 shows the percentage conversion of 1-octene using the iminophosphine Rh(I) complexes, **2.4-2.6**. These reactions were conducted using a syngas (H_2:CO, 1:1) pressure of 30 bar and a temperature of 75 °C. For these complexes there is a near quantitative conversion of 1-octene after 8 hours. More interestingly, there is a difference in the catalytic rates for the first 4 hours when using the different complexes. In the case of the mononuclear complex, **2.4**, this complex shows little to no activity over the first two hours. This behavior suggests that there is an induction period associated for the active complex to form. The first- and second-generation iminophosphine metallodendritic Rh(I) complexes **2.5** and **2.6** show results different to that of the mononuclear complex, **2.4**. For complexes **2.5** and **2.6** there is

an increase in catalytic rate over the first four hours compared to the mononuclear complex with the latter showing the highest catalytic rate. In complexes **2.4**-**2.6**, rhodium is bonded to a chloride which may cause temporary inhibition of the reaction once reacted with the hydride coordinated to rhodium to form hydrogen chloride. The induction period would therefore be expected for the metallodendrimers as well. However, this is not seen when using the iminophosphine Rh(I) metallodendrimers **2.5** and **2.6**. Therefore, there must be an alternative mechanism operating, by which hydrogen chloride is sequestered. Research conducted by Wilkinson *et al.* focused on using Rh(I) halide arylphosphines to catalyze the hydroformylation of various olefins. [9] They observed that the addition of a base like triethylamine helps remove the hydrogen chloride formed that causes inhibition of the hydroformylation reaction when working with rhodium halide complexes. The tertiary amines in the first- and second-generation PPI dendritic scaffold may serve as a possible tertiary amine source for the removal of hydrogen chloride formed, therefore rationalizing the promotional effect experienced when using the metallodendrimers. The dendrimer therefore has a promotional effect on the catalytic rate. The mononuclear complex **2.4** does not contain a tertiary amine, hence the observed induction period.

The conversion rates for 1-octene observed when using the iminopyridyl Rh(I) complexes **2.10**-**2.12** were also determined. Figure 3.3 depicts a graph for the conversion of 1-octene over an eight hour period when using these complexes.

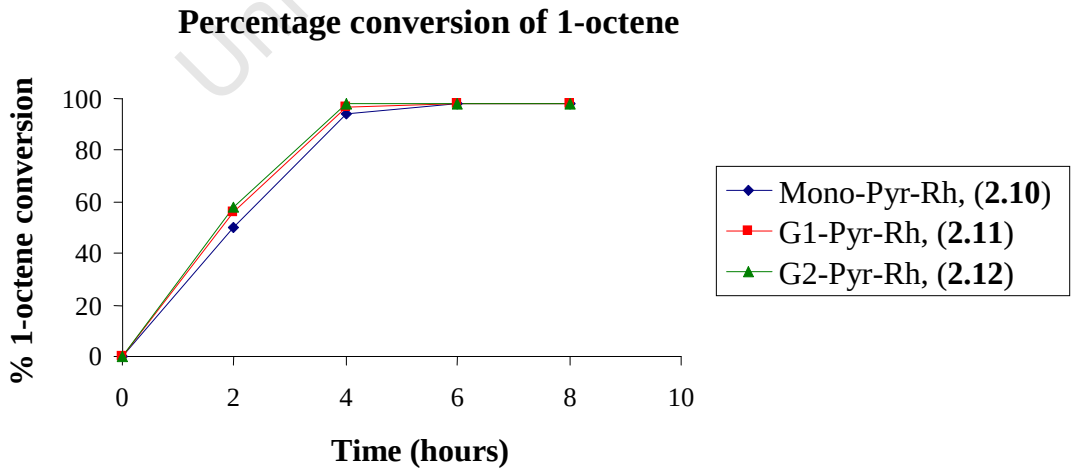

Figure 3.3: Percentage conversion of 1-octene over an 8 hour period using Rh(I) iminopyridyl complexes.

Rh(I) complexes **2.10**-**2.12** show a near-quantitative conversion of 1-octene after 8 hours. The graph shows a steady 1-octene conversion rate over the first four hours for each of the complexes. When comparing the mononuclear iminopyridyl Rh(I) complex, **2.10**, to the multinuclear iminopyridyl Rh(I) metallodendrimer complexes, **2.11** and **2.12**, there is only a small difference in the consumption of 1-octene. The dendrimers show a slight increase in the percentage conversion over that of the mononuclear complex, **2.10**, for the first four hours.

Compared to the iminophosphine Rh(I) complexes **2.4**-**2.6**, the iminopyridyl Rh(I) complexes, **2.10**-**2.12**, show no significant difference in the catalytic rates between the mononuclear Rh(I) iminopyridyl complex, **2.10**, and the multinuclear Rh(I) iminopyridyl complexes **2.11** and **2.12**. Both the iminophosphine and iminopyridyl Rh(I) complexes are metal halide complexes. Therefore, when comparing the iminopyridyl Rh(I) complexes **2.10**-**2.14** to each other you would expect to see a similar difference in catalytic conversion rates going from the mononuclear complex to the first and second generation complexes as seen amongst the iminophosphine Rh(I) complexes **2.4**-**2.6**. The formation of the active complex for these iminopyridyl Rh(I) complexes is rapid enough to overcome the inhibitory effects of the HCl formed. This can be due to the lability of the COD ligand that allows for a more coordinatively unsaturated complex and more facile coordination of H_2, CO hence formation of the active complex.

3.2.2 Hydroformylation activity

To gain more insight into the catalytic activity, the turnover frequency (TOF) was calculated based on the mole amount of aldehyde formed per mole of rhodium metal after an 8 hour period, utilizing a syngas pressure ($CO:H_2$, 1:1) of 30 bar and temperature of 75 °C. Figure 3.4 illustrates the catalytic activity in terms of TOF for the Rh(I) catalysts used in this study as well as the complex, $[Rh(acac)(CO)_2]$.

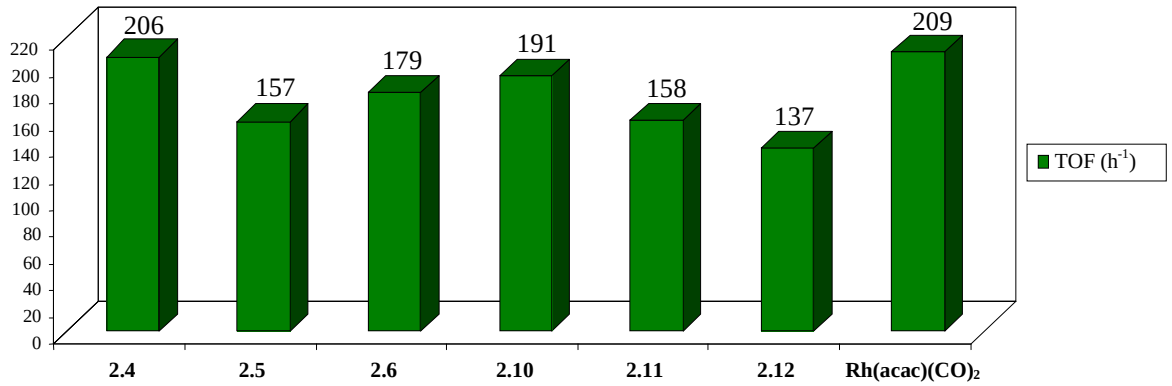

Figure 3.4: TOF for the Rh(I) catalysts investigated

Generally, the Rh(I) complexes show moderate TOF values, with activities observed in the range between 137-206 h^{-1}. It is important to realize that when comparing these complexes, two factors can affect the TOF values obtained, namely the steric bulk of the complexes and the stability of the complexes under hydroformylation conditions. In the case of the iminophosphine Rh(I) complexes **2.4-2.6**, the mononuclear complex, **2.4**, shows the highest TOF at a value of 206 h^{-1} while the first- and second-generation iminophosphine complexes **2.5** and **2.6** show values of 157 h^{-1} and 179 h^{-1} respectively. This increase in activity going from the first to the second generation metallodendritic complexes **2.5** to **2.6** respectively, may be attributed to the increased stability resulting from the more complex second generation dendritic scaffold, a feature that can help reduce metal leaching and hence help prevent deactivation of the catalyst. Comparing the metallodendritic iminophosphine Rh(I) complexes **2.5-2.6** to the mononuclear analogue, **2.4**, there is a decrease in the TOF going from the mononuclear complex to the multinuclear complexes. This decrease may be due to the decreased accessibility of the substrate to the metal complex center. In this case hydroformylation of the internal isomers to the aldehyde product is hampered since coordination of internal isomers of octene is more susceptible to inhibition caused by the steric bulk of the dendritic scaffold, a problem not experienced by the mononuclear complex. This leads to the overall decrease in aldehyde formation and decrease in TOF going from the mononuclear iminophosphine Rh(I) complex **2.4** to the multinuclear iminophosphine Rh(I) complexes, **2.5-2.6**. $Rh(acac)(CO)_2$, gives a value of 209 h^{-1} similar to that of the mononuclear Rh(I) iminophosphine complex, **2.4**.

Amongst the iminopyridyl Rh(I) complexes, **2.10**-**2.12**, the mononuclear complex **2.10** shows the highest TOF at 191 h^{-1}. The metallodendritic iminopyridyl Rh(I) complexes, **2.11** and **2.12**, show values of 158 h^{-1} and 137 h^{-1}. Comparing the mononuclear iminopyridyl Rh(I) complex (**2.10**) to the multinuclear iminopyridyl Rh(I) complexes **2.11**-**2.12**, the effects of steric bulk are more pronounced as there is a decrease going from the mononuclear complex to the first- and second-generation metallodendritic complexes. As mentioned in the previous paragraph, the decrease in TOF going from the mononuclear complex to the dendritic complex may be attributed to the steric bulk of the dendritic scaffold that hinders coordination of the internal isomers of octene and hence its subsequent hydroformylation as well.

When comparing the iminophosphine Rh(I) complexes to the iminopyridyl Rh(I) complexes there is an overall decrease in the TOF. This observation is pronounced for the second-generation Rh(I) complexes **2.6** and **2.12** where **2.6** is a more stable chelate complex. The instability of the iminopyridyl complexes was observed by the formation of a fine black precipitate in the hydroformylation mixture after a period of 4 hours. This may be deactivated rhodium that has agglomerated. This instability may be the reason for lower TOF observed when using the iminopyridyl Rh(I) complex, **2.12**. This was not observed for the iminophosphine Rh(I) complexes **2.4**-**2.6**. These are however moderate hydroformylation activity values and are comparable with values obtained for $[Rh(acac)(CO)_2]$ under the same reaction conditions.

3.2.3 Chemoselectivity

The chemoselectivity for the various catalytic systems were investigated after an eight hour period under a syngas pressure of 30 bar and temperature of 75 °C. Competitive isomerization of 1-octene occurs concurrent to the hydroformylation reaction for the complexes under investigation. Isomerization leads to the formation of the octenes, 2-octene, 3-octene and 4-octene. An investigation by Lazzaroni and co-workers studied the relationship between isomerization and the linear to branched ratio. [10, 11] They noticed that the isomerization is due to the β-hydride elimination of the iso-alkyl bond formed during a Markovnikov addition of the hydrogen to the terminal olefin. Isomerization increases with an increase in temperature and decrease in syngas pressure because this reaction has a higher free energy of activation compared to that of hydroformylation and requires a vacant site. In this

case, utilizing a temperature of 75 ºC helps increase reaction kinetics but also allows for some isomerization during the hydroformylation. Figure 3.5 illustrates the chemoselectivity data obtained from the hydroformylation runs using the previously synthesized Rh(I) complexes at an operating temperature of 75 ºC and a syngas pressure of 30 bar.

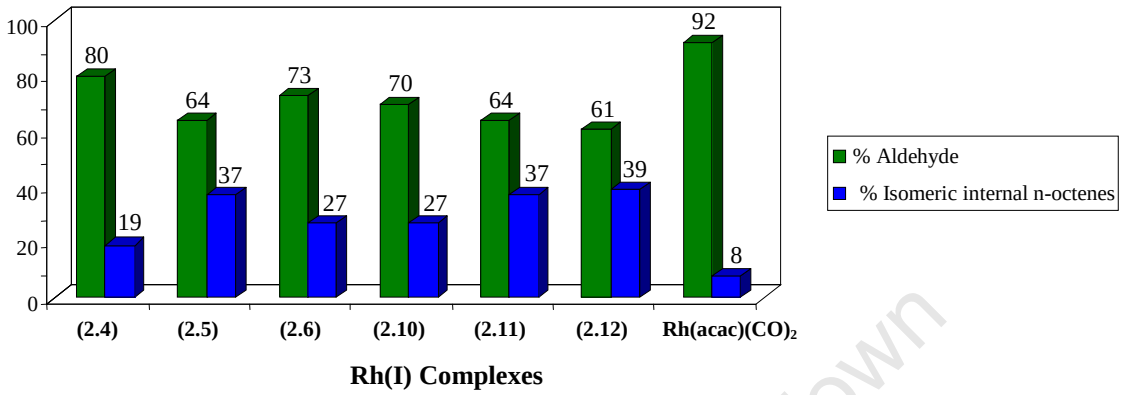

Figure 3.5: Chemoselectivity observed at 8 hours for aldehydes and isomeric internal n-octenes using the Rh(I) complexes synthesized.

The hydroformylation results for the different complexes used all show the chemoselective formation of aldehydes as main products under the given reaction conditions. The mononuclear Rh(I) complex, **2.4**, shows the highest chemoselectivity for aldehyde formation amongst the iminophosphine Rh(I) complexes. This is possibly due to the increase in reaction rate noted for the metallodendritic iminophosphine Rh(I) complexes, **2.5** and **2.6**, and the steric hindrance by the dendrimer preventing coordination of the isomeric internal n-octenes and subsequent hydroformylation. As discussed in section 3.2.2 the factors that possibly affect the hydroformylation of octenes for the Rh(I) complexes under investigation is the stability of the complexes under hydroformylation conditions and the steric bulk surrounding the metal complex. The increase in percentage aldehyde going from the first- to the second-generation iminophosphine Rh(I) complex is as previously mentioned in section 3.2.2 due to an increase in overall stability of the complex.

When considering the results for the iminopyridyl Rh(I) complexes, **2.10**-**2.12**, there is a clear decrease in the percentage aldehyde formed going from the mononuclear complex to the multinuclear complexes. A decrease in the amount of aldehyde suggests deactivation of the catalyst and therefore decreased hydroformylation activity. Catalyst deactivation is observed

by the formation of what is suspected to be free Rh particles as previously discussed for the iminopyridyl Rh(I) metallodendrimer complexes **2.11** and **2.12**. As most of the conversion of 1-octene occurs within the first four hours for the iminopyridyl Rh(I) complexes, further hydroformylation of the isomerization products occurs until eight hours is reached. However due to the decomposition of the metallodendritic iminopyridyl Rh(I) complexes **2.11** and **2.12**, the rate of hydroformylation of the isomeric internal n-octenes reduces dramatically, leading to a lower overall aldehyde percentage at eight hours in comparison to complex **2.10**. The metallodendritic iminophosphine Rh(I) complexes **2.4-2.6** do not show decomposition to Rh metal atoms that would be observed as a black precipitate and the percentage aldehyde formed increases going from the first to second generation complexes **2.5** and **2.6** respectively.

The chemoselectivity data for $Rh(acac)(CO)_2$shows the highest selectivity for aldehyde with a 90% aldehyde formation and the balance, isomerization products. Compared to the iminopyridyl and iminophosphine Rh(I) complexes, $Rh(acac)(CO)_2$ had a quicker onset of hydroformylation occurring within the first two hours. In this case the active complex was formed faster. This is most likely due to the electron-withdrawing effect of the acetylacetonato ligand coordinated to rhodium which would result in a more labile Rh-CO bond. This facilitates alkene substrate coordination and alkyl migration into the metal carbonyl bond to form the acyl intermediate favoring the hydroformylation process.

3.2.4 Regioselectivity

The regioselectivity across the double bond of 1-octene gives an indication of the selectivity of one regioisomer over the other. In this case selectivity is towards either the linear aldehyde, nonanal, or the branched aldehyde, 2-methyloctanal. It is important to note that these values are calculated based on percentages of nonanal and 2-methyloctanal formed as these are the desired products for hydroformylation of the α-olefin, 1-octene. As previously mentioned, isomerization is a competing process and hydroformylation of the isomeric internal n-octenes can lead to a higher branched product value. The hydroformylation of 2-octene can therefore also contribute to the formation of 2-methyloctanal. The n:iso ratios are therefore calculated at a time when minimal hydroformylation of isomerization products has occurred.

Table 3.1: Regioselectivity data obtained for the Rh(I) complexes used.[a]

Entry	Rh(I) Complexes	n:iso
1	Mononuclear iminophosphine, (**2.4**)[b]	73:27
2	G1 iminophosphine, (**2.5**)[c]	72:28
3	G2 iminophosphine, (**2.6**)[c]	60:40
4	Mononuclear iminopyridyl, (**2.10**)[c]	72:28
5	G1 iminopyridyl, (**2.11**)[c]	73:27
6	G2 iminopyridyl, (**2.12**)[c]	74:26
7	$Rh(acac)(CO)_2$[c]	48:52

[a] P = 30 bar, T = 75 °C, average of 2 runs, Rh = 0.0028 mmol.
[b] Regioselectivity calculated at 4 hours.
[c] Regioselectivity calculated at 2 hours.

Table 3.1 illustrates the regioselectivity data obtained using the selected catalysts. Both the iminophosphine Rh(I) complexes (**2.4-2.6**) and iminopyridyl Rh(I) complexes (**2.10-2.12**) show the regioselective formation of the linear aldehyde product, nonanal. Entries 1, 2 and 4-6 all show similar n:iso in the vicinity of ~70:30 while there is a significant change in the n:iso value for entry 3 to 60:40. To help clarify any observed trend, the regioselectivity is depicted as a bar graph in Figure 3.6 where regioselectivity is the quotient of the amount of linear and branched aldehyde.

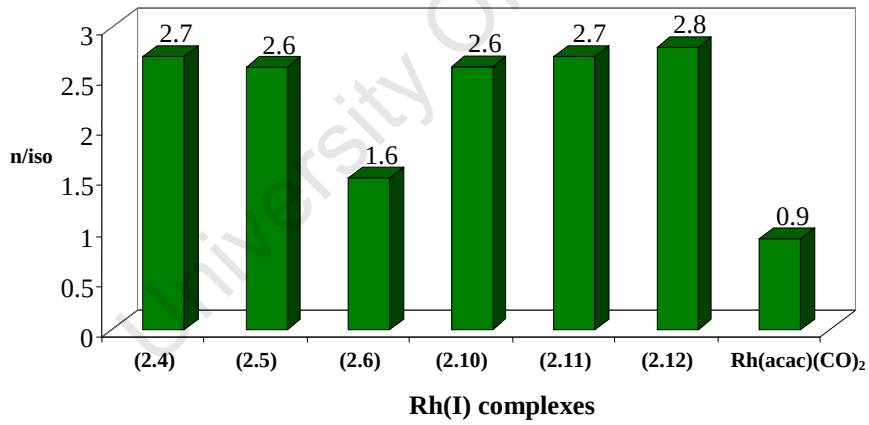

Figure 3.6: Regioselectivity data obtained from Rh(I) complexes synthesized.

The regioselectivity values obtained range from 0.9-2.8 for the various Rh(I) complexes investigated. Values below 1.0 indicate a regioselective formation of the branched aldehyde, 2-methyloctanal, and values above 1.0 indicate the regioselective formation of the linear product, nonanal.

The iminophosphine complexes, **2.4-2.6**, all showed the regioselective formation of the linear aldehyde, nonanal. Complexes **2.4** and **2.5** have values of 2.7 and 2.6 respectively. Complex **2.6** however has a lower value of 1.6 which indicates that even though the reaction was selective for nonanal formation, there is still more 2-methyloctanal forming than for the first two complexes. This lowered regioselectivity for the second generation complex could be due to the high catalytic rate observed for this catalyst. There is suspicion that hydroformylation of 2-octene formed has taken place at an earlier time period for the second generation iminophosphine Rh(I) complex, **2.6**. This was demonstrated in the graph for conversion of 1-octene. The higher catalytic rate leads to a higher isomerization rate and hydroformylation of the isomeric internal n-octenes formed occurs more rapidly resulting in a higher amount of branched aldehydes forming provided the conditions favour the isomerization in which case it does. This low n/iso value is observed for the $Rh(acac)(CO)_2$ complex where catalytic rate was highest over the first few hours of reaction compared to the Rh(I) complexes **2.4-2.6** and **2.10-2.12**. This helps clarify the lower n/iso values observed for the complexes studied.

Similarly, complexes **2.10-2.12**, show regioselective formation of the linear aldehyde indicated by regioselectivity values of 2.6-2.8. Although the mononuclear complex, **2.13**, shows a higher percentage for aldehyde formation, compared to the iminophosphine complexes it has a lower regioselectivity. The first and second generation iminopyridyl Rh(I) complexes, **2.11** and **2.12** respectively, show a minimal increase in the regioselectivity value. Steric effects from the ligand normally affect the regioselectivity of the catalyst. In the case of the regioselective formation of the linear product, ligands with large steric demand are needed. Arylphosphines are bulky ligands and can cause a higher n/iso value but a large ligand to metal ratio is needed for this giving a n/iso value of the magnitude ~20. [9, 12-14] Examining the catalyst system employed in this study, there is a 1:1 metal to ligand ratio. This is a low metal to ligand ratio and explains why the regioselectivity does not reach higher n:iso values.

The use of dendritic ligands in catalytic reactions can in some cases cause higher regioselectivities. [15, 16] With PPI-based metallodendrimers, there is the possible back folding of the dendritic arms creating a more sterically demanding macroenvironment around the metal centre. This steric bulk surrounding the metal centre should cause higher n/iso values but since the values for the mononuclear complexes are similar to those of the metallodendritic complexes, this dendritic effect might not be as pronounced. These

observations are not unprecedented as work conducted by Reetz *et al.* showed no significant difference in regioselectivity going from a mononuclear Rh(I) complex to the metallodendritic Rh(I) complex for the hydroformylation of 1-octene. [17, 18] Their rhodium metallodendrimer was also based on the PPI dendritic scaffold.

3.3 Effect of temperature and pressure on hydroformylation activity.

3.3.1 Effect of temperature

In the previous section, the catalytic performance and selectivity results for the various mononuclear and multinuclear catalytic systems were investigated at optimal reaction conditions (P = 30 bar, T = 75 °C). Prior to this investigation, a series of optimization reactions were conducted. The effects of pressure and temperature were investigated for the various catalytic systems. Syngas pressures of 5 bars and 10 bars were used at temperatures of 25 °C, 50 °C and 75 °C.

Reactions were run for 8 hours and sampled every two hours. Analyses of the results show no significant hydroformylation activity by the catalysts for temperatures below 75 °C.

3.3.2 Effect of syngas pressure

Syngas pressure is an important parameter when trying to optimize reaction conditions. Although much emphasis is placed on ligand design and how this affects selectivity, pressure influences the chemoselectivity to a great extent.

Table 3.2 shows substrate conversion and chemoselectivity results obtained using different syngas pressures at a temperature of 75 °C. The mononuclear complexes **2.4** and **2.10** and metallodendritic complexes **2.5** and **2.11** were compared. The catalysts were initially subjected to a syngas pressure of 5 bar at 75 °C. At this pressure, there is not a significant conversion of 1-octene. Comparing the results (entries 1, 4, 7 and 10), the catalytic activity increases using the mono-nuclear and first generation catalysts in the order **2.11 < 2.10 < 2.5 < 2.4**.

Table 3.2: Hydroformylation results obtained using various pressures. [a]

Rh(I) Complexes	Entry	P (bar)	% 1-octene conversion	%aldehyde	% isomeric n-octenes[b]
Mononuclear iminophosphine, (**2.4**)	1	5	16	1	99
	2	10	82	8	91
	3	30	98	80	20
Dendritic G1 iminophosphine, (**2.5**)	4	5	4.4	0	100
	5	10	57	7	93
	6	30	98	64	36
Mononuclear iminopyridyl, (**2.10**)	7	5	2	0	100
	8	10	18	7	93
	9	30	98	70	30
Dendritic G1 iminopyridyl, (**2.11**)	10	5	1	0	100
	11	10	91	6	94
	12	30	98	64	36

[a] Sampled after 8 hours. T = 75 °C. Rh = 0.0028 mmol. [b]excluding 1-octene.

The 1-octene percent conversion values occur in the range of approximately 1%-16% after an eight hour period. At a syngas pressure of 5 bar, there is only the formation of octene isomers and no hydroformylation products are observed. The syngas pressure was then increased to 10 bar (entries 2, 5, 8, 11) and 30 bar (entries 3, 6, 9, 12) in separate experiments. Upon increasing the pressure, there is a clear increase in the percentage conversion of 1-octene after a period of 8 hours for each of the complexes compared to the reactions conducted at 5 bar. For the mononuclear iminophosphine Rh(I) complex, **2.4**, there is an increase from a 16% conversion of 1-octene to 82% going from a 5 bar syngas pressure to a 10 bar syngas pressure. The percentage aldehyde formed increases for this complex with the increase in syngas pressure. This observation is met by a decrease in the percentage octene isomers formed hence increase in chemoselectivity for the aldehyde. Increasing the pressure to 30 bar led to a further increase in the catalytic rate. Conversion of 1-octene now reached approximately 99% after an 8 hour reaction period for all the catalysts used.

The chemoselectivity was positively affected by this increase in pressure now favoring the chemoselective formation of aldehyde. This increase in percent conversion and percent aldehyde with an increase in pressure was observed for all of the remaining complexes **2.10**, **2.11** and **2.5** and this lead to the utilization of a syngas pressure of 30 bar and an operating temperature of 75 °C. Enhanced diffusion of syngas into the reaction mixture upon increase in syngas pressure is responsible for the increased percentage 1-octene conversion and aldehyde formation.

3.4 Conclusion

The mononuclear and multinuclear iminophosphine and iminopyridyl Rh(I) complexes synthesized were evaluated as catalysts in the hydroformylation of 1-octene. The effect of syngas pressure on the hydroformylation reaction was investigated at this optimal temperature for syngas pressures of 5 bar, 10 bar and 30 bar. A 30 bar syngas pressure yielded the best hydroformylation results and this pressure along with a temperature of 75 °C was utilized to investigate the difference in catalytic rate, chemoselectivity and regioselectivity for the various mononuclear and multinuclear iminophosphine and iminopyridyl Rh(I) complexes. Under these conditions the catalysts showed moderate hydroformylation activity with chemoselective formation of aldehydes and some isomerization products.

3.5 References

1. R. Paciello, L. Siggel and M. Roper, *Angew. Chem., Int. Ed. Engl.*, **1999**, 38, 1920.
2. N. Brinkmann, D. Giebel, G. Lohmer, M.T. Reetz and U. Kragl, *J. Catal.*, **1999**, 183, 163.
3. H.P. Dijkstra, C.A. Kruithof, N. Ronde, R. van de Coevering, D.J. Ramón, D. Vogt, G.P.M. van Klink and G. van Koten, *J. Org. Chem.*, **2003**, 68, 675.
4. A.V. Gaikwad, V. Boffa, J.E. ten Elshof and G. Rothenberg, *Angew. Chem. Int. Ed.*, **2008**, 47, 5407.
5. D. de Groot, B.F.M. de Waal, J.N.H. Reek, A.P.H.J. Schenning, P.C.J. Kamer, E.W. Meijer and P.W.N.M. van Leeuwen, *J. Am. Chem. Soc.*, **2001**, 123, 8453.
6. R. van Heerbeek, P.C.J. Kamer, P.W.N.M. van Leeuwen and J.N.H. Reek, *Chem. Rev.*, **2002**, 102, 3717.
7. N.J. Hovestad, E.B. Eggeling, H.J. Heidbüchel, J.T.B.H. Jastrzebski, U. Kragl, W. Keim, D. Vogt and G. van Koten, *Angew. Chem. Int. Ed.*, **1999**, 38, 1655.
8. N.J. Ronde and D. Vogt, *Catalyst Separation, Recovery and Recycling; Chemistry and Process Design*, Springer edn., Dordrecht, The Netherlands, 2005.
9. D. Evans, J.A. Osborn and G. Wilkinson, *J. Chem. Soc. A*, **1968**, 3133.
10. R. Lazzaroni, G. Ucello-Barretta and M. Benetti, *Organometallics*, **1989**, 8, 2323.
11. R. Lazzaroni, A. Rafaelli, R. Settambolo, S. Bertozzi and G. Vitulli, *J. Mol. Catal.*, **1989**, 50, 1.
12. C.K. Brown and G. Wilkinson, *J. Chem. Soc. A*, **1970**, 2753.
13. D. Evans, G. Yagupsky and G. Wilkinson, *J. Chem. Soc. A*, **1968**, 2660.
14. G. Gregorio, G. Montrasi, M. Tampieri, P. Cavalieri d'Oro, G. Pagani and A. Andreetta, *Chim. Ind. (Milan)*, **1980**, 62, 389.
15. L. Ropartz, K.J. Haxton, D.F. Foster, R.E. Morris, A.M.Z. Slawin and D.J. Cole-Hamilton, *J. Chem. Soc., Dalton Trans.*, **2002**, 4323.
16. L. Ropartz, R.E. Morris, D.F. Foster and D.J. Cole-Hamilton, *Chem. Commun.*, **2001**, 361.
17. M.T. Reetz, G. Lohmer and R. Schwickardi, *Angew. Chem., Int. Ed. Engl.*, **1997**, 36, 1526.
18. M.T. Reetz, G. Lohmer and R. Schwickardi, *Angew. Chem.*, **1997**, 109, 1559.

Chapter 4

Experimental

4.1 General experimental

All reactions were performed under nitrogen gas using standard Schlenk line techniques unless otherwise stated. All solvents were dried and distilled under an inert atmosphere using the appropriate drying agents. Toluene, *n*-pentane and tetrahydrofuran were dried over sodium/benzophenone and dichloromethane with calcium hydride. Ethanol was dried over magnesium metal turnings and iodine.

2-(Diphenylphosphino)benzaldehyde, *N*,*N*,*N*′,*N*′-Tetrakis(3-aminopropyl)-1,4-butanediamine (DAB-Am-4 polypropylenimine tetraamine), 4-pyridinecarboxaldehyde, 1,5-cyclooctadiene, deuterated chloroform, 1-octene and *n*-dodecane were purchased from Aldrich. DAB-Am-8 polypropylenimine octaamine was purchased from Symo-Chem. Wilkinsons complex and $[RhCl(CO)_2]_2$ was purchased from Strem Chemicals. Anhydrous $MgSO_4$ was purchased from KIMIX. All purchased chemicals were used without further purification. Di-μ-chloro-bis(1,5-cyclooctadiene)dirhodium(I) [1] and (acetylacetonato)dicarbonylrhodium(I) [2] were prepared according to literature procedures.

Infrared absorptions were measured on the Perkin Elmer Spectrum One FT-IR Spectrometer using NaCl solution cells. Melting points were conducted on the Kofler hot stage microscope (Riechert Thermovar). Elemental analyses for C, H, and N were conducted on a Thermo Flash 1112 Series CHNS-O Analyser. Nuclear Magnetic Resonance (NMR) spectra were recorded at ambient temperature on either a Varian Mercury XR300 MHz (^{1}H at 300.08 MHz, ^{13}C 75.46 MHz, ^{31}P 121.47 MHz) or a Varian Unity XR400 MHz (^{1}H at 399.95 MHz, ^{13}C 100.58 MHz, ^{31}P 161.90 MHz). Chemical shifts for the ^{1}H and ^{13}C{^{1}H} NMR shifts were referenced using tetramethylsilane (TMS) as an internal standard and ^{31}P NMR shifts were measured relative to H_3PO_4 as external standard.

Mass spectrometry determinations were conducted on either the Waters API Q-TOF Ultima mass spectrometer, JEOL GCmateII for EI mass spectrometry, or the ULTRAFLEX (UltraflexTOF/TOF) for the MALDI-TOF.

4.2 Synthesis of the iminophosphine ligands

4.2.1 Synthesis of (2-Diphenylphosphanyl-benzylidene)-propyl-amine, **2.1** [3]

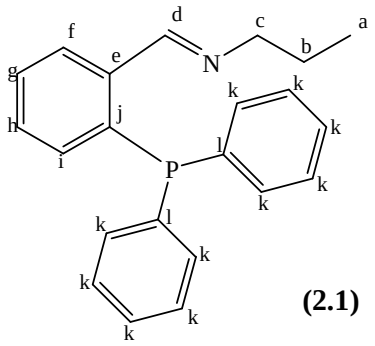

(2.1)

2-(Diphenylphosphino)benzaldehyde (1.00 g; 3.84 mmol) was transferred to a 100 cm^3 Schlenk flask and toluene (50 cm^3) added. Propylamine (0.23 g; 3.89 mmol) was syringed into the resulting solution and anhydrous $MgSO_4$ was added with stirring. The mixture was stirred for 24 hours at room temperature before being filtered by gravity and the solvent removed from the filtrate on a rotary evaporator (~30 °C). The resulting orange oil was then dissolved in dichloromethane and washed with water (6 x 50 cm^3). The organic layer was collected and dried over anhydrous $MgSO_4$. This mixture was filtered and the solvent removed from the filtrate *in vacuo* yielding an orange oil. Yield = 71%. ν_{max}(solution, CH_2Cl_2)/cm^{-1} = 1637s (C=N, imine); ^{1}H-NMR (400MHz, $CDCl_3$): 0.76 (t, 3H, H_a), 1.55 (m, 2H, H_b), 3.45 (t, 2H, H_c), 6.89 (m, 1H, H_f), 7.34 (m, 12H, H_g, H_h, H_k), 7.99 (m, 1H, H_i), 8.89 (d, 1H, H_d, $^4J_{PH}$ = 4.5 Hz); ^{31}P-NMR (121 MHz, $CDCl_3$): -13.4 (s)

4.2.2 Synthesis of the first-generation DAB iminophosphine ligand, **2.2** [4]

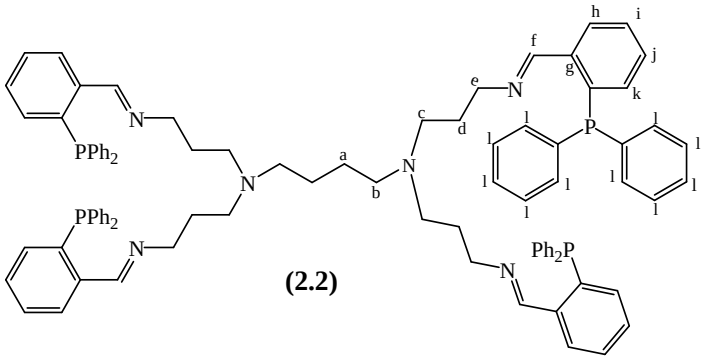

(2.2)

A solution of DAB-$(NH_2)_4$ (0.37 g; 1.18 mmol) in dichloromethane/absolute ethanol (99%) (50:50 by v/v%) (20 cm^3) was transferred to a Schlenk flask. 2-(Diphenylphosphino) benzaldehyde (1.37 g; 4.75 mmol) in dichloromethane/absolute ethanol (60 cm^3) solution was syringed into the Schlenk flask and the solution stirred. Anhydrous $MgSO_4$ (~6 g) was transferred to the stirring solution and resulting mixture stirred for 48 hours. The mixture was then filtered and the solvent removed from the filtrate on the rotary evaporator (~30°C). The resulting orange oil was dissolved in dichloromethane (60 cm^3) and washed with water (6 x 50 cm^3). The yellow organic layer was collected and dried over anhydrous $MgSO_4$, filtered and the solvent removed from the filtrate using the rotary evaporator (~30°C). The resulting orange oil was further dried *in vacuo* to yield a pale-yellow foam-like solid. Yield = 76%. M.p.: 56-58 ºC; ν_{max}(solution, CH_2Cl_2)/cm^{-1} = 1637s; ^{1}H-NMR (300MHz, $CDCl_3$): 1.29 (br qn, 4H, H_a), 1.59 (br qn, 8H, H_d), 2.28 (br m, 12H, H_b and H_c), 3.44 (br t, 8H, H_e), 6.86 (m, 4H, H_k), 7.29 (br m, 48H, $H_{i, j, m, n, o, p}$), 7.94 (m, 4H, H_h), 8.85(d, 4H, H_f, $^4J_{PH}$ = 4.5 Hz); ^{13}C-NMR (100MHz, $CDCl_3$): 25.2-59.6 (DAB-*dendr*-$(NH_2)_4$ core), 127.6-139.8 (aromatic), 159.4 (d, $^3J_{PC}$ = 20.7 Hz, C_f); ^{31}P-NMR (121MHz, $CDCl_3$): -13.4 (s); Elemental Analysis for **2.2**: Found: C = 77.40%, H = 6.53%, N = 5.79%. $C_{92}H_{92}N_6P_4.¼CH_2Cl_2$ requires C = 77.65%, H = 6.53%, N = 5.89%; ESI-MS: m/z 703 $[M]^{2+}$ (doubly charged ion)

4.2.3 Synthesis of the second-generation DAB iminophosphine ligand, **2.3** [4]

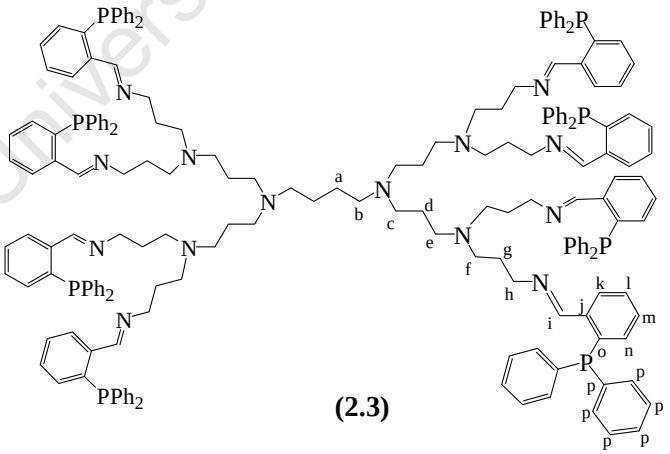

(2.3)

Compound **2.3** was synthesised in a similar method to **2.2** using DAB-$(NH_2)_8$ (0.09 g; 0.12 mmol) and 2-(diphenylphosphino)benzaldehyde (0.29 g; 0.99 mmol). The pale-yellow solid foam-like solid that forms upon removal of solvent *in vacuo* was triturated with n-pentane (20 cm^3). Yield = 68%. M.p.: 61-63 ºC; ν_{max}(solution, CH_2Cl_2)/cm^{-1} = 1637s; ^{1}H-NMR

(300MHz, $CDCl_3$): 1.55 (br qn, 4H, H_a), 1.59 (br qn, 24H, H_d, H_g), 2.29-2.39 (2 x br s, 36H, H_b, H_c, H_e, H_f), 3.42 (m, 16H, H_h), 6.85 (m, 8H, H_k), 7.27-7.39 (br m, 96H, $H_{l, m, p}$), 7.94 (m, 8H, H_n), 8.84 (d, 8H, H_i); ^{13}C-NMR (100 MHz, $CDCl_3$): 23.7, 24.2, 27.2, 50.6, 51.3, 53.4, 58.6, 126.7-138.8 (aromatic), 158.2 (d, $^3J_{PC}$ = 20.7 Hz, C_i); ^{31}P-NMR (121MHz, $CDCl_3$): -13.4 (s); Elemental Analysis for **2.3**: Found: C = 73.05%, H = 6.48%, N = 6.12%. $C_{192}H_{200}N_{14}P_8.3CH_2Cl_2$ requires C = 73.09%, H = 6.46%, N = 6.13%; MALDI-TOF-MS: m/z 2951 $[M]^+$

4.3 Reactions of the iminophosphine ligands with $[RhCl(CO)_2]_2$

4.3.1 Reaction of (2-Diphenylphosphanyl-benzylidene)-propyl-amine (**2.1**) with $[RhCl(CO)_2]_2$ to form compound **2.4** [4]

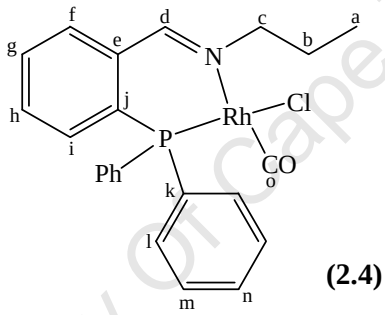

(2.4)

$[RhCl(CO)_2]_2$ (0.07 g; 0.17 mmol) was transferred to a Schlenk tube in a nitrogen purged glovebox. Tetrahydrofuran (THF) (5 cm^3) was syringed into the Schlenk tube to dissolve the $[RhCl(CO)_2]_2$ complex. A solution of **2.1** (0.13 g; 0.38 mmol) in THF (5 cm^3) was added dropwise to the stirring $[RhCl(CO)_2]_2$ solution causing a colour change from orange to red. The reaction was stirred for 2 hours at room temperature during which time a precipitate forms. The orange precipitate was collected on a Hirsch funnel, washed with cold THF (2 x 5 cm^3) and further dried *in vacuo*. Yield = 54%. M.p.: decomposes without melting > 250 °C; ν_{max}(solution, CH_2Cl_2)/cm^{-1} = 1628w (C=N), 2000s (C=O); ^{1}H-NMR (300MHz, $CDCl_3$): 0.47 (t, 3H, H_a), 1.68 (sx, 2H, H_o), 4.11 (t, 2H, H_c), 6.90 (t, 1H, H_g), 7.47 (m, 13H, $H_{f, h, I, l, m, n}$), 7.93 (s, 1H, H_d); ^{13}C-NMR (100 MHz, $CDCl_3$): 10.8, 24.3, 66.9, 128.8-135.4 (aromatic), 163.8 (s, C=N), 189.5 (dd, $^2J_{PC}$ = 17.0 Hz, $^1J_{RhC}$ = 72.0 Hz, CO); ^{31}P-NMR (121 MHz, $CDCl_3$): 48.3 (d, $^1J_{RhP}$ = 167 Hz); Elemental Analysis for **2.4**: Found: C = 55.49%, H = 4.10%, N = 2.58%. $C_{23}H_{22}NOPRhCl$ requires C = 55.49%, H = 4.45%, N = 2.81%; EI+-MS: m/z 496.76 $[M]^+$

4.3.2 Reaction of the first-generation iminophosphine DAB dendrimer, **2.2**, with $[RhCl(CO)_2]_2$, to form compound **2.5** [4]

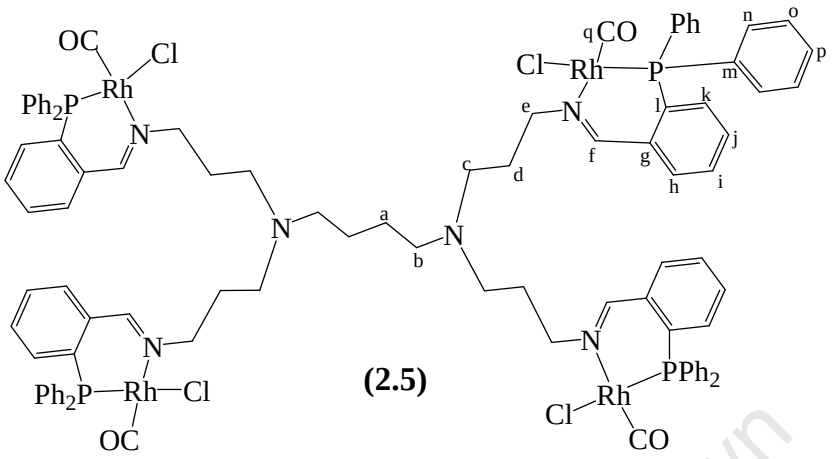

(2.5)

$[RhCl(CO)_2]_2$ (0.07 g; 0.17 mmol) and **2.2** (0.18 g; 0.12 mmol) was transferred to a Schlenk tube. THF (10 cm^3) was syringed into the Schlenk tube to dissolve the reactants. The reaction was stirred for 24 hours at room temperature after which the reaction volume was reduced to ~3 cm^3 by removing solvent *in vacuo*. *n*-Pentane was syringed into the solution to precipitate the product as an orange solid that was collected on a Hirsch funnel, washed with n-pentane (2 x 5 cm^3) and further dried *in vacuo*. The compound was further purified by precipitation from a DCM solution using n-pentane. Yield = 63%. M.p.: >300 ºC decomposes without melting; ν_{max}(solution, CH_2Cl_2)/cm^{-1} = 1630m (C=N), 2001s (C=O); ^{1}H-NMR (300MHz, $CDCl_3$): 1.45 (br s, 4H, H_a), 1.84 (br s, 8H, H_d), 2.27 (br s, 12H, H_b and H_c), 4.07 (br s, 8H, H_e), 6.82 (m, 4H, H_i), 7.43 (br m, 48H, $H_{j, k, m, n, o, p}$), 7.91 (m, 4H, H_h), 8.49(s, 4H, H_f); ^{13}C-NMR (100 MHz, $CDCl_3$): 25.8 (br), 62.0 (br), 68.2, 125.6-136.6 (aromatic), 167.1 (br, C=N), 189.4. (dd, $^2J_{PC}$ = 17.0 Hz, $^1J_{RhC}$ = 72.0 Hz, CO). ^{31}P-NMR (121MHz, $CDCl_3$): 48.5 (d, $^1J_{RhP}$ = 163 Hz); Elemental Analysis for **2.5**: Found: C = 51.83%, H = 4.38%, N = 3.61%. $C_{96}H_{92}N_6O_4P_4Rh_4Cl_4.2½CH_2Cl_2$ requires C = 51.81%, H = 4.28%, N = 3.68%; ESI-MS: m/z 1038 $[M]^{2+}$ (doubly charged ion)

4.3.3 Reaction of the second-generation iminophosphine DAB dendrimer, **2.3**, with $[RhCl(CO)_2]_2$, to form compound, **2.6**[4]

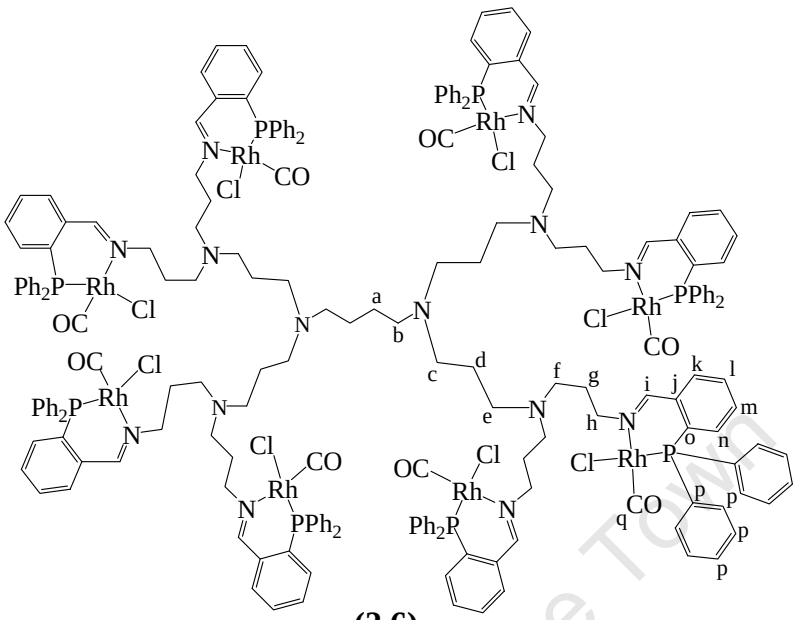

(2.6)

A THF (10 cm^3) solution of **2.3** (0.27 g; 0.09 mmol) was syringed into a THF (10 cm^3) solution of $[RhCl(CO)_2]_2$ (0.14 g; 0.36 mmol) stirring in a Schlenk tube. The reaction was stirred for 24 hours during which a colour change from orange to red occurred. The solvent volume was reduced *in vacuo* and *n*-pentane added to form a precipitate. The precipitate was collected on a Hirsch funnel, washed with *n*-pentane and dried *in vacuo* yielding a yellow-brown solid. Yield = 88%. M.p.: >300 ºC decomposes without melting; ν_{max}(solution, CH_2Cl_2)/cm^{-1} = 1630w (C=N); 1996s (C=O); ^{1}H-NMR (300MHz, $CDCl_3$): 1.64 (br s, 28H, $H_{a,\ d,\ g}$), 2.35 (br s, 36H, $H_{b,\ c,\ e,\ f}$), 4.11 (m, 16H, H_h), 6.79 (m, 8H, H_k), 7.92 (br m, 96H, phenyl), 7.92 (m, 8H, H_n), 8.54 (br s, 8H, H_i); ^{13}C-NMR (100 MHz, $CDCl_3$): 22.4 (br), 51.4 (br) 62.1, 125.9-136.3 (aromatic), 166.2 (br,C=N), 190.0 (dd, $^2J_{PC}$ = 17.0 Hz, $^1J_{RhC}$ = 72.0 Hz, CO); ^{31}P-NMR (121 MHz, $CDCl_3$): 48.5 (d, PPh_2, $^1J_{RhP}$ = 164 Hz); Elemental Analysis for **2.6**: Found: C = 50.57%, H = 4.54%, N = 3.62%. $C_{200}H_{200}N_{14}O_8P_8Rh_8Cl_8$.$7CH_2Cl_2$ requires C = 50.98%, H = 4.42%, N = 4.02%

4.4 Synthesis of the iminopyridyl ligands

4.4.1 Synthesis of propyl-pyridin-4-ylmethylene-amine, **2.7** [5]

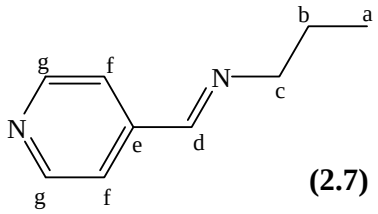

(2.7)

Propylamine (1.33 g, 22.49 mmol) was syringed into a stirring mixture of anhydrous toluene (50 cm^3), 4-pyridinecarboxaldehyde (2.24 g, 20.95 mmol) and anhydrous $MgSO_4$. The mixture was stirred at room temperature for 24 hours. The mixture was filtered and the solvent removed from the filtrate using the rotary evaporator (~ 30 °C). The residual yellow-orange oil was dissolved in DCM (30 cm^3) and washed with water (6 x 50 cm^3). The organic layer was collected and dried over anhydrous $MgSO_4$. The mixture was filtered and the solvent removed from the filtrate *in vacuo* yielding a yellow-orange oil. Yield = 52%. ν_{max}(solution, CH_2Cl_2)/cm^{-1} = 1647s (C=N, imine), 1598s (C=N, pyridyl); ^{1}H-NMR (300MHz, $CDCl_3$): 0.95 (t, 3H, H_a), 1.73 (m, 2H, H_b), 3.61 (t, 2H, H_c), 7.57 (d, 2H, H_f), 8.24 (s, 1H, H_d), 8.66 (d, 2H, H_g); ^{13}C-NMR (100 MHz, $CDCl_3$): 11.8 (C_a), 23.8 (C_b), 63.6 (C_c), 121.9 (C_f), 143.1 (C_e), 150.4 (C_g), 158.8 (C_d).

4.4.2 Synthesis of the first-generation DAB iminopyridyl ligand, **2.8** [5]

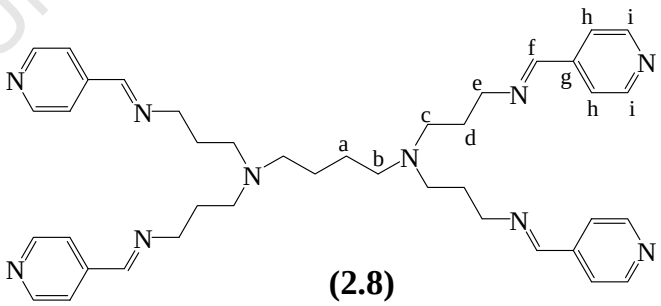

(2.8)

DAB-$(NH_2)_4$ (1.04g; 3.30 mmol) was dissolved in toluene (20 cm^3) and added to a stirring mixture of anhydrous $MgSO_4$ (~7g) in toluene (30 cm^3). 4-Pyridinecarboxaldehyde (1.45 g; 13.51 mmol) was then added to the reaction and was stirred at room temperature for 48 hours. The mixture develops a pale-straw colour as the reaction progresses. The mixture was then

filtered by gravity and the solvent removed from the filtrate on the rotary evaporator (~ 30 °C) yielding a crude yellow oil. The oil was dissolved in DCM (50 cm^3) and washed with water (12 x 50 cm^3). The organic layer was then collected and dried over $MgSO_4$. The mixture was filtered and the solvent removed from the filtrate *in vacuo* yielding the product as a yellow oil. Yield = 68%. ν_{max}(solution, CH_2Cl_2)/cm^{-1} = 1648s (C=N, imine), 1599s, (C=N, pyridyl); ^{1}H-NMR (400MHz, $CDCl_3$): 1.42 (m, 4H, H_a), 1.83 (qn, 8H, H_d), 2.38 (br t, 4H, H_b), 2.52 (m, 8H, H_c), 3.63 (t, 8H, ^3J = 7.53 Hz, H_e), 7.52 (d, 8H, ^3J = 6.04, H_h), 8.23 (s, 4H, H_f), 8.63 (d, 8H, ^3J = 6.02 Hz, H_i); ^{13}C-NMR (100MHz, $CDCl_3$): 25.3, 28.3, 51.7, 54.1, 59.8 (CH_2), 121.8, 143.0 (C, Ar pyr), 150.4 (Ar pyr), 159.0 (s, C_i); Elemental Analysis for **2.8**: Found: C = 68.42%, H = 7.50%, N = 20.02%. $C_{40}H_{52}N_{10}.½CH_2Cl_2$ requires C = 68.00%, H = 7.47%, N = 19.58%; FAB-MS: m/z 673 $[M]^+$

4.4.3 Synthesis of the second-generation DAB iminopyridyl ligand, **2.9** [5]

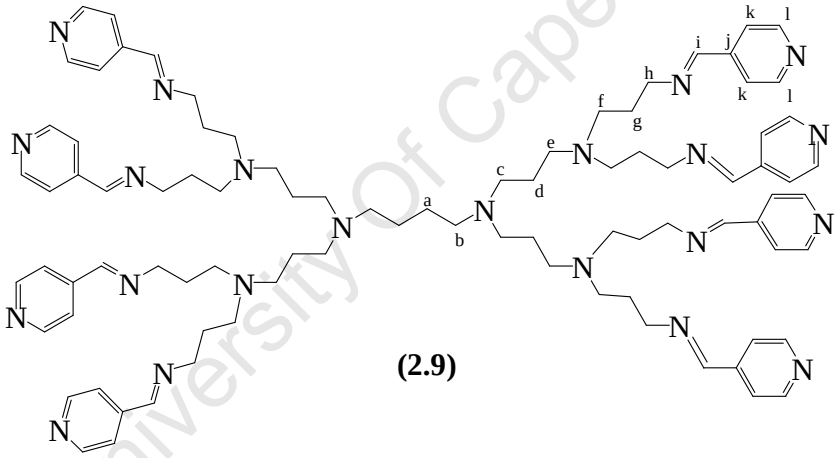

(2.9)

Compound **2.9** was synthesized in a similar method to **2.8** using DAB-$(NH_2)_8$ (0.57 g; 0.66 mmol) and 4-pyridinecarboxaldehyde (0.60 g; 5.62 mmol). The compound is an orange oil. Yield = 76%. ν_{max}(solution, CH_2Cl_2)/cm^{-1} = 1648s (C=N, imine), 1599s (C=N, pyridyl); ^{1}H-NMR (300MHz, $CDCl_3$): 1.39 (br s, 4H, H_a), 1.56 (br s, 8H, H_d), 1.72 (br s, 16H, H_g), 1.94 -2.44 (br m, 36H, $H_{b, c, e, f}$), 3.56 (br t, 16H, ^3J = 6.49 Hz, H_h), 7.48 (d, 16H, ^3J = 6.03 Hz, H_k), 8.17 (s, 8H, H_i), 8.57 (d, 16H, ^3J = 5.99 Hz, H_l); ^{13}C-NMR (75MHz, $CDCl_3$): 24.8, 25.2, 28.3, 51.7, 52.2, 52.3, 54.3, 59.8, 121.8, 150.4, 142.9, 159.0 (s, C_i); Elemental Analysis for **2.9**: Found: C = 69.24%, H = 8.18%, N = 20.49%. $C_{40}H_{52}N_{10}.½CH_2Cl_2$ requires C = 69.54%, H = 7.98%, N = 20.16%

4.5 Reactions of the iminopyridyl ligands with $[RhCl(COD)]_2$

4.5.1 Reaction of propyl-pyridin-4-ylmethylene-amine (**2.7**) with $[RhCl(COD)]_2$ to form compound **2.10**

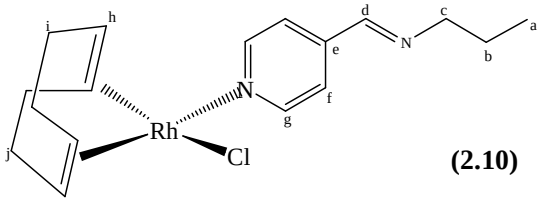

(2.10)

A solution of propyl-pyridin-4-ylmethylene-amine (0.06 g; 0.40 mmol) in DCM (5 cm^3) was added dropwise to a DCM (5 cm^3) solution of $[RhCl(COD)]_2$ (0.09 g; 0.19 mmol) in a Schlenk tube. The reaction was allowed to stir for 1 hour at room temperature after which the solvent was removed. The resulting yellow solid was washed with diethyl ether (5 cm^3), then n-pentane (5 cm^3) and dried *in vacuo*. Yield = 58%. M.p.: 124-127 °C; ν_{max}(solution, CH_2Cl_2)/cm^{-1} = 1612m (C=N, pyridyl), 1646m (C=N, imine); ^{1}H-NMR (300MHz, $CDCl_3$): 0.91 (t, 3H, H_a), 1.69 (m, 2H, H_b), 1.81 (m, 4H, H_i), 2.51 (m, 4H, H_j), 3.62 (m, 2H, H_c), 4.17 (m, 4H, H_h), 7.59 (d, 2H, H_f), 8.18 (s, 1H, H_d), 8.79 (d, 2H, H_g). ^{13}C-NMR (100MHz, $CDCl_3$): 11.8 (C_a), 23.7 (C_b), 30.9 ($C_{i,j}$), 63.6 (C_c), 80.5 (C_h), 122.7 (C_f), 144.1 (C_e), 151.3 (C_g), 157.4 (C_d); Elemental Analysis for **2.10**: Found: C = 51.04%, H = 6.12%, N = 6.93%. $C_{17}H_{24}N_2RhCl$ requires C = 51.85%, H = 6.39%, N = 7.11%

4.5.2 Reaction of the first-generation iminopyridyl DAB ligand, **2.8**, with $[RhCl(COD)]_2$ to form compound **2.11**

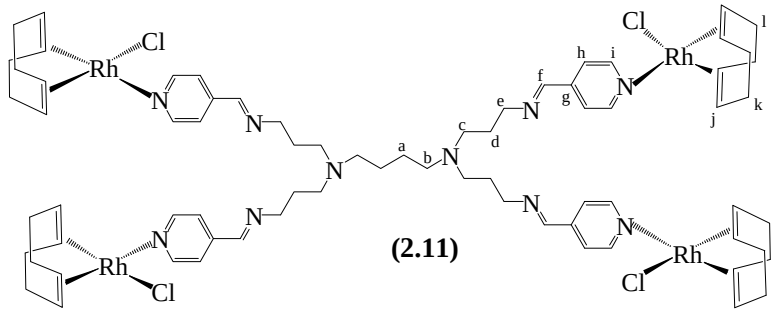

(2.11)

A solution of **2.8** (0.07 g; 0.09 mmol) in DCM (5 cm^3) was syringed dropwise into a stirring solution of $[RhCl(COD)]_2$ (0.10 g; 0.20 mmol) in DCM (5 cm^3) in a Schlenk tube. The

solution darkens over the course of the reaction. The reaction was stirred for 24 hours at room temperature after which the volume was reduced to approximately 5 cm^3. Diethyl ether was added to precipitate yellow solid. The solid was filtered and washed with diethyl ether (5 cm^3), n-pentane (5 cm^3) and dried *in vacuo*. Yield = 70%. M.p.: 133-137 °C; ν_{max}(solution, CH_2Cl_2)/cm^{-1} = 1646w (C=N, imine), 1612w (C=N, pyridyl); ^{1}H-NMR (300MHz, $CDCl_3$): 1.29 (br s, 4H, H_a), 1.83 (br m, 24H, H_d, H_l), 2.48 (br s, 28H, H_b, H_c, H_k), 3.59 (br s, 8H, H_e), 4.18 (br s, 16H, H_j), 7.50 (d, 8H, H_h), 8.21(s, 4H, H_f), 8.75 (d, 8H, H_i); ^{13}C-NMR (100MHz, $CDCl_3$): 25.1, 28.2, 30.8, 51.5, 53.9, 59.6, 80.4, 122.7, 143.9, 151.4, 157.6; Elemental Analysis for **2.11**: Found: C = 49.48.%, H = 6.06%, N = 7.38%. $C_{72}H_{120}N_{10}Rh_4Cl_4.1½CH_2Cl_2$ requires C = 49.41%, H = 5.81%, N = 7.84%

4.5.3 Reaction of the second-generation iminopyridyl DAB ligand, **2.9**, with $[RhCl(COD)]_2$ to form compound **2.12**

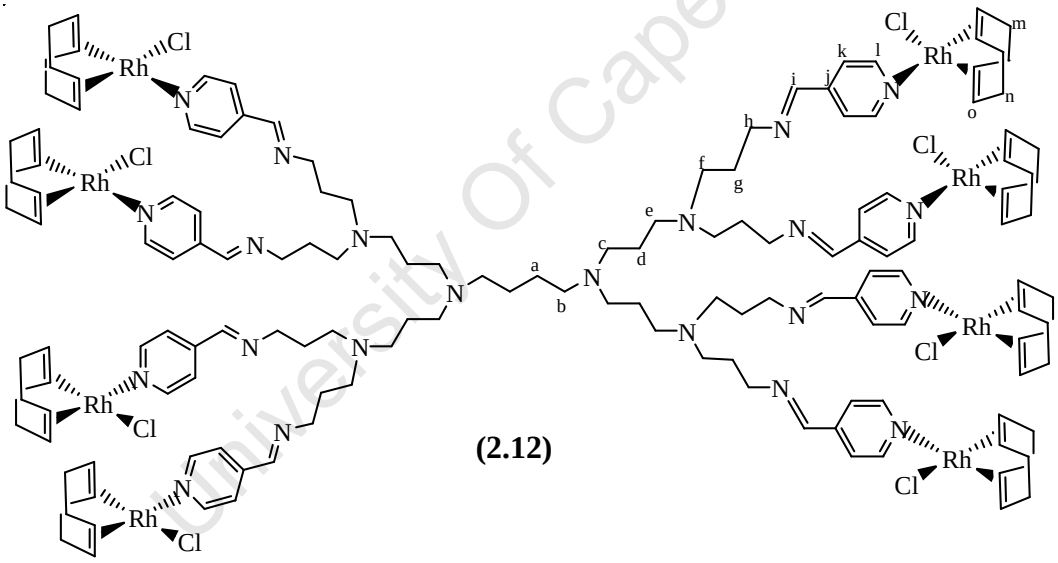

(2.12)

$[RhCl(COD)]_2$ (0.14 g; 0.28 mmol) was transferred to a Schlenk tube and DCM (5 cm^3) was added to dissolve it. A solution of **2.9** (0.10 g; 0.07 mmol) in DCM (5 cm^3) was then added dropwise. The solution was stirred for 24 hours after which the volume of the solution was reduced to approximately 5 cm^3 by removing solvent *in vacuo*. n-Pentane was added to precipitate the crude product. The product was triturated with n-pentane and then collected on a Hirsch funnel, washed with n-pentane (2 x 5 cm^3) and dried *in vacuo* yielding a yellow solid. Yield = 74 %. M.p.: >170 °C decomposes without melting; ν_{max}(solution, CH_2Cl_2)/cm^{-1} = 1646 (C=N, imine), 1612, (C=N, pyridyl); ^{1}H-NMR (300MHz, $CDCl_3$): 1.36

(br s, 4H, H_a), 1.54 (br s, 8H, H_d), 1.78 (br s, 48H, H_g and COD-CH_2), 2.45 (br s, 68H, $H_{b, c, e, f}$ and COD-CH_2), 3.60 (br s, 16H, H_h), 4.13 (br s, 32H, COD-CH), 7.54 (br s, 16H, H_k), 8.17 (br s, 8H, H_i), 8.74(br s, 16H, H_l); ^{13}C-NMR (100MHz, $CDCl_3$) : 28.0 (s), 30.8 (s), 51.5 (s), 52.0 (s), 59.6 (s), 80.6 (s), 122.7 (s), 143.8 (s), 151.3 (s), 157.8 (s); Elemental Analysis for **2.12**: Found: C = 50.28%, H = 6.25%, N = 8.13%. $C_{72}H_{120}N_{10}Rh_4Cl_4.2½CH_2Cl_2$ requires C = 50.55%, H = 6.07%, N = 8.39%

4.6 Reactions of the iminopyridyl ligands with [$RhCl(PPh_3)_3$]

4.6.1 Reaction of propyl-pyridin-4-ylmethylene-amine (**2.7**) with [$RhCl(PPh_3)_3$] to form compound **2.13**

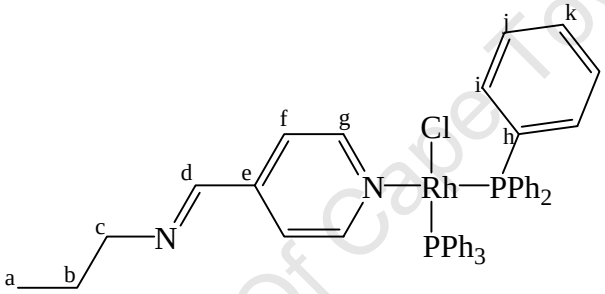

(2.13)

A solution of **2.7** (0.02 g, 0.16 mmol) in DCM (5 cm^3) was syringed drop wise into a stirring solution of [$RhCl(PPh_3)_3$] (0.14 g, 0.15 mmol) in DCM (5 cm^3) in a Schlenk tube. The reaction was stirred for 2 hours at room temperature at which time the volume was reduced to approximately 3-5 cm^3. n-Pentane was added to precipitate a beige solid. The solid was filtered and washed with n-pentane (5 cm^3 x 2). The beige solid was then dried *in vacuo*. Yield = 27% ν_{max}(solution, CH_2Cl_2)/cm^{-1} = 1614m (C=N, pyridyl), 1646m (C=N, imine); ^{1}H-NMR (300MHz, $CDCl_3$): 0.92 (m, 3H, H_a); 1.70 (s, 2H, H_b), 3.61 (t, 2H, H_c), 7.48 (d, 33H, H_{d-k}); ^{31}P NMR (121 MHz, $CDCl_3$): 29.20 s

4.6.2 Reaction of the first-generation iminopyridyl DAB ligand, **2.8**, with [RhCl(PPh$_3$)$_3$] to form compound **2.14**

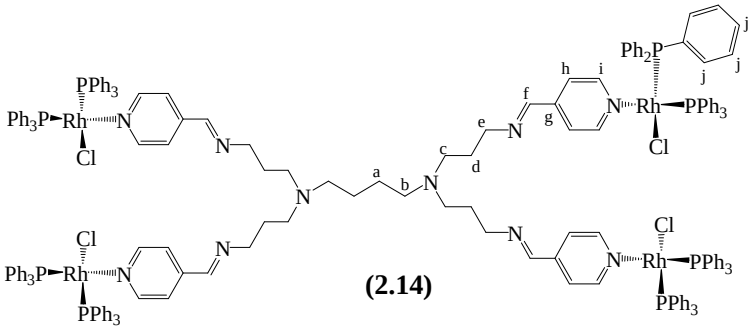

(2.14)

A solution of **2.8** (0.02 g, 0.02 mmol) in DCM (5 cm^3) was syringed dropwise into a stirring solution of [RhCl(PPh$_3$)$_3$] (0.10 g, 0.10 mmol) in DCM (5 cm^3) in a Schlenk tube. The reaction proceeded for 24 hours at room temperature after which the volume was reduced to approximately 5 cm^3. n-Pentane was added to precipitate a beige solid. The solid was filtered and washed with n-pentane (5 cm^3 x 2) and dried *in vacuo*. Yield = 71% ν_{max}(solution, CH_2Cl_2)/cm^{-1} = 1646 (C=N, imine), 1614 (C=N, pyridyl); ^{1}H-NMR (400MHz, $CDCl_3$): 1.27 (br m, 4H, H_a), 1.89 (br s, 8H, H_d), 2.42 (br s, 4H, H_b), 2.52 (br s, 8H, H_c), 3.73 (br s, 8H, H_e), 7-8 ppm (m, 60H, H_j), 8.25(s, 4H, H_f), 8.98 (d, 8H, H_i)

4.6.3 Reaction of the second-generation iminopyridyl DAB ligand, **2.9**, with [RhCl(PPh$_3$)$_3$] to form compound **2.15**

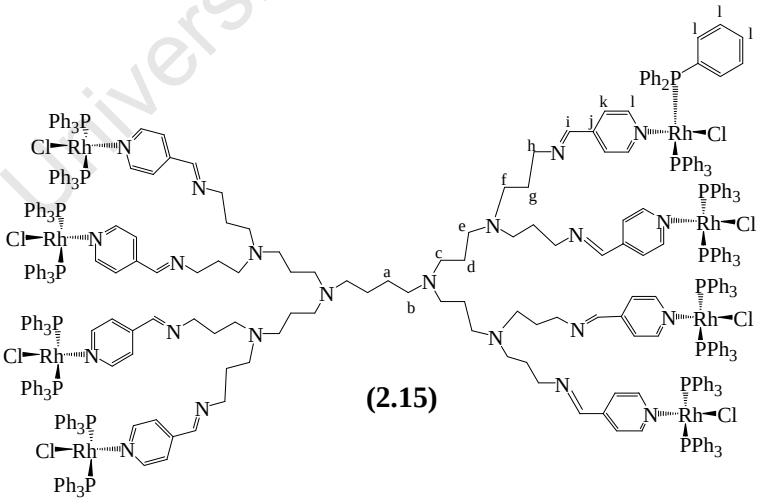

(2.15)

A solution of **2.9** (0.08 g, 0.05 mmol) in DCM (5 cm^3) was syringed dropwise into a stirring solution of [RhCl(PPh$_3$)$_3$] (0.40 g, 0.43 mmol) in dichloromethane (5 cm^3) in a Schlenk tube. The reaction proceeded for 24 hours at room temperature after which the volume was reduced

to approximately 3-5 cm^3. n-Pentane was added to form a precipitate. The beige solid was collected on a Hirsch funnel, washed with n-pentane (5 cm^3 x 2) and dried *in vacuo*. Yield = 62%. ν_{max}(solution, CH_2Cl_2)/cm^{-1} = 1646 (C=N, imine), 1614 (C=N, pyridyl); ^{1}H-NMR (400MHz, $CDCl_3$): 1.42 (br s, 12H, $H_{a,d}$), 1.76 (br s, 16H, H_g), 2.41 (br s, 36H, $H_{b, e, c, e, f}$), 3.57 (br s, 16H, H_h), 7.34 (m, 264H, H_i, phenyls), 8.68(broad s, 16H, H_l)

4.7 Preliminary chemical reactivity studies

4.7.1 Reaction of the iminophosphine Rh(I) complexes with methyl iodide

The respective iminophosphine Rh(I) complex (**2.4, 2.5** or **2.6**) was transferred to a Schlenk tube under nitrogen. Anhydrous DCM (10 cm^3) was syringed into the Schlenk tube and the resulting solution stirred. A molar excess of methyl iodide was syringed into the Schlenk tube and the solution stirred.

The reaction was sampled every ten minutes by removing 1cm^3 of the solution and removing all solvent to yield a dark maroon solid. The solid was redissolved in DCM 0.5 cm^3 and the infrared spectrum obtained.

4.7.2 Reaction of the iminopyridyl Rh(I) COD complexes with triphenylphosphine

A general procedure was followed for this series of preliminary chemical reactivity studies. The respective iminopyridyl Rh(I) complex (**2.10, 2.11** or **2.12**) was transferred to a Schlenk tube under nitrogen. DCM (5 cm^3) was syringed into the Schleck tube to dissolve the complex. Maintaining a Rh(I) complexes:PPh_3 ratio of 1:2, 1:8 and 1:16 for complex **2.10**, **2.11** and **2.12** respectively, a solution of triphenylphosphine in DCM (5 cm^3) was syringed into the stirring metal complex solution. The reactions change colour from yellow to orange upon reaction of the triphenylphosphine with the metal complexes. The reaction volume was then reduced to approximately 3 cm^3 and n-pentane added to precipitate a beige solid.

4.8 General hydroformylation procedure

The reactions were conducted in a 10 cm^3 stainless steel autoclave equipped with a magnetic stirrer. The autoclave was charged with toluene (6 cm^3), 1-octene (6.38 mmol) and rhodium complex (0.0028 mmol) resulting in a substrate to rhodium ratio of 2279:1. The autoclave was then flushed five times with syngas ($CO:H_2$, 1:1) to purge by displacement. The autoclave was then pressurized and heated to the desired syngas pressure and temperature respectively. Samples were taken every two hours and analyzed using gas chromatography (GC) with n-dodecane as internal standard. GC analyses were conducted using a Varian 3900 gas chromatograph equipped with a HP-PONA column for quantification. The identity of isomeric octenes and aldehydes were validated using GCMS on an Agilent Technologies 5973 Network Mass Selective Detector equipped with an identical column. Mass spectra were analyzed against the Wiley and NIST02 databases.

4.9 X-Ray crystallography

Reflection data for the single crystal was collected on a Stoe Image Plate Diffraction System (Stoe & Cie, 2000) using graphite monochromated MoKα radiation. The structure was solved using direct methods with the program SHELXS-97. [6] The refinement and all further calculations were conducted using SHELLXL-97 [7]. Packing diagrams were generated using the program PovRay and the graphical interface X-seed. [8] Non-H atoms were refined anisotropically using weighted full-matrix least-square on F^2 with 254 parameters. Drawings detailing the molecular structure were rendered using ORTEP. [9]

4.10 References

1. J. Chatt and L. M. Venanzi, *J. Chem. Soc.*, **1957**, 4735.
2. M. A. F. Hernandez-Gruel, J. J. Perez-Torrente, M. A. Ciriano, L. A. Oro and D. Krogstad, *Inorg. Synth.*, **2004**, 34, 127.
3. C.A. Ghilardi, S. Midollini, S. Moneti, A. Orlandini and G. Scapacci, *J. Chem. Soc., Dalton Trans.*, **1992**, 3371.
4. N.C. Antonels, B. Therrien, J.R. Moss and G.S. Smith, *Inorg. Chem. Commun.*, **2009**, 12, 716.
5. P. Govender, N.C. Antonels, J. Mattsson, A.K. Renfrew, P.J. Dyson, J.R. Moss, B. Therrien and G.S. Smith, *J. Organomet. Chem.*, **2009**, 694, 3470.
6. G.M. Sheldrick, *Acta Crystallogr.*, **1990**, A46, 467.
7. G.M. Sheldrick, SHELXS-97, SHELXL-97, University of Göttingen, Göttingen, Germany, 1999.
8. L.J. Barbour, *J. Supramol. Chem.*, **2001**, 1, 189.
9. L.J. Farrugia, *J. Appl. Cryst.* , **1997**, 30, 565.